Identification of active sites for N2O activation over iron containing pentasil zeolites

Please check the document version of this publication:

• A submitted manuscript is the version of the article upon submission and before peer-review. There can be important differences between the submitted version and the official published version of record. People interested in the research are advised to contact the author for the final version of the publication, or visit the DOI to the publisher's website.
• The final author version and the galley proof are versions of the publication after peer review.
• The final published version features the final layout of the paper including the volume, issue and page numbers.

Link to publication

IDENTIFICATION OF ACTIVE SITES FOR N$_2$O ACTIVATION OVER IRON CONTAINING PENTASIL ZEOLITES

PROEFSCHRIFT

ter verkrijging van de graad van doctor aan de
Technische Universiteit Eindhoven, op gezag van de
Rector Magnificus, prof.dr. R.A. van Santen, voor een
commissie aangewezen door het College voor
Promoties in het openbaar te verdedigen
op maandag 15 December 2003 om 14.00 uur

door

Zhu Qingjun

Geboren te Hulin
(China)

Dit proefschrift is goedgekeurd door de promotoren:

prof.dr. R.A. van Santen
en
prof.dr. F.Kapteijn

Copromotor:
dr.ir. E.J.M.Hensen

To my parents

Contents

Chapter 1

Introduction

Abstract

This thesis deals with the study of catalytic properties of iron-containing pentasil zeolites with a focus on reactions involving the activation of nitrous oxide. These include the decomposition of nitrous oxide and the selective oxidation of benzene to phenol using nitrous oxide as oxidant. The main objectives of the research are to identify the active sites in the catalysts, to establish the structure-reactivity relationships and to design catalysts based on the acquired knowledge. The methodology is to incorporate iron either at framework positions of the zeolites (via isomorphous substitution) followed by controlled migration to extra-framework positions or directly at extra-framework positions (via sublimation of $FeCl_3$), characterize the resulting materials and compare their catalytic activities. This introductory section provides a background to this research subject.

1.1 Heterogeneous catalysis and catalyst

The modern concept of catalysis was defined by Berzelius as follows "*Catalysis is a process whereby a reaction occurs faster than the uncatalyzed reaction, the reaction being accelerated by the presence of a catalyst*" (1). Catalysis by solid materials has been observed quantitatively at temperatures as low as 78 K and as high as 1500 K, at pressures between 10^{-9} and 10^3 bar. Its yields can be as low as 10^{-5} s^{-1} (one turnover per day) and as high as 10^9 s^{-1} (2). In brief, a catalyst is a substance that changes the kinetics but not the thermodynamics of a chemical reaction (3). Practically, catalysts are used in more than 70% of all industrial chemical processes. Moreover, the production of catalysts themselves accounts for a significant part of chemical manufacture (4). In 1998, world-wide catalyst sales totalled no less than $7.4 billion and some $10 trillion worth of chemicals and materials are produced each year through catalytic processes (5). While catalysts are widely employed in chemical process industries, much of its usage is in three categories: making petrochemicals and speciality chemicals, petroleum refining and environmental protection.

Environmental catalysis is required for cleaner air, soil and water. Catalysts are applied in environmental technologies to convert environmentally hazardous materials into harmless compounds. Examples are Selective Catalytic Reduction (SCR) of NO_x, removal of Volatile Organic Compounds (VOC), the decomposition of NO and N_2O and oxidation of CO from exhaust gas. A variety of catalysts, such as noble metal catalysts, promoted oxide catalysts and zeolite catalysts are employed for these reactions (6,7).

1.2 Nitrous oxide abatement

Nitrous oxide (dinitrogen oxide, N_2O) is a clear, colorless gas under ambient condition with a slightly sweet odor. The product is stable and inert at room temperature. After blended with O_2, it is widely used as a mild anaesthetic for dental surgery and obstetrics. However, pure nitrous oxide will cause asphyxiation, resulting ultimately in respiratory arrest (8,9).

Measurements of the amount of N_2O entrapped in the polar ice show that the global concentration of N_2O is higher now than any time during the past 45000 years. After the last ice age, the N_2O concentration remained at 275 ppb for around 10000 years until 19th century. Since then, the concentration of N_2O has increased significantly due to anthropogenic contributions (10). The atmospheric concentration is now about 315 ppb, and it has been increasing at the rate of 0.8 ppbv per year (11). The half-life of N_2O is estimated to be 120

years so even a small increase results in an accumulation and any concentration perturbation that occurs will last for centuries. N_2O is a kind of greenhouse gases with a global warming potential about 310 times that of CO_2 (table 1) (12). Moreover, N_2O is the main source of stratosphere NO_x which is an important sink for stratospheric ozone (13).

Table 1. The contributions of various gas, relative to CO_2, to the greenhouse effect. Calculations are based on emitted amounts and consideration has been given to the gases' decay in the atmosphere; ppbv, parts per billion by volume (12).

Species	Concentration (ppbv)	Rate of increase (% per year)	Relative contribution	
			Mass basis (kg^{-1})	Mole basis (mol^{-1})
CO_2	353×10^3	0.5	1	1
CH_4	1.7×10^3	1	45	15
N_2O	310	0.2	300	300
O_3	10-50	0.5	3	4
CFC-11	0.28	4	4000	11000
CFC-12	0.48	4	8000	2000

Less than 50% of all nitrous oxide emissions are caused by mankind activities. In chemical industry, N_2O is formed as an unwanted by-product during the catalytic oxidation of ammonia in air over platinum-rhodium catalyst gauzes in the ammonia converter of nitric acid plants (14,15).

$$4NH_3 + 5O_2 \longrightarrow 4NO + 6H_2O \qquad \text{desired}$$
$$4NH_3 + 4O_2 \longrightarrow 2N_2O + 6H_2O \qquad \text{undesired}$$
$$4NH_3 + 3O_2 \longrightarrow 2N_2 + 6H_2O \qquad \text{undesired}$$
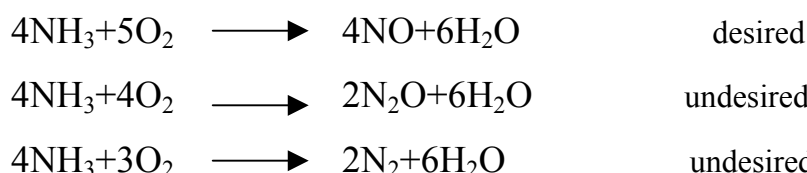
Many companies, such as BASF and Norsk Hydro, are trying to develop industrial processes to reduce the emission of N_2O. The approaches include (i) modification of the catalyst for ammonia oxidation with the aim to inhibit nitrous oxide formation (16) (ii) thermal or catalytic decomposition of nitrous oxide in the tail gas (17).

1.3. Benzene oxidation to phenol with N_2O as oxidant

Currently, the hydroxylation of paraffins and aromatics into alcohols and phenols are produced via complex multi-step processes that are unfriendly to the environment. For

instance, for the production of phenol the currently applied reaction route is the cumene process (figure 1) Although it is widely applied in industry, the cumene process has some important disadvantages: a poor ecology, an explosive intermediate (cumene hydroperoxide), low yield (85%) and the unwanted by-product of acetone (18).
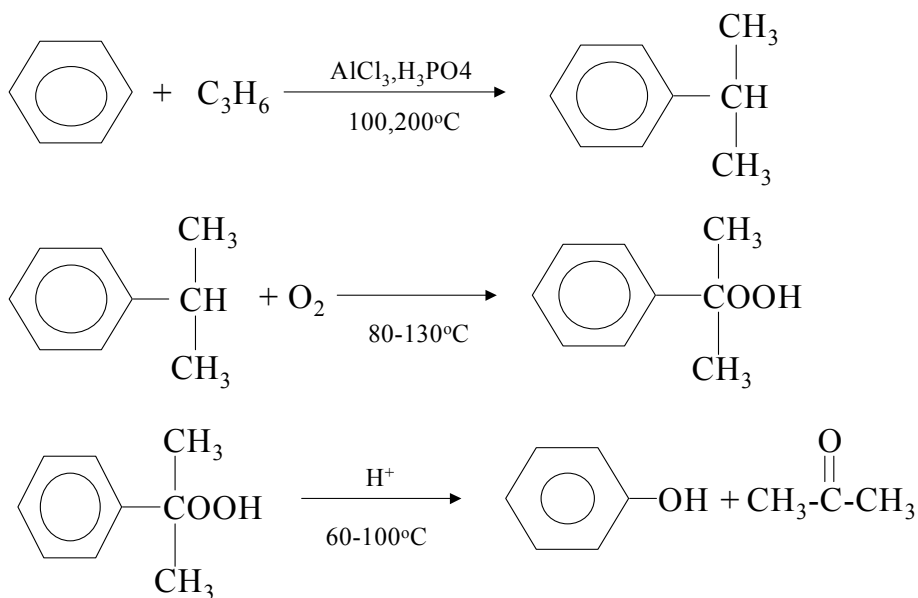
Figure 1: The three step cumene process for the production of phenol from benzene.

Nitrous oxide is a potentially interesting oxidant for selective oxidation of organic substrates since it contains 36 wt.% oxygen and the by-product of an oxidation reaction would be environmentally benign molecular nitrogen. Implementation of a one-step process of benzene oxidation to phenol using nitrous oxide as oxidant is potentially viable for the production of the adipic acid precursor to nylon (19). In this process, nitric acid is used and its production leads to nitrous-oxide-containing tail gases. In this way, the nitrous oxide could be efficiently reused to oxidize benzene. Selective oxidation of benzene to phenol using N_2O as oxidant was first reported by Iwamoto over vanadia (20) but later pilot plant development turned out to be disappointing due to low selectivity to phenol. Alternatively, Fe/ZSM-5 catalysts was found to be more promising catalyst with better selectivity and Solutia Inc. adapted the process to pilot plant scale (21).

Compared with the cumene process, this direct oxidation step is more environmental friendly. It is well known that methane monoxygenase (MMO) in methanotrophic bacteria

4

catalyzes the selective oxidation of methane to methanol by oxygen under ambient conditions (22, 23). The proposal that the active site of Fe/ZSM-5 involves the analogue of binuclear Fe cluster as found in MMO has attracted much academic interest (18). In addition, N_2O was also found recently to selectively oxidize the primary and secondary alcohols to aldehydes and ketons over the vanadium-containing keggin-type polyoxomolydbate that indicates the potential application of N_2O in selective oxidation chemistry (24).

1.4. Nature of Fe/ZSM-5 zeolites

Zeolites, which are crystalline aluminosilicate, have pores or channels formed by alumina and silica tetrahedra linked by oxygen bridges (3). However, unpromoted zeolites show limited applications so addition of the promoters such as transition metal ions is necessary (25). Many papers are published on the characterization and reactivity of such transition-metal-containing zeolites. Among those, iron in the MFI zeolites is of considerable interest to catalysis. Iron-loaded MFI zeolite was employed to catalyze the isomerization or dehydrogenation of alkanes (26), the selective oxidation of ammonia (27), the conversion of syngas to light olefins (28) and methane to aromatics (29). The most extensively studied reaction involving Fe/ZSM-5 in the last decade is the hydroxylation of benzene to phenol with N_2O as oxidant (30-38) and the selective catalytic reduction of NO_x with hydrocarbons (39-46). The pioneering work of Panov's group in selective benzene oxidation has been followed up by a wealth of literature on these materials. An exciting result is the possibility to oxidize methane to methanol at room temperature, which forms a potential route to the chemical use of the large deposits of natural gas (35). Compared to Fe/ZSM-5 prepared by isomorphous substitution, another type of Fe/ZSM-5 widely studied for the selective catalytic reduction of NO_x and involves the post-synthesis incorporation of Fe. Feng and Hall announced active and durable Fe/ZSM-5 catalyst made by ion exchange from an iron oxalate solution (39,40). It was reported that the conversion of NO to N_2 was 100% in combination with a high resistance against H_2O and SO_2 poisoning. However, the results of these experiments were difficult to reproduce (46). Later, Chen and Sachtler reexamined the FeZSM-5 catalyst in the same reaction using a different preparation procedure, anaerobic sublimation of volatile $FeCl_3$, and again noted remarkable poisoning resistance and stability of the catalyst (41-45). The reasons for these unique catalytic properties as well as the nature of active sites in Fe/ZSM-5 of zeolites, which are not typical for oxidation reactions, are

widely debated (39-50). It is therefore important to identify the iron species present in the cavities of ZSM-5.

The introduction of iron into extra-framework position of zeolites can be achieved by impregnation, ion exchange, including solid state ion exchange or sublimation of a suitable iron precursor. By contrast, the hydrothermal synthesis of [Fe]ZSM-5 introduces Fe at framework positions (51). These materials generally need to be activated to remove part of Fe to extra-framework positions. In general, iron ions can occupy three positions in the matrix of ZSM-5: (i) as isolated ions in framework positions, (ii) as cationic or neutral iron oxo complexes in the intracrystalline micropore space and (iii) as clusters or finely dispersed iron oxide particles on the external surface of the zeolite crystals. Many attempts have been made to elucidate the active structures and functioning of the redox sites, but no defintie conclusions have been drawn yet.

Conventionally, it has been supposed that dehydrogenation of two $Fe(OH)^+$ results in [Fe-O-Fe]$^{2+}$ and the complex is a possible oxygen carrier. This chemistry has been well established for Fe/Y for a Si/Al ratio of 2.5 allowing a close proximity of the negatively charged Al occupying tetrahedra (52). This simple compensation chemistry has been generally accepted for many years for a variety of divalent cations in faujasite systems. They found this to act as an oxygen carrier that can be reduced with H_2 and oxidized with O_2. The model was confirmed by Hall *et al.* and both Fe-Y and Fe-Mor (53) have been reported to act as oxygen carriers where the oxygen atom is to be located at bridging positions. Nevertheless, Pierce *et al.* found no evidence for the bridging oxygen atoms from x-ray diffraction (54). An alternative possibility was suggested by Segawa *et al.*(55). Because of the mobility of iron in the zeolite structure and the ability of zeolites to trap cations at sites of high accessibility, Fe^{3+} could be held by an O in the supercages, where the [FeO]$^+$ complex could readily participate in the redox reactions. Support for this idea was found in IR and Mössbauer studies on FeY. A similar iron-oxygen-iron bridge reportedly forms in the main channel of Fe/Mor and the location of the Fe would be along the main channel of the mordenite where the redox reaction is likely to occur. Some molecular form of oxygen is bonded to the zeolite even under vacuum at 773 K that is supposed to be superoxo (O^{2-}) compound of type [Fe-O-O-Fe]$^{2+}$ (56).

Panov *et al.* assumed that an iron complex stabilized in ZSM-5 zeolites produces a new form of surface oxygen (denoted as α-oxygen) upon the decomposition of N_2O (30 - 38). The α- sites is proposed to be a binuclear iron complex stabilized in the zeolite micropore system.

The complexes are formed presumably by Fe atoms leaving the framework during thermal treatment of the [Fe]ZSM-5. The following steps are proposed for the reaction mechanism over such centers.

Step 1. *Deposition of oxygen from nitrous oxide*

$$N_2O + (\ )_\alpha \ \rightarrow \ N_2 + (O)_\alpha$$
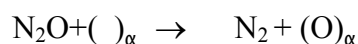
The α-sites are inert to oxidation by molecular oxygen and their peculiarity is the ability to decompose nitrous oxide at relatively low temperature and produce a new reactive form of surface oxygen. The state of Fe in these α- sites is of considerable interest and it is recently reported to be Fe^{2+} (57) although it is Fe^{3+} that is used for the synthesis.

Step 2. *Reaction of α-oxygen with a hydrocarbon, e.g. benzene*

$$C_6H_6 + (O)_\alpha \ \rightarrow \ (C_6H_6O)_\alpha$$
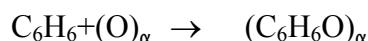
Next to the often studied oxidation of benzene to phenol, the reactivity of this α-oxygen allows also the conversion of methane to methanol at room temperature. This conforms to the very high reactivity found for oxygen in methane monooxygenases and thus mimics its ability for the selective oxidation at ambient temperatures.

Step 3. *Formation of phenol*

$$(C_6H_6OH)_\alpha \ \rightarrow \ C_6H_6O + (\ )_\alpha$$
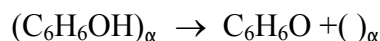
The final step involves the removal of phenol from the surface regenerating the vacancy. Recent quantum-chemical calculations by Kachurovskaya *et al.* (58) provide further insight into the mechanism (figure 2), showing the intermediate formation of an arene oxide and that removal of the hydroxylated product is a difficult step in the mechanism.

Although this model explains several of the experimental observations and most notably allows to titrate the number of active sites by studying the low temperature decomposition of nitrous oxide (59), it does not answer questions on the exact nature of the active sites, their location and the debated necessity of Fe. That is, competing views have stressed the importance of Brønsted acid sites (60,61) or Al Lewis acid sites (62).
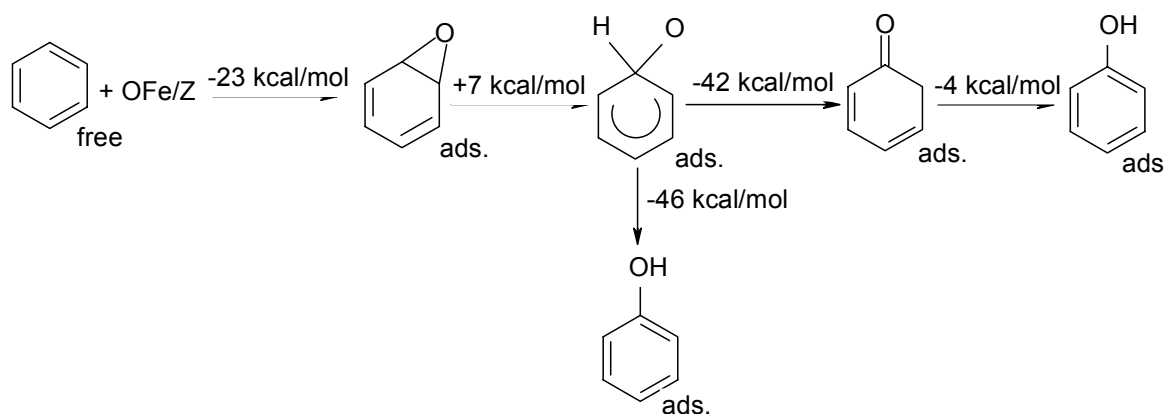
Figure 2: Mechanism of selective oxidation of benzene to phenol over Fe/ZSM-5.

Interestingly, the binuclear model has attracted the most attention. Chen and Sachtler (41-45) proposed a binuclear oxygen bridged complex, $[HO-Fe-O-Fe-OH]^{2+}$, based on the analogy with $[Cu-O-Cu]^{2+}$ in the same zeolite and the ability of Fe^{3+} to hydrolyze. This binuclear cluster can be reduced by removing the bridging oxygen. H_2-TPR and CO-TPR show that this reduction requires a higher temperature (about 673 K) than removal of the bridging oxygen from the corresponding $[Cu-O-Cu]^{2+}$ complex in CuZSM-5 which takes place near 300 K. It is therefore clear that the oxidation activity of Fe/ZSM-5 is much lower than that of Cu/ZSM-5. Remarkably, Marturano *et al.* (63) and Battiston *et al.* (64) independently reported the presence of diferric oxo/hydroxo-bridged clusters using EXAFS data although the application of such technique is debated for this heterogeneous system (9,65,66). Recent publications strongly support that only a small part of the Fe species is catalytically active (9,65,66). Nevertheless, indications were found that these sites contain a binuclear Fe structure. Furthermore, reports that the iron valence is transformed from Fe^{3+} to Fe^{2+} in He atmosphere at elevated temperature add more complexity to this system (9,57,66).

1.5 The scope of this thesis

This thesis deals with the study of active sites in iron-containing MFI zeolites, prepared either by sublimation of $FeCl_3$ on HZSM-5 or by introduction of Fe in the framework via isomorphous substitution followed by its extraction. These two types of Fe/ZSM-5 have attracted world-wide academic and industrial attention during the last decade. Typically, these materials show promising performances in environmentally related reactions, *i.e.* in the reduction of NO_x and in the decomposition of N_2O in tail gases. Moreover, it forms the basis of a potentially new route to phenol from benzene. Despite the extensive research in this

field, various aspects are not clarified yet. For instance, the nature of the active sites are much debated as well as the various described activation procedures. Iron can be conveniently introduced by the chemical vapor deposition of FeCl$_3$ in HZSM-5. Chapter 2 concerns the extensive characterization of those materials and specifically deals with subsequent high-temperature calcination or steaming treatments. The reactivity of these well-characterized catalysts is addressed in chapter 3. The activation of nitrous oxide is studied by nitrous oxide decomposition and the selective oxidation of benzene to phenol, while selective reduction of NO by iso-butane is studied for the sake of comparison. The understanding obtained for sublimed Fe/ZSM-5 is applied to address the importance of Fe and Al in iron-containing ZSM-5 in those reactions where nitrous oxide activation is required (chapter 4). Here, zeolites are prepared via hydrothermal synthesis and Fe or Al or a combination of both elements is built into the framework positions. Chapter 5 extends the study of this route and addresses the influence of the Fe and Al content on the structure and reactivity. Finally, a summary and outlook will be given.

References

1. J.J.Berzelius, Ann. Chim. Phys. (Paris) 61 (1836) 146.
2. M. Boudart, In: G. Ertl, H. Knözinger and J. Weitkamp (Eds.), Handbook of Heterogeneous Catalysis, Vol. 1, Wiley-VCH, Weinheim, Germany, 1997, p.1 .
3. Catalysis: An Integrated Approach to Homogeneous, Heterogeneous and Industrial Catalysis, J.A. Moulijn, P.W.N.M. van Leeuwen and R.A. van Santen (Eds.), Elsevier, Amsterdam, 1993.
4. Catalysis looks to the future, National Academy Press, Washington, 1992.
5. M. Mccoy , C&EN News, Sep 20th (1999) 17.
6. R.A.van Santen, In: Environmental Catalysis, F.J.J.G. Janssen and R.A. van Santen (Eds.), Imperial College Press, London, 1999.
7. H. Meinemann, In: G. Ertl, H.Knözinger and J.Weitkamp (Eds.), Handbook of Heterogeneous Catalysis, Vol. 1, Wiley-VCH, Weinheim, Germany, 1997, p. 44.
8. F. Kapteijn, J. Rodriguez-Mirasol and J.A. Moulijn, Appl.Catal. 9 (1996) 25.
9. J. Pérez-Ramírez, Catalyzed N$_2$O activation: promising (new) catalysts for abatement and utilization. Ph.D. thesis, 2002, Delft University of Technology, Delft.
10. M. Leuenberger and U. Siegenthaler, Nature, 360 (1992) 449.
11. W.C. Trogler, Coord.Chem.Rev. 187 (1999) 303.

12. H. Rodhe, Science, 248 (1990) 1217.

13. T.E. Graedel and P.J. Grutzen, Atmospheric change: an Earth System Perspective, Freeman, New York, 1993.

14. M. Schwefer, R. Maurer, M. Groves and K.U. GmbH, In: Proceedings of International Conference & Exhibition of Nitrogen 2000,, Vienna, 2000 p.61

15. Kirk-Othmer Encyclopedia of Chemical Technology, Vol.17.Wiley, New York, 1997, p.84.

16. G. Centi, S. Perathoner, and F. Vazzana, CHEMTECH, 29 (1999) 48.

17. J. Pérez-Ramírez, F. kapteijn, K. Schöffel and J.A.Moulijn, Appl. Catal. B 44 (2003) 117.

18. G.I. Panov, CatTech 4 (2000) 18.

19. A.M. Thayer, C&Eng News, April 6th (1998) 21.

20. M. Iwamoto, K. Matsukami and K. Kagawa, J. Phys. Chem. 87 (1983) 903.

21. P. Notté, Top. Catal. 13 (2000) 387.

22. N. Elango, R. Radhakrishnan, W. A. Froland, B. J. Wallar, C. A. Earhart, J. D. Lipscomb and D. H. Ohlendorf, Protein Sci. 6 (1997) 556.

23. M.J.Rataj, J.E. Kauth and M.I.Donnelly, J. Biol. Chem. 261 (1991) 18684.

24. R. Ben-Daniel and R. Neumann, Angew. Chem. Int. Ed. 42 (2003) 92.

25. P.M.M. Blauwhoff, J.W. Gosselink, E.P. Kieffer, S.T. Sie and W.H.J. Stork, In: Catalysis and Zeolites Fundamentals and Applications, J.Weitkamp and L.Puppe (Eds.) chapter.7,Springer Press, NewYork, 1999.

26. P.B. Venuto, Microporous Mat. 2 (1994) 297.

27. R.Q. Long and R.T. Yang, J. Catal. 207 (2002) 224.

28. D. Das, G. Ravichandran and D. K. Chakrabarty, Catal. Today 36 (1997) 285.

29. B.M. Weckhuysen, D. Wang, M.P. Rosynek and J. H. Lunsford, J. Catal. 175 (1998) 347.

30. G.I. Panov, V.I. Sobolev and A.S. Kharitonov, J. Mol. Catal. 61 (1990) 85.

31. V.I. Sobolev, G.I. Panov, A.S. Kharitonov, V.N. Romannikov, A.M. Volodin and K.G.Ione, J. Catal. 139 (1993) 435.

32. V.I. Sobolev, K.A. Dubkov, E.A. Paukshtis, L.V. Pirutko, M.A. Rodkin, A.S. Kharitonov and G.I .Panov, Appl. Catal. A. 141 (1996) 185.

33. G.I. Panov, V.I. Sobolev, K.A. Dubkov, V.N. Parmon, N. S. Ovanesyan, A.E.Shilov and A.A. Shteinman, React. Kinet. Catal. Lett. 61 (1997) 251.

34. K.A. Dubkov, V.I. Sobolev, E.P. Talsi, M.A. Rodkin, N.H. Watkins, A.A. Shteinman and G.I. Panov, J. Mol. Catal. 123 (1997) 155.

35. G.I. Panov, V.I. Sobolev, K.A. Dubkov and A.S. Kharitonov, Stud. Surf. Sci. Catal. 101 (1996) 493.

36. A.K. Uriarte, M.A. Rodkin, M.J. Gross, A.S. Kharitonov, G.I. Panov, Stud. Surf. Sci. Catal. 110 (1996) 857.

37. G.I. Panov, A.K. Uriarte, M.A. Rodkin, V.I. Sobolev, Catal. Today.41 (1998) 365.

38. L.V. Pirutko, V.S. Chernyavsky, A.K. Uriarte and G.I. Panov, Appl. Catal. A. 227 (2002) 143.

39. X. Feng and W.K. Hall, Catal. Lett. 41 (1996) 45.

40. X. Feng and W.K. Hall, J. Catal. 166 (1997) 368.

41. H.-Y. Chen, T. Voskoboinikov and W.M.H. Sachtler, Catal. Today 54 (1999) 483.

42. H.-Y. Chen and W.M.H. Sachtler, Catal. Lett. 50 (1998) 125.

43. H. -Y. Chen, T.V. Voskoboinikov and W.M.H. Sachtler, J. Catal. 180 (1998) 171.

44. Q. Sun, Z.-X. Gao, H.-Y. Chen and W.M.H. Sachtler, J. Catal. 201 (1998) 89.

45. T.V. Voskoboinikov, H.-Y. Chen and W.M.H. Sachtler, Appl. Catal. B. 19 (1998) 279.

46. X. Feng and W.K. Hall, Catal. Lett. 52 (1997) 13.

47. R. Joyner and M. Stockenhuber, J. Phys. Chem.B. 103 (1999) 5963.

48. L.J. Lobree, I. -C. Hwang , J.A. Reimer and A.T. Bell, J. Catal. 186 (1999) 242.

49. G. Centi and F. Vazzana, Catal. Today. 53 (1998) 683.

50. El-M. El-Malki, R.A. van Santen and W.M.H. Sachtler, J. Catal. 196 (2000) 212.

51. P. Ratnasamy, R. Kumar, Catal. Today, 9 (1991) 329.

52. W.N. Delgass, R.L. Garten and M. Boudart. J. Phy. Chem. 73 (1969) 2970.

53. J. Leglise, J.O. Petunchi and W.K. Hall, J. Catal. 86 (1984) 392.

54. J.R. Pierce, W.J. Mortier and J.B. Vytterhoeren, J. Chem. Soc. Faraday Trans. 7 (1987) 937.

55. K. Segawa. , Y. Chen, J.E. kubsh, W.N. Delgass, J.A. Dumesic and W.K. Hall. J Catal. 76 (1982)112.

56. R.L. Garten, J. Gallard-Nechtschein and M. Boudart.   Ind. Eng. Chem Fundam. 12 (1973) 299.

57. K.A. Dubkov, N.S. Ovanesyan, A.A. Shteinman, E.V. Starokon and G.I. Panov, J. Catal. 207 (2002) 341.

58. N.A.Kachurovskaya, G.M. Zhidomirov, E.J.M. Hensen and R.A. van Santen, Catal. Lett. 86.(2003) 25.

59. K.A. Dubkov, V.I. Sobolev and G.I. Panov, Kinet. Katal. 39 (1998) 79.

60. E. Suzui, K. Nakashiro and Y. Ono, Chem. Lett. (1988) 953.

61. R. Burch and C. Howitt, Appl. Catal. A. 103 (1993) 135.

62. R. J.L. Motz, H. Heinrichen and W.F. Hölderich, J. Mol. Catal.A 136 (1998) 175.

63. P. Marturano, L. Drozdová, A. Kogelbauer and R. Prins, J. Catal. 192 (2000) 236.

64. A.A. Battiston, J.H. Bitter and D.C. Kongingsberger, Catal. Lett. 66 (2000) 75.

65. H.-Y Chen, El-M. El-Malki, X. Wang, R.A. van Santen and W.M.H. Sachtler, J. Mol. Catal. 162 (2000) 159.

66. E.J.M. Hensen, Q. Zhu, M.M.R.M. Hendrix, A.R. Overweg, P.J. Kooyman, M.V. Sychev and R.A. van Santen, Physicochemical characterization of Fe/ZSM-5 prepared by chemical vapor deposition of $FeCl_3$, Accepted by J. Catal.

Chapter 2

Characterization of Fe/ZSM-5 prepared by chemical vapor deposition of FeCl$_3$

Abstract

Various techniques were employed to characterize Fe/ZSM-5 prepared by the sublimation method and its counterparts treated under severe conditions (high- temperature calcination and steaming). It is concluded that a variety of Fe species are co-present in Fe/ZSM-5, including iron oxide aggregates on the external surface and neutral and charge-compensating Fe species occluded in the micropores of the zeolites. High-temperature treatment induces the growth and ordering of the iron oxide aggregates next to a protolysis reaction between occluded neutral iron oxide nanoparticles and Brønsted acid sites. These effects are more pronounced in the case of steaming at 973 K, a treatment leading to more extensive dealumination. Relatively low Fe-Fe coordination numbers were derived from Fe K-edge EXAFS measurements. This is as an indication of disordered nature of the abundantly present iron oxide aggregates rather than as evidence for the predominant presence of binuclear clusters. More importantly from a catalytic point of view, we conclude that high-temperature treatments lead to a larger number of sites active in decomposing nitrous oxide at relatively low temperature. The number of such active sites, however, is quite small and constitutes only a small fraction of the total iron content. Moreover, the amount of active sites correlates with the amount of Fe^{2+} as probed by ^{57}Fe Mössbauer spectroscopy at 4.2 K. Tentatively, the observation that approximately one oxygen atom is deposited per two Fe^{2+} atoms agrees with the earlier proposed binuclear nature of the active sites.

2.1 Introduction

The limited dimensions of zeolite micropores allow stabilization of small transition metal oxide complexes with unique catalytic properties (1,2). The redox properties of iron containing zeolites, most notably those with the MFI topology, have attracted widespread attention for a number of potential catalytic applications. Most importantly, such zeolites catalyze the selective insertion of an oxygen atom into the C-H bonds of aromatics and alkanes (3) when nitrous oxide is the oxidant. The particular case of benzene hydroxylation to phenol forms the basis for a potential alternative to the environmentally stressing three-step cumene process (4). Moreover, these materials may be suitable for abatement of nitrous oxide emissions from nitric acid plants (5-10). Another potential application field is NO_x reduction for diesel or lean-burn Otto engines which has resulted in a number of studies using ammonia (*e.g.*,11) or hydrocarbons (12-15) as reductant.

Although there appears to be no general consensus on the nature of the active sites, especially regarding the activation of nitrous oxide with proposals stressing the importance of Brønsted acid sites (16,17), Lewis acid sites created upon hydrothermal treatment (18-20) and Fe redox sites (21-23) coming in for their share of attention, the latter type of species have been assigned the specific catalytic activity most frequently. It is suggested that the active sites have a dimeric iron structure with the property to adsorb a single oxygen atom upon nitrous oxide decomposition (22,23). Although their exact structure remains unknown, the close proximity of such sites to the zeolite framework has been stressed (24-27). In general, there are two methods to prepare Fe/ZSM-5, *i.e.* (i) controlled removal of framework Fe species of isomorphously substituted MFI type zeolite (25,28-37) (ii) post synthesis dispersion of Fe^{3+} through ion-exchange of iron-containing compounds either in solution or in the gas phase (9,10,12,13,38-47). The first method guarantees a high dispersion of iron which results in selective and stable catalysts for phenol production. The post-synthesis introduction of iron, mainly via gas phase deposition of $FeCl_3$ followed by extensive washing to remove chloride, has also been extensively employed. This sublimation method offers the possibility to obtain over-exchanged ZSM-5 catalyst, the term "over-exchanged" stressing the iron content in excess of the expected $Fe^{n+}/Al=1/n$ with n=2 or 3. Materials prepared using this method are interesting due to their high activity in the selective reduction of NO_x. Benzene oxidation has been described less frequently for these materials and appears to be less preferred due to lower phenol selectivities (48). There are conflicting views on the nature of Fe species in iron containing MFI zeolite prepared by this method. The heterogeneous

nature of such samples has been stressed (9,10,36) with particles of different nuclearity including large iron oxide particles on the external surface, neutral iron oxide nanoparticles in the micropores and iron complexes (mono-, bi, oligonuclear) at cation-exchange positions. On the other hand, several authors have pointed out that rather well-defined structures are obtained via the sublimation method (42-45,47,49) in which the catalysts were carefully calcined, resulting in the dominant presence of binuclear iron oxo complexes. This finding is based on the observation of Fe-Fe coordination numbers derived from Fe K-edge EXAFS measurements close to unity (42-45,47). As extensively outlined by Panov and co-workers (22,23), the specific catalytic property of the presumed binuclear cluster, denoted as α-sites, is the abstraction of one oxygen atom from a nitrous oxide molecule. In view of this specificity for nitrous oxide, the relevance of such binuclear clusters for nitric oxide reduction remains to be determined.

In this chapter, it is aimed to obtain insight into the changes in the active phase and zeolite matrix upon severe treatments of the Fe/ZSM-5 prepared by the sublimation method. Detailed characterization of the catalysts was carried out by various characterization techniques, *i.e.* ^{57}Fe Mössbauer adsorption spectroscopy, ESR, TEM, Fe K-edge EXAFS, IR, and ^{27}Al NMR *et al*. The aim is to identify the Fe species in the Fe/ZSM-5. Most importantly, the focus is on determining the active sites in sublimed Fe/ZSM-5 and the influence of various treatments. Since Panov (3,22,23) uses high temperature or steaming pretreatment to form so-called α-sites whereas this step is not necessarily applied in the over-exchanged Fe/ZSM-5, similar treatments (high-temperature calcination or steaming) were employed on the sublimed Fe/ZSM-5 samples.

2.2 Experimental section

2.2.1 Catalyst preparation

Parent NH$_4$ZSM-5 zeolites with different Si/Al ratios (20, 30 and 45) were kindly provided by Akzo-Nobel. Anhydrous FeCl$_3$ (reagent grade 99.9 %) was obtained from Aldrich. HZSM-5 was prepared by calcining NH$_4$ZSM-5 at 823K in a flow of O$_2$ (100 ml·min^{-1}). Fe/ZSM-5 was prepared by the sublimation method developed by Sachtler *et al* (15). The setup is shown schematically in figure 1.
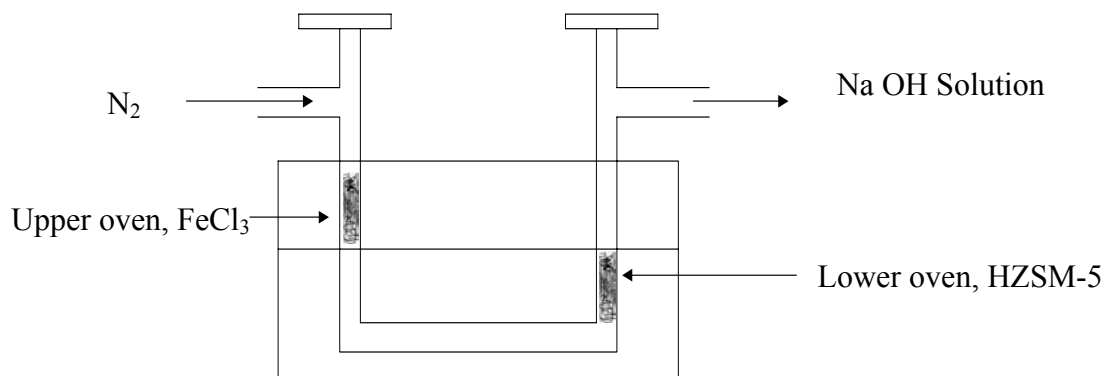
Figure 1: Schematic layout of the setup for sublimation method.

Sublimation was carried out in a two-zone oven. $FeCl_3$ was contained in the upper part at a temperature of 573 K (boiling point 588 K), while the dehydrated zeolite was present in the lower one at 593 K. A nitrogen flow induced the vapor of gaseous iron chloride to the zeolite. A scheme is shown in figure 1. Subsequently, the sample was washed in 2500 ml deionized water twice by stirring for 1 h each time. After drying in an oven at 383 K overnight, 1 g Fe/ZSM-5 was calcined at 823 K in a flow of 20 vol. % O_2/He (200 ml·min^{-1}) for 2 h.

Table 1: Elemental analysis for the various catalysts

	Si/Al	Al content (wt. %)	Fe content (wt.%)	Fe/Al
Fe/ZSM-5(20)	19.4	1.79	3.60	0.97
Fe/ZSM-5(30)	27.5	1.34	3.62	1.30
Fe/ZSM-5(45)	45	0.88	2.63	1.44

Table 1 shows the elemental composition of the various Fe/ZSM-5 samples (the number in parenthesis indicates Si/Al ratio of the samples). Despite the lower Al content of Fe/ZSM-5(30), the Fe content is similar to Fe/ZSM-5(20). This implies almost four times over-exchange compared to an ordinary ion-exchange method. Moreover, for Fe/ZSM-5(45) , the ratio of Fe to Al is even higher than those Fe/ZSM-5 with lower Si to Al ratio (20 or 30).

The proposal of the reaction (Z represents Al or Fe in the framework)

$$Z\text{-OH} + FeCl_3 \longrightarrow [Z\text{-O}]^-[FeCl_2]^+ + HCl\uparrow \quad (1)$$
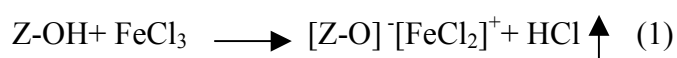
explains a three-fold higher exchange compared to ion exchange. However, in the gas phase, $FeCl_3$ exists in the binuclear form of Fe_2Cl_6 that has a puckered four-membered Fe_2Cl_2 ring

(50). In relatively Al-rich ZSM-5 zeolites where the distance between the aluminum occupying oxygen tetrahedra is small, the reaction may proceed as

$$2\ Z\text{-OH} + Fe_2Cl_6 \longrightarrow 2[Z\text{-O}]^-[Fe_2Cl_4]^{2+} + 2HCl\uparrow \quad (2)$$
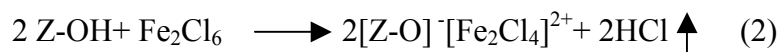
For high Si/Al ratio, the concentration of vicinal protons is low and part of the reaction can be described as

$$ZOH + Fe_2Cl_6 \longrightarrow [Z\text{-O}]^-[Fe_2Cl_5]^+ + HCl\uparrow \quad (3)$$

This reaction provides a way of introducing two Fe^{3+} for one proton into the zeolite. Consequently, Fe/ZSM-5 of different Si to Al ratio may have similar Fe content. As pointed out by Dědeček *et al.* (51), the Al distribution in silicon-rich zeolite is not random, but depends on the chemical composition and the condition of synthesis. This may lead to three or even less chlorine atoms in the adsorbed iron complex.

Since Fe/ZSM-5(20) has an ideal Fe to Al ratio of nearly 1, further research is mainly focused on Fe/ZSM-5 with an Si to Al ratio of nearly 20. This sample is denoted as Fe/ZSM-5. Further treatment of the original calcined catalyst was carried out at relatively high temperature: (a) 0.2g original Fe/ZSM-5 was calcined in a flow of 20 vol.% O_2/He (200 ml·min^{-1}) at 973 K for 3 h, the catalyst is referred to as high temperature calcined Fe/ZSM-5, denoted as Fe/ZSM-5(HTC). (b) 0.2g original catalyst was steamed in a flow of 20 vol.% O_2/He (200 ml.min^{-1}) with 10% water vapor at 973 K for 3 h, the catalyst is designated as high temperature steamed Fe/ZSM-5, denoted as Fe/ZSM-5(HTS). No change in elemental composition is found after further treatment (973 K calcination or steaming) of Fe/ZSM-5.

HZSM-5(HTC) or HZSM-5(HTS) starting from the parent zeolites, were also prepared via similar pretreatments as Fe/ZSM-5 for comparison in the N_2O decomposition and selective benzene to phenol reaction. It is worth pointing out that the parent commercial zeolite has an Fe impurity of 0.024 wt. % that is very common in industrially prepared HZSM-5. Fe/SiO$_2$ with 3.0 wt. % Fe was prepared by pore volume impregnation of high surface area silica (Grace) with iron nitrate as the precursor.

2.2.2 Catalyst Characterization

The elemental composition was determined by OES-ICP after dissolving the sample in a mixture of HF and HNO$_3$.

Power x-ray diffractograms were measured using a Rigaku diffractometer. Typically, an XRD spectrum was recorded in the range $5^o < 2\theta < 50^o$ using Cu Kα radiation with a scanning speed of 0.01^o min^{-1}.

Nitrogen adsorption at 77 K was carried out in a Micromeritics ASAP 2000 apparatus. Prior to nitrogen adsorption, samples were evacuated at 623 K for 16 h.

UV-Vis spectra was recorded on Shimadzu UV-2401 PC spectrometer. $BaSO_4$ was used as reference sample

For the H_2-TPR measurements, 100 mg sample was placed in a fixed-bed reactor and exposed to the H_2/N_2. The measurements were performed with 4 vol. % H_2/N_2 (8 ml·min^{-1}), heating from RT to 1073 K (ramp 5K·min^{-1}) then holding at 1073 K for 2 h. The H_2 signal is determined by a thermistor. Prior to measurements, the samples were flushed in N_2 for 0.5 h at room temperature.

Infrared spectra of self-supporting 10 mg catalyst wafers were recorded at room temperature on a Brukers. IFS113 Fourier Transform IR spectrometer with DTGS detector at a resolution of 4cm^{-1}. Prior to IR measurement, the catalyst was pretreated *in-situ* at 773 K for 1 h *in vacuo* (pressure $< 10^{-6}$ mbar). Normalization of the overtones of framework vibration (1870 cm^{-1} - 1950 cm^{-1}) was applied to achieve quantification of the amount of Brønsted acid sites.

Solid-state ^{27}Al magic-angle spinning NMR spectra were obtained on a Bruker Ultrashield 500 spectrometer at a magnetic field of 11.7 T equipped with a 4 mm MAS probe head. The Al resonance frequency at this field was 130 MHz. The sample rotation speed was 12.5 kHz. The ^{27}Al chemical shifts were referenced to a saturated $Al(NO_3)_3$ solution.

ESR experiments were carried out on a Bruker ESP 300E spectrometer, operating with an X-band standard cavity (9.44 GHz), an ER 035 M NMR Gauss meter, and a HP 5350B frequency counter. A 100 kHz modulation of 5 Gauss and 2 mW microwave power were used to record the spectra. The field axis was corrected for the variations in frequency in different spectra. The spectra were recorded at 10 K with the use of an Oxford continuous flow cryostat and variable temperature unit.

For transmission electron microscopy, a catalyst sample was mounted on a microgrid carbon polymer supported on a copper grid by placing a few droplets of a suspension of ground sample in ethanol on the grid, followed by drying at ambient conditions. High resolution transmission electron microscopy was performed using Philips CM30ST electron microscopes with a field emission gun as the source of electrons at 300 kV. EDX elemental analysis was performed using a LINK EDX system

A number of Positron Emission Profiling experiment were carried out on Fe/ZSM-5(HTS) using $N_2^{15}O$. A thorough description of the principles and procedures to perform the PEP (Positron Emission Profiling) experiments is given in a number of references (52,53). The catalyst was pretreated at 20 vol. % O_2/He before measurement at 673K overnight at a ramp rate of 2 K·min^{-1}. Subsequently, the feed is changed to helium only to remove the residual O_2. The PEP experiments were performed by pulse injection of a mixture of $N_2^{15}O$/N_2O onto the catalyst (pulse mode) at 723 K.

Fe-K-edge XAFS measurements were performed at beamline 17C of the national Synchrotron Radiation Research Center in Hsinchu (Taiwan). The electron energy and ring current were 1.5 GeV and 160 mA, respectively. The spectra were recorded with sampling steps of 0.5 eV in the XANES region and of 1 to 2 eV in the EXAFS region. An amount of catalyst was pressed into a self-supporting wafer, calculated to have an absorbence μx of 2.5, and placed in a controlled atmosphere transmission cell. Prior to measurement, the sample was heated at a rate of 2 K·min^{-1} to 673 K in a flow of 20 vol. % O_2 in He to remove physisorbed water. Fe K-edge spectra were recorded in transmission mode at ambient temperature in He atmosphere. EXAFS data were extracted from the measured adsorption spectra with the XDAP code (54). The pre-edge was subtracted using a modified Victoreen curve, while the background was subtracted by using cubic spline routines. Finally, normalization took place by dividing the subtracted absorption spectra by the intensity of the spectrum at 50 eV above the Fe K-edge. Structural information was determined by multiple-shell fitting in *R*-space (55). The fits were checked by k^1 and k^3 weighting. Errors in the obtained numerical values are estimated ±10% for the coordination numbers (CN), ±1% for the coordination distances(R), ±5% for the Debye-Waller factor ($\Delta\sigma^2$) and ±10% in the inner-potential correction (ΔE_0). Two reference were used, ferric acetylactonate for Fe-O and α-Fe_2O_3 for Fe-Fe generated by FEFF7 according to parameters provided by Battiston *et al.*(47).

^{57}Fe Mössbauer spectra were measured on a constant acceleration spectrometer in a triangular mode using a ^{57}Co: Rh Source. All Mössbauer spectra have been recorded at 300 K, both in air and under high vacuum conditions (pressure lower than 10^{-6} mbar), at 77 K (pressure lower than 10^{-6} mbar) and at 4.2 K under high vacuum. The overall spectra were deconvoluted with calculated Mössbauer spectra that consisted of Lorentzian-shaped lines. In the case of quadrupole doublets the line widths and the adsorption areas of the constituent lines were constrained to be equal. Positional parameters were not constrained in the fitting procedure. The isomer shift values are reported relative to sodium nitroprusside.

Temperature-programmed decomposition of adsorbed isopropylamine (IPA_m) was used to determine the amount of acidic sites. In a typical experiment, 100 mg of catalyst was dried in He flow of 100 ml·min^{-1} while heating at a rate of 2 K·min^{-1} to 723 K. The sample was kept at this temperature for 1 h and subsequently cooled to 323 K. A He flow saturated with IPA_m at 273 K was led over the catalyst bed until no further adsorption was observed by on-line mass spectrometry; subsequently, the larger part of physisorbed IPA_m was removed by purging in a He flow for 16 h at 323 K. Temperature-programmed decomposition of IPA_m was started by heating the sample at a rate of 5 K·min^{-1} to 773 K. The number of acidic sites was calculated from the number of propene molecules deriving from IPA_m decomposition. Special attention was paid to correct for desorption of the residual IPA_m which also yields propene molecules during mass spectrometric analysis. Kofke *et al.* (56) have demonstrated that exactly one IPA_m molecule is chemisorbed per acidic site.

The low-temperature (523 K) decomposition of nitrous oxide was carried out in a static vacuum setup equipped with an online mass spectrometer for determining the gas-phase composition. A catalyst sample of approximately 0.6 g was placed into a quartz reactor tube and subjected to the following treatment: heating to 823 K in 30 min *in vacuo* followed by an isothermal period of 30 min, a treatment for 1 h in 1.3 mbar of oxygen and cooling to 523 K in oxygen. After evacuation of the setup, the catalyst was exposed to a known amount of nitrous oxide (typically 2×10^{19} molecules N_2O). In a typical experiment, dinitrogen formation was observed without the production of dioxygen. This allows calculation of the number of stoichiometrically deposited oxygen atoms. For higher accuracy, also isotopic exchange of the adsorbed ^{16}O with $^{18}O_2$ was carried out. To this end, the sample saturated with oxygen atoms was cooled to 323 K. After evacuation, $^{18}O_2$ (purity > 95%) was admitted to the catalyst. The exchange of the two types of oxygen was followed and the number of initially deposited oxygen was calculated from the equilibrium composition (22,57,58). Subsequently, a third method was applied which consisted of heating the sample up to 723 K while recording the amount of released oxygen. A comparison was made of the results of these three methods.

2.3 Results

XRD
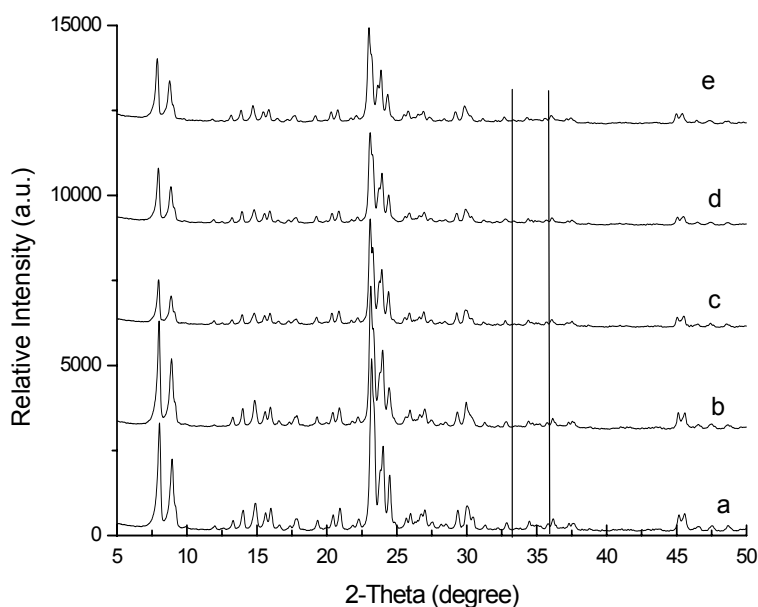
Figure 2: XRD of the samples: (a) HZSM-5, (b) HZSM-5 (HTS), (c) Fe/ZSM-5 (d) Fe/ZSM-5 (HTC), (e) Fe/ZSM-5 (HTS).

The x-ray diffactograms of various samples are collected in figure2. All samples display the typical diffraction pattern of the MFI framework. No indications for the formation of α-Fe_2O_3 (major reflections at $2\theta = 33.2\,^\circ$ and 35.7°) or any other iron oxide were observed.

Nitrogen adsorption

Table 2: The surface area (S_{Lang}) and micropore volume (V_{Lang}) derived from the Langmuir equation, the surface area (S_{D-R}) and micropore volume (V_{D-R}) calculated using the Dubinin-Radushkevich method and the Dubinin-Astakhov limiting micropore volume (V_{D-Ast}).

Sample	S_{Lang} $(m^2.g^{-1})$	V_{Lang} $(cm^3.g^{-1})$	S_{D-R} $(m^2.g^{-1})$	V_{D-R} $(cm^3.g^{-1})$	V_{D-Ast} $(cm^3.g^{-1})$
HZSM-5	440	0.156	417	0.148	0.168
Fe/ZSM-5	334	0.119	340	0.121	0.121
Fe/ZSM-5(HTC)	341	0.121	337	0.120	0.128
Fe/ZSM-5(HTS)	371	0.132	359	0.128	0.138

The textual properties of the catalyst samples (HZSM-5 and the sublimed samples) were investigated by nitrogen adsorption. The isotherms all exhibit type I adsorption isotherms as expected for microporous solids. The BET method, based on multilayer N_2 adsorption, is inadequate to describe the adsorption process in medium-pore zeolites due to the restricted pore sizes (59). This is exemplified by the fact that we derived negative C values for all isotherms. For a qualitative analysis of the isotherms, the Langmuir equation, the Dubinin-Radushkevich(D-R) and Dubinin-Astakhov(D-Ast) methods were employed (59). The results collected in table 2 for HZSM-5 and Fe/ZSM-5 clearly points to the incorporation of species into the micropore space of HZSM-5. This is reflected by the lower surface area and micropore volume. The large decrease is most probably related to some degree of pore blocking. The increase in micropore volume (V_{D-Ast}) for FeZSM-5(HTC) may point to changes in the nature of extra-framework species rather than changes in the pore structure. The latter type of changes is not expected since dealumination of HZSM-5 upon high-temperature calcination appears to be small. Steaming, however, results in a significant increase in the surface area and pore volume as derived by the different analysis methods. This points to the creation of larger pores occurring concomitantly with removal of aluminium from framework positions. Alternatively, this can be taken as an indication of the migration of small iron species from the micropores to the external surfaces.

UV-Vis

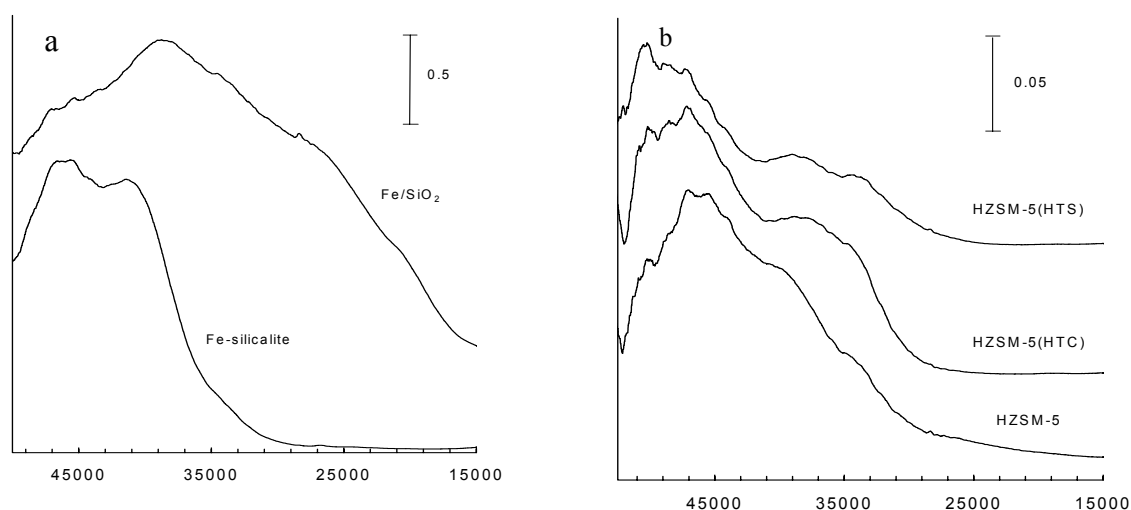**Figure 3**: (a) UV-Vis spectra of Fe/SiO$_2$ and Fe-Silicalite, (b) UV-Vis spectra of various HZSM-5.

The UV-Vis spectra of two reference materials, Fe-silicalite and Fe/SiO$_2$, and of the HZSM-5 materials are presented in Fig.3a and 3b, respectively. Fe-silicalite exhibits two major bands around 46000 cm^{-1} and 41000 cm^{-1}, corresponding to the $t_1 \rightarrow t_2$ and $t_1 \rightarrow e$

transitions of FeO_4 tetrahedral.(32,60) This strongly indicates that the majority of iron species are occupying framework positions in this sample. We note here that the template was not removed in Fe-silicalite because this would lead to partial removal of Fe from framework positions. The silica-supported iron oxide sample (Fe/SiO_2) exhibits various bands. The most dominant band at 38574 cm^{-1} is due to small clusters of iron oxide (60). The poorly resolved peak at 27626 cm^{-1} may be related to iron in γ - FeOOH species (32). The shoulder around 20000 cm^{-1} is due to an asymmetric peak of large iron oxide aggregates. The UV-Vis spectrum of HZSM-5 (figure 3b) indicates that this material contains a small amount of iron in accordance with the elemental analysis. Clearly, the majority of the few Fe species are tetrahedrally coordinated iron species as evidenced by the charge transfer band around 46800 cm^{-1}. However the band around 39000 cm^{-1} points to the formation of small clustered Fe^{3+} species, most probably deriving from dislodgement of iron from the framework during template removal. This is underpinned by a visual comparison with the spectrum for Fe-silicalite. After high temperature calcination and steaming, the intensity of the charge-transfer band corresponding to tetrahedrally coordinated iron, close to 46800 cm^{-1}, decreases strongly after steaming indicating the migration of additional framework Fe atoms to extra-framework positions. Concomitantly, an increase of the band at 39000 cm^{-1} is observed deriving from an increased contribution of small extra-framework iron oxide clusters. The absence of bands around 20000 cm^{-1} indicates that no bulky iron oxide particles are formed.

The UV-Vis spectra of the sublimed samples are presented presented in figure 4. Fe/ZSM-5 contains a poorly resolved band (around 45000cm^{-1}) assigned to tetrahedrally coordinated Fe species. An unambiguous interpretation of the band at 39000 cm^{-1} is difficult. It is close to the band found for Fe/SiO_2 at 38574 cm^{-1} that corresponds to small clustered Fe species. The spectrum resembles the one reported by Centi *et al.* (60) for a similarly prepared sample, although in their case the band at 45000 cm^{-1} is more pronounced. Our spectrum is much more diffuse than the well-defined UV-Vis spectrum obtained by Marturano *et al.* (44). A poorly resolved peak at 28207 cm^{-1} is related to iron in mixed tetra- and octahedral coordination. The absence of a band around 20000 cm^{-1} indicates that no bulk iron oxide agglomerates are formed after mild calcination. For Fe/ZSM-5(HTC), the poorly resolved band around 20000 cm^{-1} points to the formation of larger iron oxide species. Steaming of Fe/ZSM-5 causes further distribution of the band intensities and widths. The contribution of the band corresponding to clustered Fe species becomes larger. Steaming also causes an increased contribution of large iron oxide aggregates.
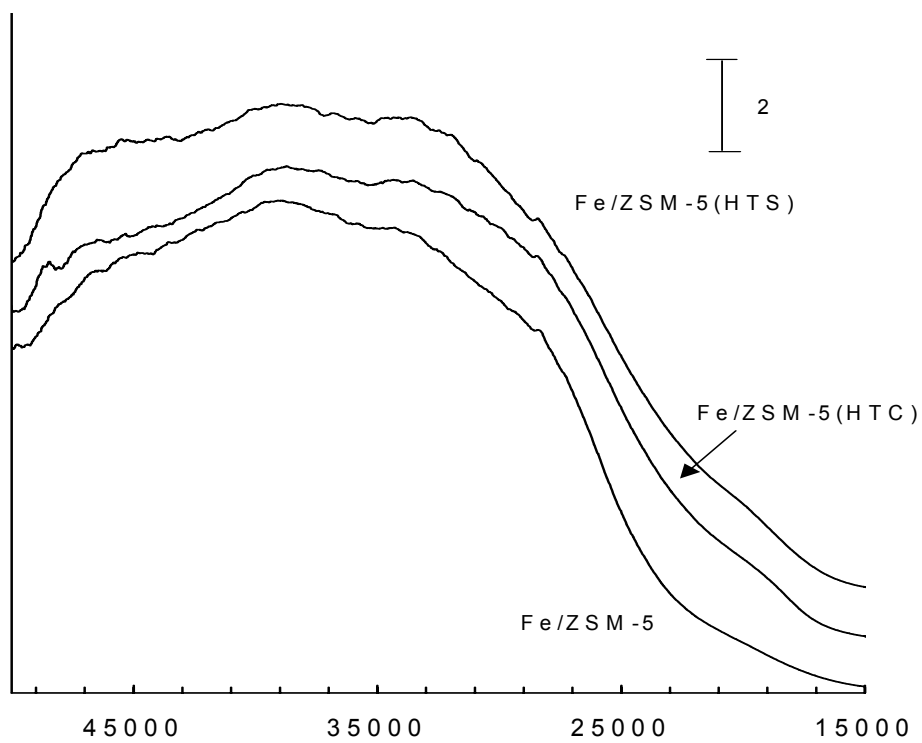
Figure 4: UV-Vis spectra of various Fe/ZSM-5 samples.

H₂-TPR
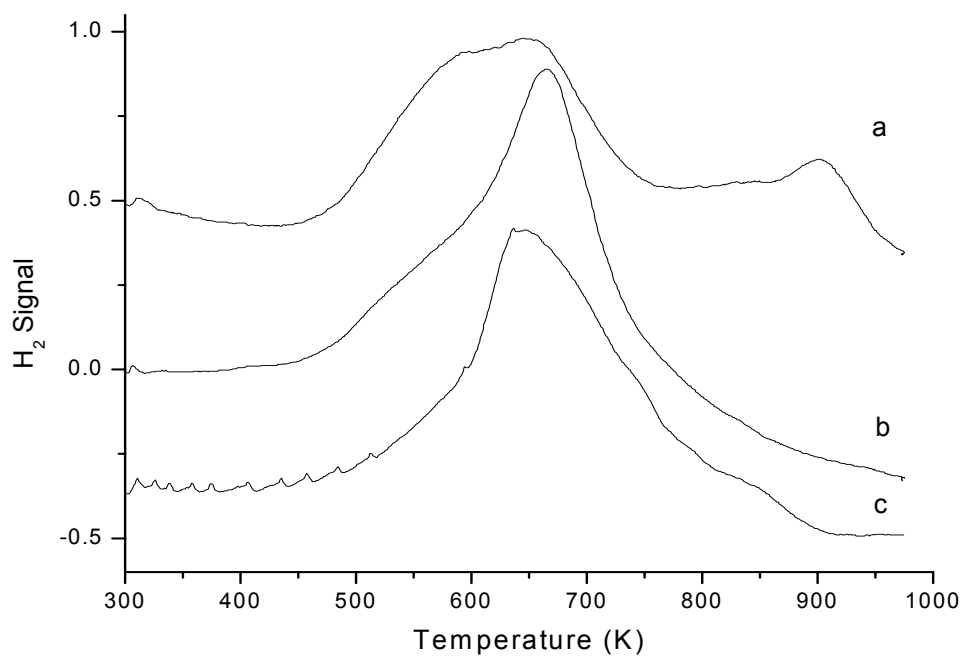
Figure 5: H$_2$-TPR of various Fe/ZSM-5 (a) Fe/ZSM-5, (b) Fe/ZSM-5(HTC), (c) Fe/ZSM-5(HTS).

The temperature-programmed reduction profiles of various Fe/ZSM-5 samples in H_2 are presented in figure 5. Literature reports the reduction of bulk Fe_2O_3 in two main steps at 693 K and 963 K with a small shoulder at 863 K. The band at 693 K is assigned to the reduction from Fe_2O_3 to Fe_3O_4 and the band of 963 K is due to the reduction of Fe_3O_4 to Fe. Since the reduction of Fe_3O_4 proceeds via FeO, the small shoulder at 863 K is assigned to the reduction of Fe_3O_4 to FeO (61). For Fe/ZSM-5, three bands at 573 K, 683 K and 923 K are distinguished on the spectra. However, after severe treatments, it seems there are changes of the Fe species in the zeolites, evidenced by the disappearance of the band at 923K.

IR
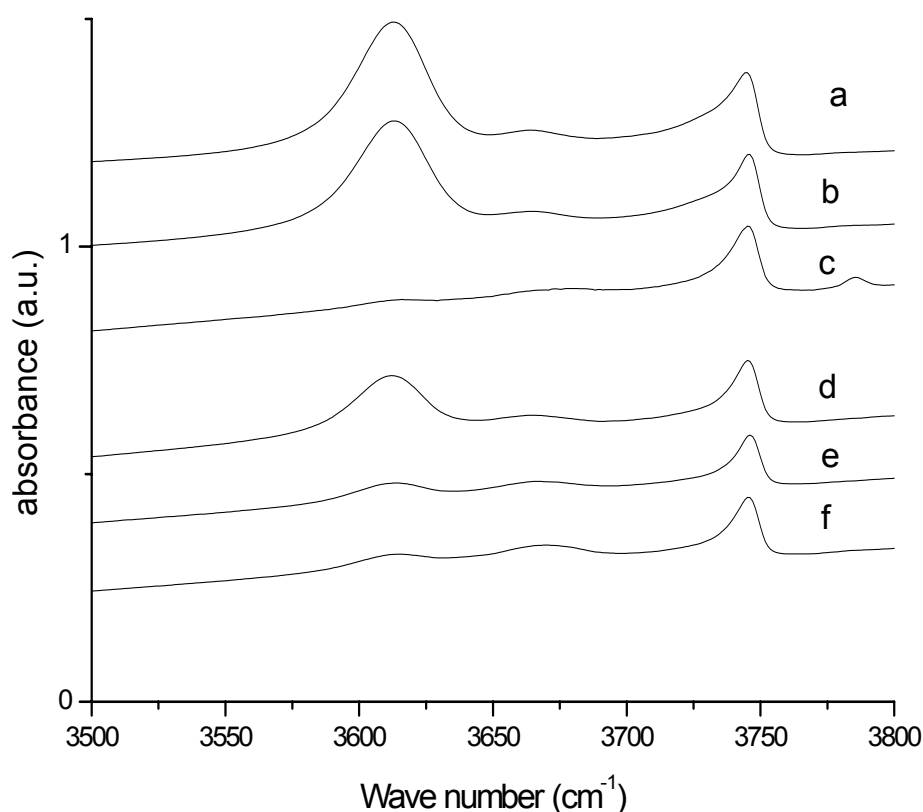
Figure 6: IR of various Fe/ZSM-5 (a) HZSM-5 (b) HZSM-5(HTC) (c) HZSM-5(HTS)
(d) Fe/ZSM-5 (e) Fe/ZSM-5(HTC) (e) Fe/ZSM-5(HTS)

Figure 6 displays infrared spectra of the hydroxyl region of the various Fe-containing and parent zeolites. For HZSM-5, the bands of bridging hydroxyl groups (3613 cm^{-1}), silanol groups (3745 cm^{-1}) and a weak band (3665 cm^{-1}) assigned to the hydroxyl groups connected

to the extra-framework aluminium species can be clearly distinguished. While the deposition of FeCl$_3$ results in the disappearance of all bridging hydroxyl groups in the parent zeolite (39), further treatment (hydrolysis, drying and calcination at 723 K) results in restoration of about 50% of the original Brønsted acid sites. After calcination at 973 K, the band at 3613 cm^{-1} has further decreased in intensity and we calculate that approximately 15% of the original Brønsted acid sites persists in Fe/ZSM-5(HTC). We note here that the disappearance of these protons is reversible to some extent by exposure to water vapor at 773 K as described in chapter 3. A similar but more pronounced decrease is observed after steaming of Fe/ZSM-5, with approximately 10% of the acid sites remaining. In this case, a small but noticeable increase in the band at 3665 cm^{-1} points to partial dealumination of the zeolite structure. A comparison of the hydroxyl band region of HZSM-5, HZSM-5(HTC) and HZSM-5(HTS) shows that dehydroxylation is relatively small upon high temperature cacination, but extensive in the case of high-temperature steaming (around 90 %)

^{27}Al NMR

Figure 7: ^{27}Al NMR of HZSM-5 and various Fe/ZSM-5 prepared by sublimation method

^{27}Al MAS NMR spectra were recorded for the three sublimed samples. The spectra are reported in Figure 7 together with the spectrum of HZSM-5. This latter spectrum contains a dominant resonance at 54 ppm assigned to tetrahedrally coordinated Al in framework positions. Additionally, a small amount of extra-framework Al with octahedral coordination resulting in a resonance at 0 ppm i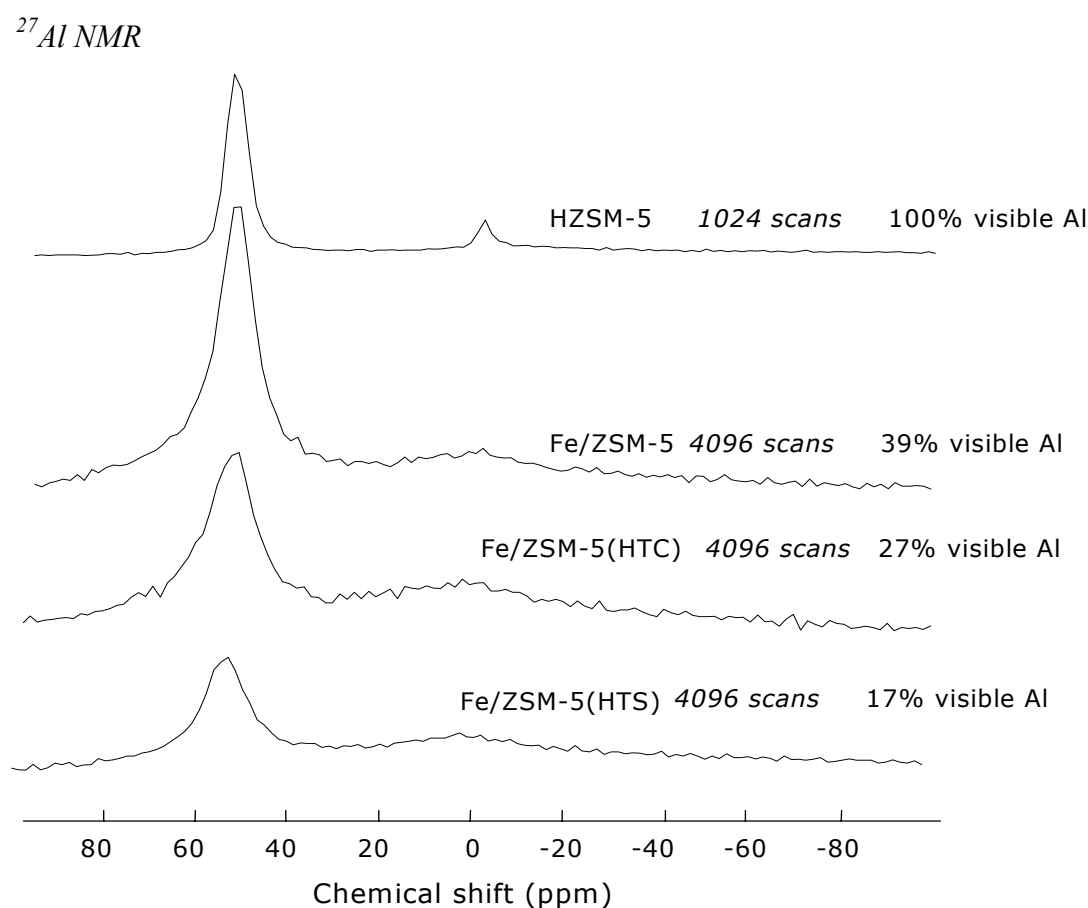s present. The resonance at 54 ppm is strongly reduced in Fe/ZSM-5. This is due to the paramagnetism of the iron. The local magnetic field generated by its unpaired electrons strongly perturbs the resonance of the ^{27}Al nuclei. Also, the sharp resonance at 0 ppm is transformed into a broad signal around this value. Although it is difficult to ascertain, some dealumination might have taken place in line with the report by Maturano *et al.* (43). Quantification of the areas of the resonance at 54 ppm for HZSM-5 and Fe/ZSM-5 shows that only about 39% of the original tetrahedral Al signal is observed in the sublimed sample. This observation points to a close proximity of Fe species to Al sites and provides a tentative explanation for the decrease of the intensity of the IR band corresponding to bridging hydroxyl groups. The decrease of the resonance signal at 54 ppm is even more pronounced in Fe/ZSM-5(HTC) and Fe/ZSM-5(HTS), leaving about 27% and 17% of the aluminum detected, respectively. This again parallels the IR observations and is in agreement with our conclusion of a protolysis reaction between iron oxide particles and Brønsted acid sites upon high temperature calcination that is reversible. Steaming results in a stronger decrease of the resonant signal at 54 ppm and extensive removal of Al from framework positions is assumed to take place. Most importantly, we conclude that high temperature treatments lead to a closer proximity of Fe and Al in sublimed catalysts. Moreover, after steaming, a new broad peak is detected at 37 ppm. 2D MQ MAS ^{27}Al NMR (chapter 4) confirms the presence of such Al species. Typically, this peak is attributed to non-framework tetrahedrally or pentahedrally coordinated aluminum Such Al may exist in the MFI micropores as Al_2O_3 without associated hydroxyl group. Apparently, such extra framework aluminum is produced by steaming. On the contrary, the absence of a peak around 37 ppm for the high-temperature calcined Fe/ZSM-5(HTC) also indicates that the disappearance of Brønsted acidity must originate from the reaction of the protons with Fe species at 973 K.

TEM
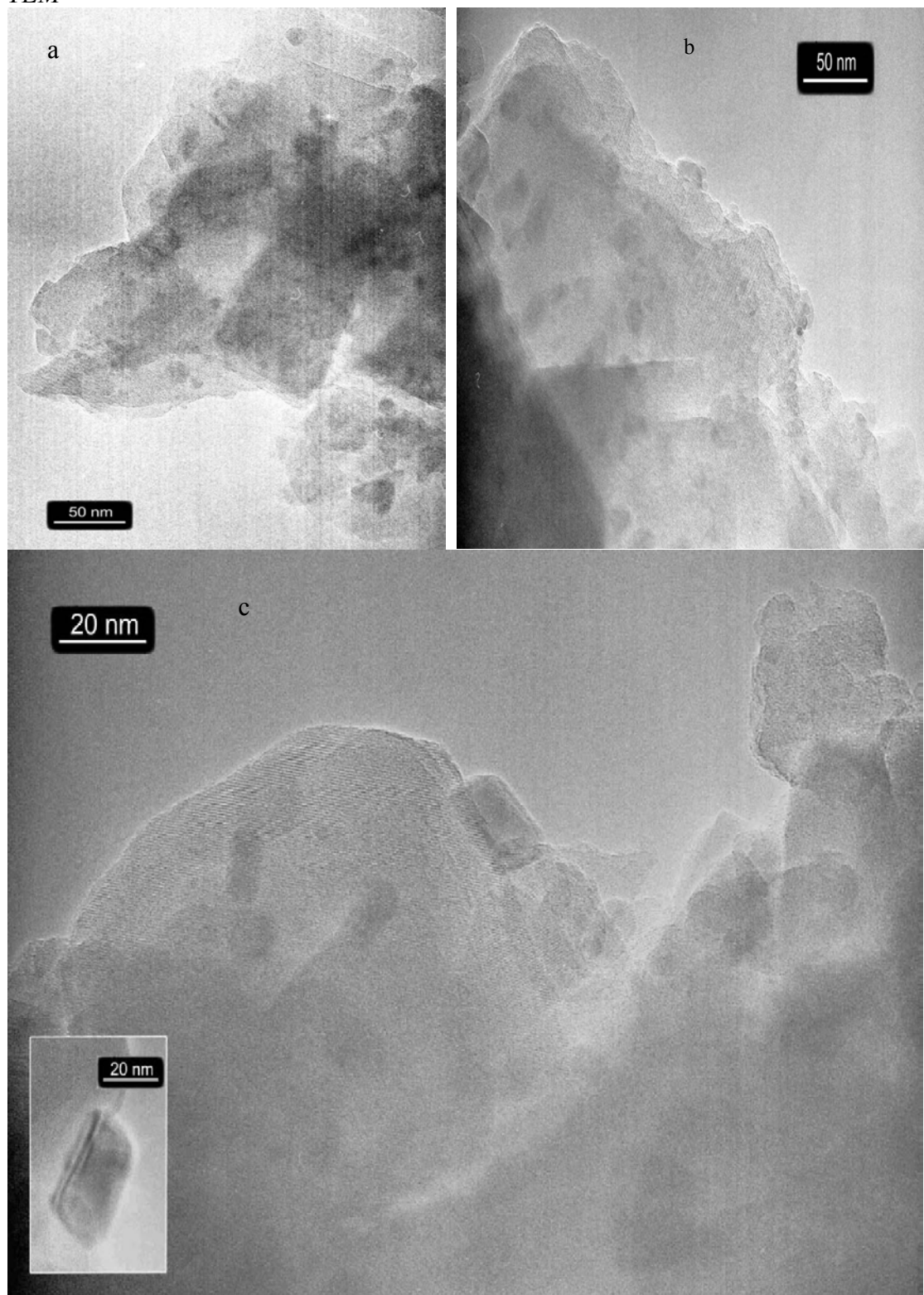
Figure 8: TEM images of various Fe/ZSM-5, (a) Fe/ZSM-5 (upper left), (b) Fe/ZSM-5(HTC) (upper right), (c) Fe/ZSM-5$_S$ (below).

Figure 8 shows representative TEM micrographs of Fe/ZSM-5 and its high- temperature calcined and steamed counterparts. All three samples clearly show the presence of iron oxide

particles on the external zeolite surface as confirmed by EDX analysis. The presence of iron oxide particles on the external zeolite surface was noted by Chen and Sachtler (39), although the particles appear to be smaller in the present study. The exact distribution of Fe species is strongly dependent on the calcination procedure (39,46,47). While these iron oxide particles are quite homogeneously distributed over the surface with dimensions of 1-4 nm in the case of Fe/ZSM-5 with some larger particles up to 10 nm present, they tend to sinter to some degree upon high temperature treatments. The particles in the 2-10 nm size range remain dominantly, but particles in the range 10-20 nm can also be found. Especially, steaming results in the formation of larger agglomerates. Most probably, the effect of water induces a higher mobility of iron oxide species, which may provide a partial explanation for the relative strong increase in micropore volume upon steaming (table 2).

ESR
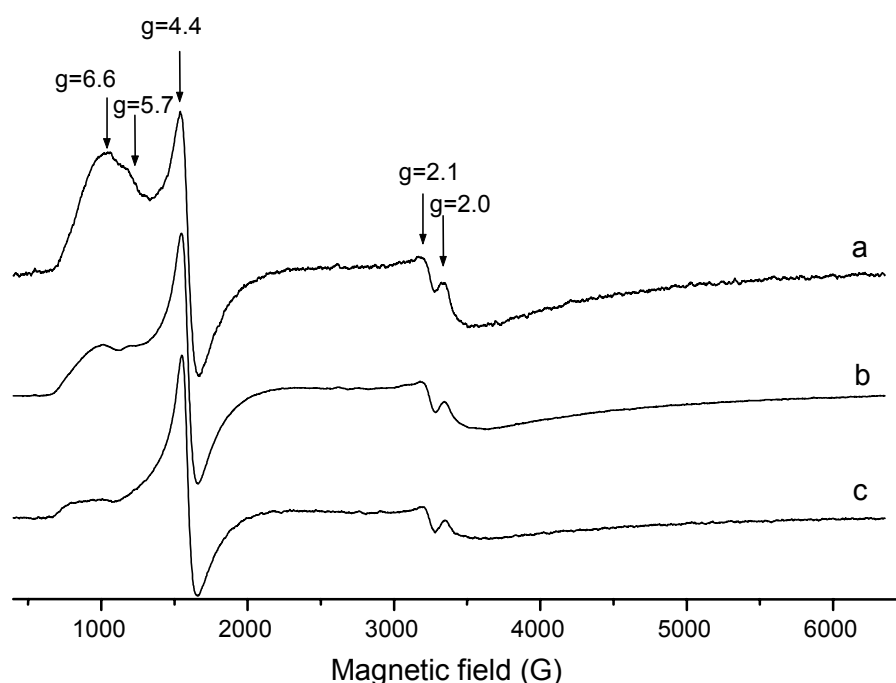
Figure 9: ESR spectra of various Fe/ZSM-5, (a) Fe/ZSM-5, (b) Fe/ZSM-5(HTC), (c)Fe/ZSM-5(HTS) at 10K.

Since the ferric iron, with unpaired electrons in the 3d shell, is paramagnetic in both the low-spin and high-spin electronic configurations, ESR spectroscopy is a powerful and sensitive method to characterize the Fe species although the assignment and identification of Fe species by this technique is by no means conclusive (33,62,63).

The ESR spectra of all Fe/ZSM-5 samples, recorded at 10 K are reported in figure 9. The spectra at this temperature show a better resolution of the overlapping lines than the spectra at room temperature (not shown). The original Fe/ZSM-5 shows significant signals at g values of 4.4, 5.7 and 6.6 with a broad line in the low field. At high field, a broad line centered at g = 2.1 is obvious with a shoulder at g = 2.0. These signals have been reported in the literature, but their assignments to various Fe-species is not unequivocal. In general, the signal at g = 4.4 is assigned to isolated tetrahedrally coordinated Fe with a strong rhombic distortion, while the g = 5.7 and g = 6.6 signals are assigned to strongly axially distorted tetrahedrally coordinated Fe-species (63). It is worth pointing out that the narrow line of g = 4.4 can not be used to exclusively confirm the presence of Fe^{3+} in the zeolite framework positions (62). We propose that part of the signal g = 4.4 is due to the mononuclear $(Fe=O)^{+}$ that is strongly distorted by the negative charge of vicinal framework Al. Generally, the signals at g = 5.7 and g = 6.6 are assigned to isolated Fe^{3+} cations in distorted tetrahedral coordination. The weak signal at 2.0 is attributed to octahedral Fe^{3+} in the zeolite. The various spectra indicate a signal at g = 2.1 that we assign to an agglomerate of iron oxide on the external zeolite surface. Further treatments of the original Fe/ZSM-5 cause some changes in the ESR spectra. Most significantly, the signals at g = 5.7/6.6 drastically decrease for both the calcination and the steaming treatment. It is worth pointing out that in the ESR spectra of Fe/ZSM-5(30) (not shown), we also observe a similar decrease of the signals at g = 5.7/6.6 and an increase of the signal g = 4.4, when applying the same amount of the various samples.

^{57}Fe Mössbauer spectroscopy

Figure 10 displays ^{57}Fe Mössbauer absorption spectra (MAS) of three Fe/ZSM-5 catalysts recorded at 300 K, in air (only shown for the steamed sample) and under higher vacuum conditions. The complex nature of the spectra points to the presence of several species. At 300 K one doublet with an isomer shift (IS) of 0.61 mm.s^{-1} and a quadrupole splitting (QS) of 1.02 mm.s^{-1} is detected for Fe/ZSM-5. This well-resolved doublet means that the Fe phase is relatively dense (no paramagnetic hyperfine splitting is observed), but it also indicates that the iron oxide particles are smaller than about 6 nm. This component is also present in the high-temperature calcined sample. Additionally, one observes the onset of a six-line pattern indicative for the presence of a high spin Fe^{3+} contribution. This is the result of the superparamagnetic behaviour of relatively large iron oxide particles. A small shoulder can be observed on the high-energy line of the Fe^{3+}doublet. The fit parameters (IS = 1.33mm.s^{-1} and

QS = 3.19 mm.s^{-1}) point to the presence of Fe^{2+}. This Fe^{2+} component is also present in the steamed sample, Fe/ZSM-5(HTS), under high-vacuum conditions. For Fe/ZSM-5(HTS), the Mössbauer spectrum was also recorded in air. In this case, the Fe^{2+} component was not observed. The broad singlet at 0.60 mm.s^{-1}, observed on Fe/ZSM-5(HTS) at 300K can most probably be related to superparamaganetic iron oxide particles close to the superparamanetic transition temperature. This is underpinned by the development of a sextuplet at 77 K for this sample (*vide infra*).
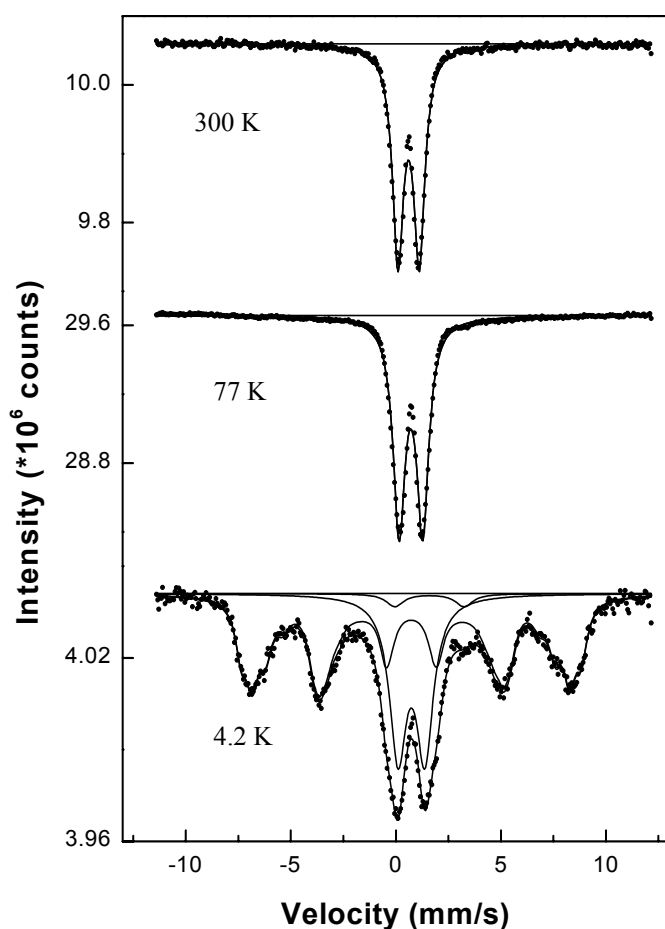
Figure 10: (a) Mössbauer spectroscopy of Fe/ZSM-5.

Additional measurements of Mössbauer spectra at 77 K and 4.2 K allow further insight into the particle size distribution of small iron oxide particles and the relative abundance of various Fe species. This latter point should be addressed with care, since the recoil-free fraction for clustered iron oxide may be significantly different from that of mono- or oligonuclear species. Nevertheless, we will employ the contributions of the various Fe states to the total resonant absorption area at 4.2 K as an estimate of their relative abundance. The resulting spectral fit parameters are listed in table 3. For Fe/ZSM-5, a full grown sextuplet is
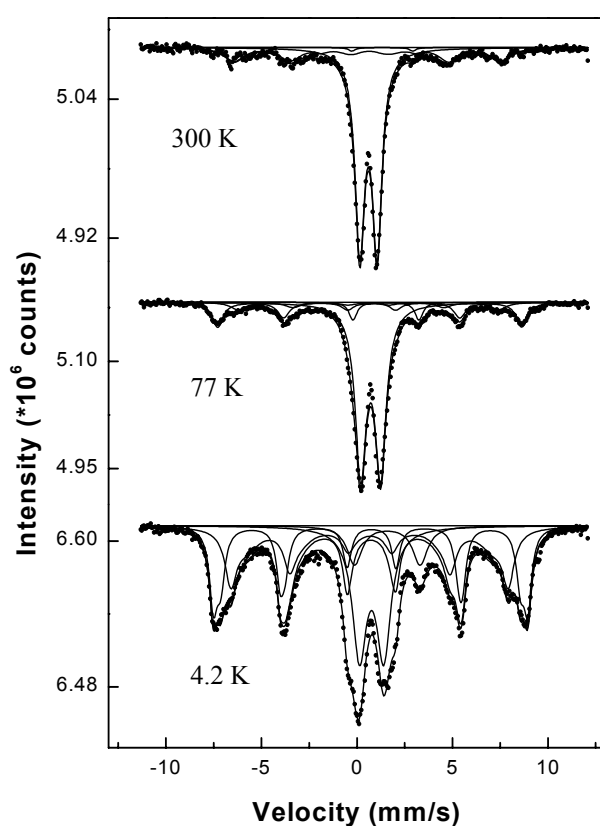
Figure 10: (b) Mössbauer spectroscopy of Fe/ZSM-5(HTC).

only observed in the Mössbauer spectrum at 4.2 K. The absence of this pattern at temperature of 77 K points to the presence of relatively small iron oxide particles (*ca.* 2 nm) in line with the TEM observations. The relatively broad lines of the sextuplet in Fe/ZSM-5 stress the amorphous character of the associated iron oxide particles, with a lower hyperfine field (45.5 T) than in bulk α-Fe_2O_3 (54.4 T at 0 K). The spectral contribution of these particles amounts

up approximately 66% at 4.2 K. The Fe^{3+} doublet (IS = 0.74 mm.s^{-1} and QS = 1.28 m.s^{-1}) with a contribution of 31% relates to very small Fe species occluded in the zeolite micropores space. We can not draw conclusions on the nuclearity of such species. The contribution of Fe^{2+} doublet with fit parameters close to those obtained after fitting of room temperature spectrum of the severely treated samples was 3%.

Table 3: Mössbauer parameters for Fe/ZSM-5 samples

	Isomer shift (mm/s)	Quadrupole splitting (mm/s)	Hyperfine field (T)	Spectral contribution (%)
Fe/ZSM-5				
300 K	0.61	1.02		100
77 K	0.72	1.13		100
4.2 K	0.73	0.01	45.5	65.9
	0.74	1.28		31.4
	1.60	3.30		2.7
Fe/ZSM-5(HTC)				
300 K	0.60	0.06	43.6	25.2
	0.60	0.91		73.8
	1.33	3.19		1.0
77 K	0.72	0.05	47.6	27.7
	0.72	1.05		67.1
	1.52	3.46		5.2
4.2 K	0.68	0.02	43.1	15.7
	0.74	0.02	50.4	31.1
	0.76	1.27		27.4
	1.59	3.43		8.8
Fe/ZSM-5(HTS)				
300K, air	0.60	0.88		84.6
	0.60			15.4
300 K, HV*	0.61	0.90		79.0
	0.60			16.9

	1.42	3.28		4.1
77 K	0.72	0.96		71.5
	0.75	0.00	48.3	17.4
	1.41	3.43		5.0
	1.72	3.61		6.1
4.2 K	0.72	0.02	47.3	71.6
	0.73	1.53		15.8
	1.40	3.55		3.6
	1.82	3.42		9.0

A broad particle size distribution is observed for Fe/ZSM-5(HTC). Relatively large iron oxide crystallites (> 8 nm) are present as derived from the occurrence of a sextuplet in the room temperature spectrum of this sample. Additionally, the fit parameters show the presence of a relatively large fraction of 2-4 nm-sized particles. This qualitatively agrees with the TEM observations of some sintering of iron oxide particles on the external surface of the zeolite. The spectrum at 4.2 K clearly shows the presence of two sextuplet contributions, one with hyperfine field of 43.1 T and another with a hyperfine field of 50.4 T. At the moment, the structure of these iron oxide phases is unclear, although the latter contribution may point to nanocrystalline α-Fe_2O_3 particles. At 4.2 K, the spectral contribution of the components related to large iron oxide particles does not significantly increase after high-temperature calcination. Nevertheless, the spectral contribution of the Fe^{2+} doublet has increased slightly.

The high-temperature steamed sample, Fe/ZSM-5(HTS), presents a relatively large fraction of iron oxide particles in the range of 2-4 nm. The relative contribution of this fraction has grown slightly compared to Fe/ZSM-5. The Fe^{3+} doublet has significantly decreased in this sample. We attribute this partly to the migration of very small iron oxide particles from the zeolite pores to the external surface. The presence of water during steaming may play an important role in the higher mobility of iron oxide particles when compared to the high-temperature calcination treatment. On the other hand, also the Fe^{2+} contribution appears to increase resulting in the presence of two doublets, with the fit parameters IS = 1.40 mm·s^{-1}, Q.S = 3.55 mm·s^{-1} and IS = 1.82 mm·s^{-1}, QS = 3.42mm·s^{-1}. The occurrence of two

Fe^{2+} states was previously reported by Pérez-Ramírez *et al.* (64) and by Dubkov *et al.* (58) for activated isomorphously-substituted Fe/ZSM-5.
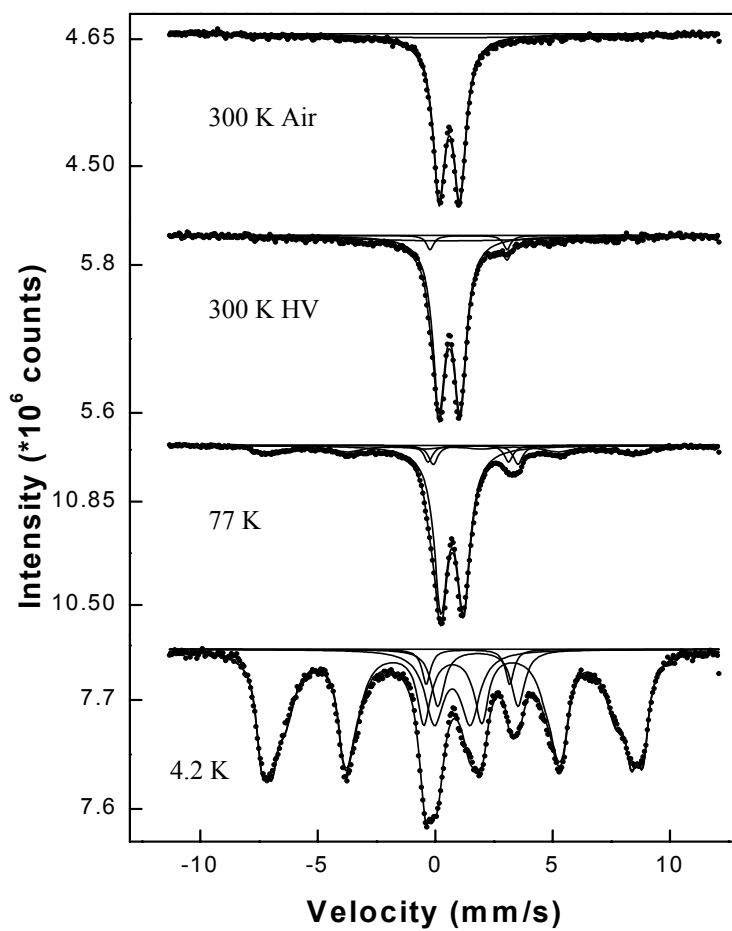

Figure 10: (c) Mössbauer spectroscopy of Fe/ZSM-5(HTS).

IPA_m decomposition

Table 4: Amount of acid sites determined from isopropylamine decomposition

Sample	Number of acid sites (mmol.g^{-1})		
	583K	653K	683K
HZSM-5	0.083	0.001	0
HZSM-5(HTC)	0.079	0.001	0
HZSM-5(HTS)	0.021	0.001	0.01
Fe/ZSM-5	0.047	0.009	0.012
Fe/ZSM-5(HTC)	0.034	0.011	0.013
Fe/ZSM-5(HTS)	0.021	0.007	0.007

The Brønsted acid site densities determined by the decomposition of isopropyl amine for the various catalysts are shown in table 4. The value for HZM-5 (0.083 mmol H$^+$·g^{-1}) is close to the theoretical amount corresponding to a framework Si/Al ratio of 19.4. High-temperature calcination of HZSM-5 results in a small decrease in acidity. This is in agreement with the IR measurement of a small decrease of the hydroxyl band at 3613 cm^{-1}. On the other hand, steaming results in a substantial decrease in Brønsted acidity (higher decomposition temperature of IPA$_m$) which most probably relates to OH groups of extra framework species. The acid site density of Fe/ZSM-5 amounts to 0.047 mmol H$^+$·g^{-1}, which is in rather good agreement with the quantitative data obtained from IR spectroscopy. Subsequent high-temperature treatments further decrease the number of protons. The decrease after high-temperature calcination is due to the protolysis reaction of small occluded neutral iron oxide particles. This also parallels the observed decrease in the resonance area of tetrahedral Al species determined from ^{27}Al NMR, explained by a closer proximity of the Al nuclei to the paramagnetic Fe centres. Steaming results in a further decrease of the acid site density (0.021 mmol H$^+$·g^{-1}). The amount of hydroxyl groups derived from infrared spectroscopy is somewhat lower. This may suggest that some protons are strongly perturbed by the presence of extra-framework species, possible iron oxide particles. Notably, the iron-containing samples clearly show the presence of two extra protonic species with a lower acidity. The absence of such contributions in the HZSM-5 samples stresses that these species are related to iron oxide particles, although their nature remains unclear at the moment.
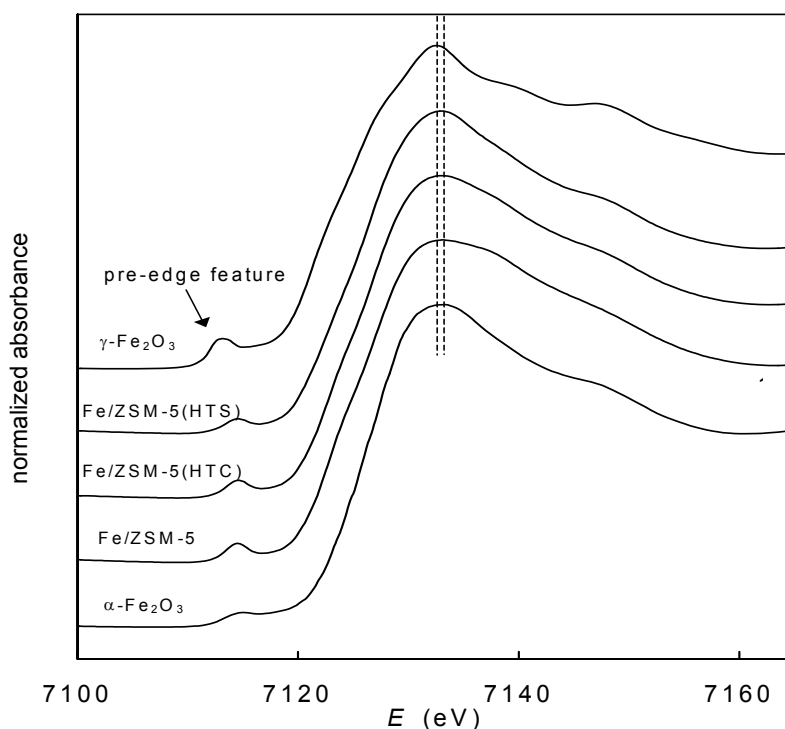
Figure 11: XANES of α-Fe$_2$O$_3$, γ-Fe$_2$O$_3$ and the sublimed catalysts after in situ calcination.

Figure 11 displays a comparison of the near edge regions of the x-ray adsorption spectra of α - Fe$_2$O$_3$, γ - Fe$_2$O$_3$ and the three sublimed catalysts. The edge positions of the Fe/ZSM-5 catalysts are in line with those in reference oxides indicating the predominant presence of Fe^{3+}. The pre-edge absorption feature due to 1s→3d transition is forbidden for octahedral coordination but arises in distorted octahedral and tetrahedral symmetries. For γ - Fe$_2$O$_3$ with 50% of Fe^{3+} in tetrahedral symmetry, this feature is more intense than for α - Fe$_2$O$_3$ with Fe^{3+} in distorted symmetry (65) which is in agreement with a recent report by Heinrich *et al.* (46). All three samples show a pre-edge feature intermediate between those of two reference oxides. This indicates the presence of tetrahedral Fe^{3+} although its contribution should be less than 50%. Moreover, the scattering feature just above the adsorption maximum becomes more pronounced for the catalysts which have been severely treated. In particular, the steamed sample shows a pronounced order in the higher coordination spheres in line with the results from EXAFS data analysis (*vide infra*).
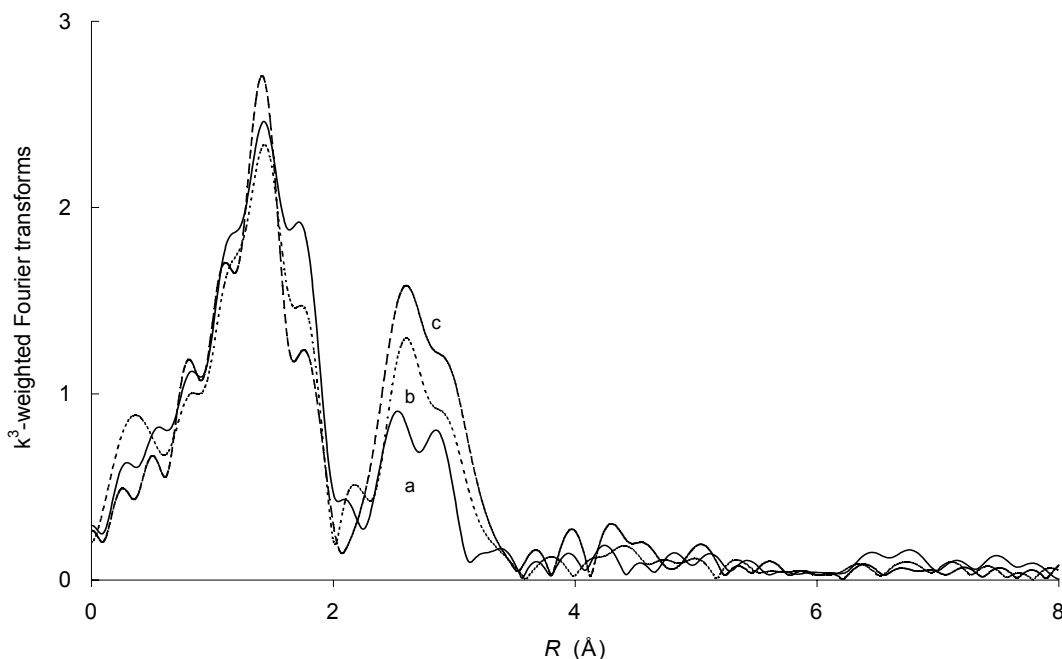
Figure 12: Absolute part of the k^3–weighted spectra for (a)Fe/ZSM-5, (b)Fe/ZSM-5(HTC) and (c)Fe/ZSM-5(HTS).

Figure 12 shows the absolute part of the k^3–weighted spectra for the catalyst samples. Conspicuously, the samples do not differ to a great extent from each other except for the intensities. Multiple shell analysis of these EXAFS data was performed taking into account the models postulated by Battiston *et al.*(47). Especially we use their result that the first oxygen shell can be fitted by six oxygen atoms at two different distances. In agreement with their results, this led to better fit results than the use of three different Fe-O shells. Moreover, a third Fe-O shell at a larger distance (R = 3.9-4.2 Å) considerable improved the fitting results. The k^1–weighted Fourier transform and the corresponding best fit for Fe/ZSM-5 are presented in figure 13a. The fit results are listed in Table 5.

Two oxygen shells were fitted producing a total Fe-O coordination number (CN) of six in the first shell. The second shell consists of two Fe-Fe contributions, because fitting with one Fe-Fe shell did not produce satisfactory results. The coordination number of Fe-Fe$_1$ is 1.2 while a value of 0.9 is found for the Fe-Fe$_2$ shell. The results for the second shell are close to those reported recently by Battiston *et al.* (47). Most notably, the CN of the two Fe-Fe shells in the Fe/ZSM-5 sample of the present work are between those of two samples obtained after mild calcination and severe calcination in the study of Battiston *et al.* Given that our calcination procedure for Fe/ZSM-5 is of intermediate severity, the somewhat higher value

for the coordination number of Fe-Fe$_2$ shell is in rather good agreement with these earlier results. On the other hand, the coordination distances are somewhat lower and appear to agree better with the results of Heinrich *et al.*(46).

Table 5: Fit parameters of multiple shell analysis of the EXAFS data for Fe/ZSM-5, Fe/ZSM-5(HTC) and Fe/ZSM-5(HTS)

Shell	CN	R(Å)	$\Delta\sigma^2(10^{-3}$ Å)	ΔE_0(eV)	k^1-variance(%)	
Fe/ZSM-5					Im.part	Abs.part
Fe-O$_1$	3.0	1.87	3.46	-4.57	0.07	0.04
Fe-O$_2$	3.0	1.99	1.68	6.33		
Fe-Fe$_1$	1.2	2.93	6.24	-8.46		
Fe-Fe$_2$	0.9	3.32	3.58	9.70		
Fe-O$_3$	1.2	3.91	11.2	-3.53		
Fe/ZSM-5(HTC)					0.14	0.06
Fe-O$_1$	3.3	1.88	2.85	0.05		
Fe-O$_2$	2.8	2.01	1.33	11.9		
Fe-Fe$_1$	1.4	2.93	6.39	-1.54		
Fe-Fe$_2$	1.2	3.36	3.64	5.39		
Fe-O$_3$	1.2	3.91	10.9	-3.51		
Fe/ZSM-5(HTS)					0.06	0.02
Fe-O$_1$	3.0	1.89	1.96	0.54		
Fe-O$_2$	3.0	2.01	6.11	12.06		
Fe-Fe$_1$	1.8	2.97	6.11	-8.50		
Fe-Fe$_2$	1.1	3.36	1.53	4.87		
Fe-O$_3$	1.6	4.13	11.6	-10.1		
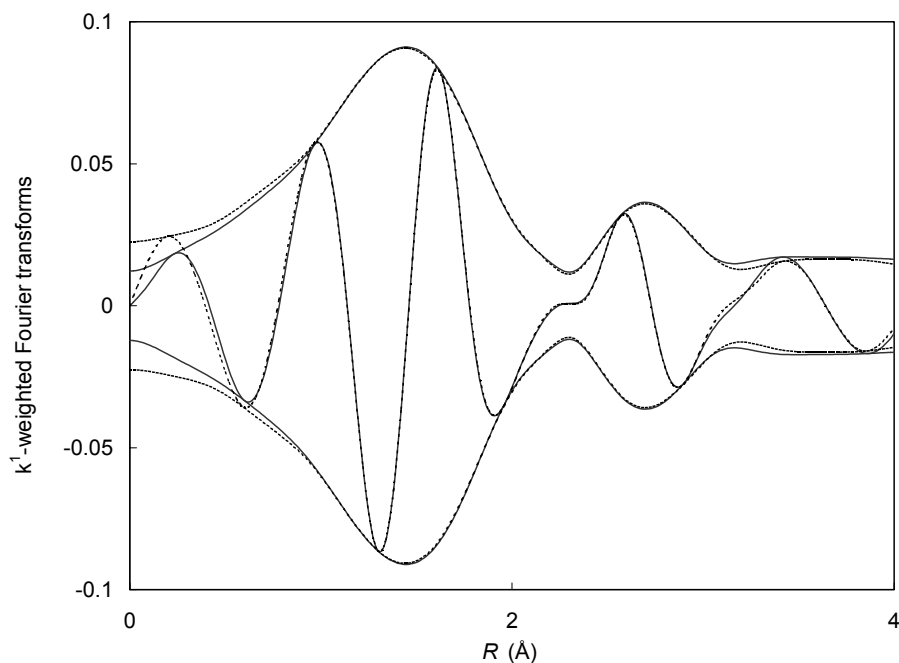
Figure 13: (a) k^1- FT experimental (solid line) and fitted (dashed line) for Fe/ZSM-5.

Figures 13b and 13c produce the k^1 –weighted Fourier transforms and best fits for the Fe/ZSM-5(HTC) and Fe/ZSM-5(HTS), respectively. Large changes are observed for the two Fe-Fe shells, whereas the first iron-oxygen shell remains unaltered. The fit results indeed show that there are no large changes in this latter shell. The coordination numbers for the two Fe-Fe shells strongly increase upon high temperature treatments.

This points to further ordering and/or particle growth of the iron oxide phases. This qualitatively agrees with the observations of Battiston *et al.*(47) comparing mildly and severely calcined Fe/ZSM-5 precursors. While the quite severe calcination temperature has led to the segregation of a large part of iron into iron oxide particles, the low coordination number for the Fe-Fe shell for the Fe/ZSM-5 is attributed to structural disorder of the iron oxide aggregates. Increasing severity of treatment induces a further growth and ordering of such particles, which are reflected by increasing Fe-Fe coordination numbers. This notion is in line with the presence of clustered iron oxide particles observed by UV-Vis spectroscopy and of large iron oxide aggregates observed by TEM and derived from [57]Fe Mössbauer spectroscopy.
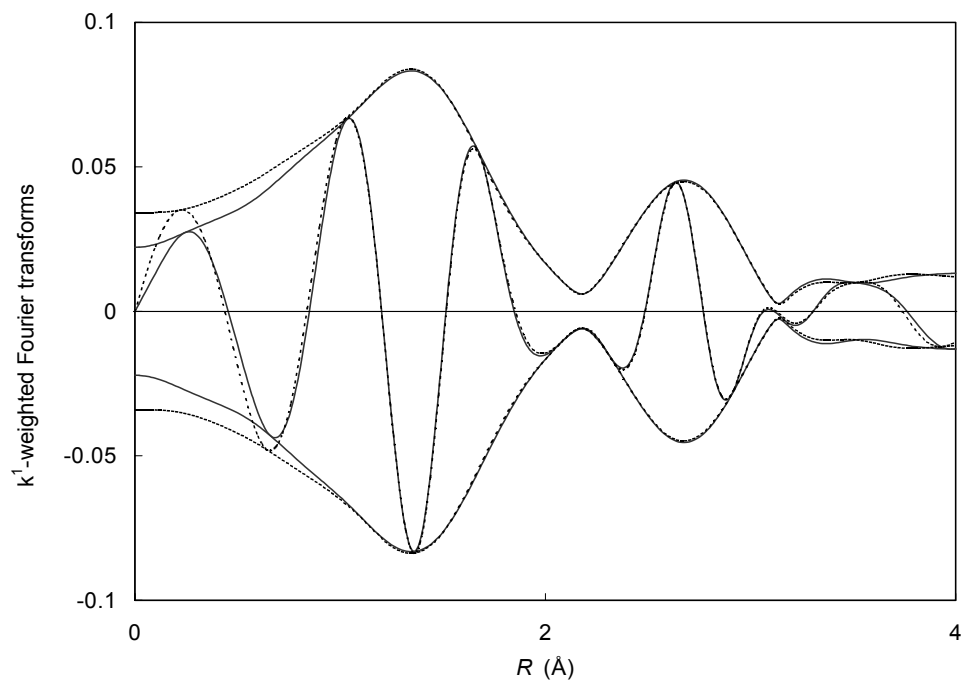
Figure 13 (b): k^1-FT experimental (solid line) and fitted (dashed line) for Fe/ZSM-5(HTC).
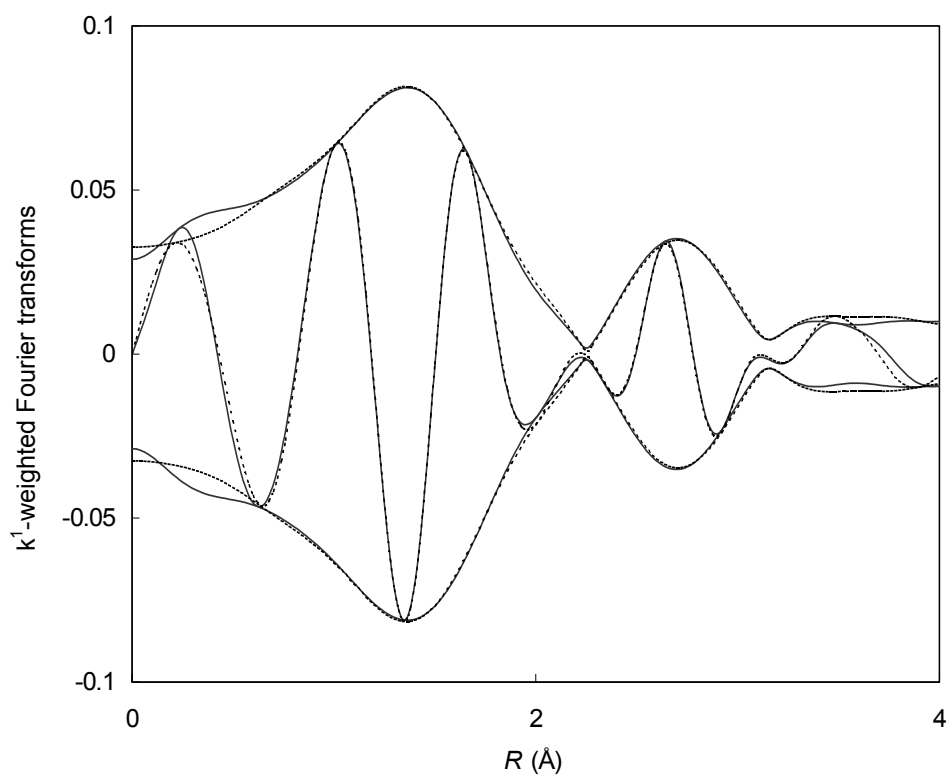

Figure 13 (c): k^1-FT experimental (solid line) and fitted (dashed line) for Fe/ZSM-5(HTS).

41

Low-temperature nitrous oxide decomposition

Nitrous oxide decomposition at relatively low temperature allows the stoichiometric deposition of one oxygen atom on active centers under the release of dinitrogen (22,23). Such sites are thought to consist of binuclear Fe centers, have been coined α-sites by the group of Panov and have been reported to be created upon high-temperature activation leading to reduction of some Fe^{3+} species to Fe^{2+} (58). These species are stable in the presence of molecular oxygen and can be reoxidized by nitrous oxide. Table 6 lists the number of deposited oxygen atoms (N_{N2O}) as determined by low-temperature (523 K) nitrous oxide decomposition, subsequent room temperature isotopic exchange with $^{18}O_2$ and O_2 desorption.

Table 6: The number of sites able to decompose nitrous oxide at low temperature, the number of exchangeable deposited oxygen atoms and the number of oxygen atoms desorbing in a TPD experiment

Sample	Number of active sites		
	N_2O decomposition	^{18}O exchange	O_2 desorption
Fe/ZSM-5	8.8×10^{18}	5.8×10^{18}	1.5×10^{19}
Fe/ZSM-5(HTC)	1.6×10^{19}	1.5×10^{19}	2.0×10^{19}
Fe/ZSM-5(HTS)	1.7×10^{19}	1.9×10^{19}	1.8×10^{19}
HZSM-5(HTS)	-	5.0×10^{17}	7.2×10^{17}

Qualitatively, the amount of deposited oxygen atoms increases in the order: HZSM-5$_{HTS}$<FeZSM-5<Fe/ZSM-5(HTC)<Fe/ZSM-5(HTS). The agreement between the various methods is not perfect and especially the values obtained after oxygen desorption are somewhat higher. This is most probably due to some auto-reduction of aggregated iron oxide species. From a chemical point of view, the $^{18}O_2$ exchange experiments are most reliable since they relate to measurements carried out close to room temperature. It is expected that only the most reactive oxygen species are isotopically exchanged under these reaction conditions. Comparing the present results to those obtained by Dubkov *et al.* (58) for a sample prepared by hydrothermal synthesis, we can conclude that the amount of deposited oxygen atoms is an order of magnitude higher for our sublimed samples to be attributed to the higher Fe content. In agreement with Dubkov *et al.* (58), an increase is found with increasing treatment temperature and the presence of water vapor during pretreatment. There are several indications that the activity in nitrous oxide and benzene-to-phenol conversion correlates to

sites capable of decomposing nitrous oxide at low temperature. We have reached similar conclusions. Interestingly, the titration data imply that the number of Fe atoms involved in such specific sites in catalysts prepared by sublimation of $FeCl_3$ is very small. This amount is smallest for Fe/ZSM-5, *i.e.* 0.098 wt. % and increases to 0.32 wt.% and 0.45 wt% for Fe/ZSM-5(HTC) and Fe/ZSM-5(HTS), respectively. On the other hand, the value obtained by low-temperature nitrous oxide decomposition for HZSM-5(HTS) suggests that about one third of the total iron content in HZSM-5 (approximately 0.0083 wt.% of the total content of 0.024wt%) is associated with these specific sites. This higher fraction of catalysts with a lower iron content agrees with the report of Dubkov *et al.*(58).

Positron Emission Profiling
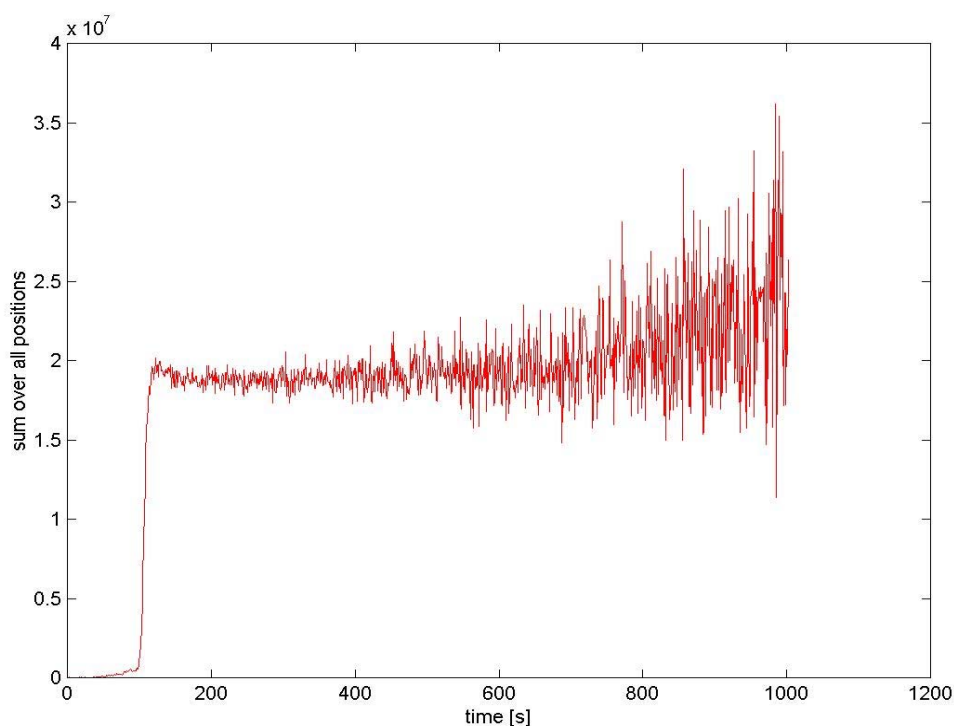
Figure 14: Time profile for the decomposition of $N_2{}^{15}O$ over Fe/ZSM-5(HTS) at 523K

The phenomenon of oxygen deposition of N_2O with concomitant release of N_2 is also confirmed by PEP measurements with $N_2{}^{15}O$. The decomposition of N_2O on Fe/ZSM-5 has been analyzed with $N_2{}^{15}O$. The behaviour of the labelled nitrous oxide can be followed with the PEP detectors as it passes through the catalyst bed. Figure 14 shows the time profiles for the Fe/ZSM-5(HTS) (response measured as a function of time at a specific position in a catalyst bed).

The main observation is that radioactivity is retained on the catalyst. Although in principle, it is not possible to distinguish physically adsorbed $N_2{}^{15}O$ and ^{15}O, online mass spectrometry clearly indicates the production of N_2 while part of the corresponding O_2 is missing. We thus conclude that the retention of the radioactivity is related to the deposition of the oxygen atom from nitrous oxide. This technique provides possibilities to study the interaction of hydrocarbon molecule with the deposited oxygen atoms (52, 53).

Relation between the Fe^{2+} and the active sites
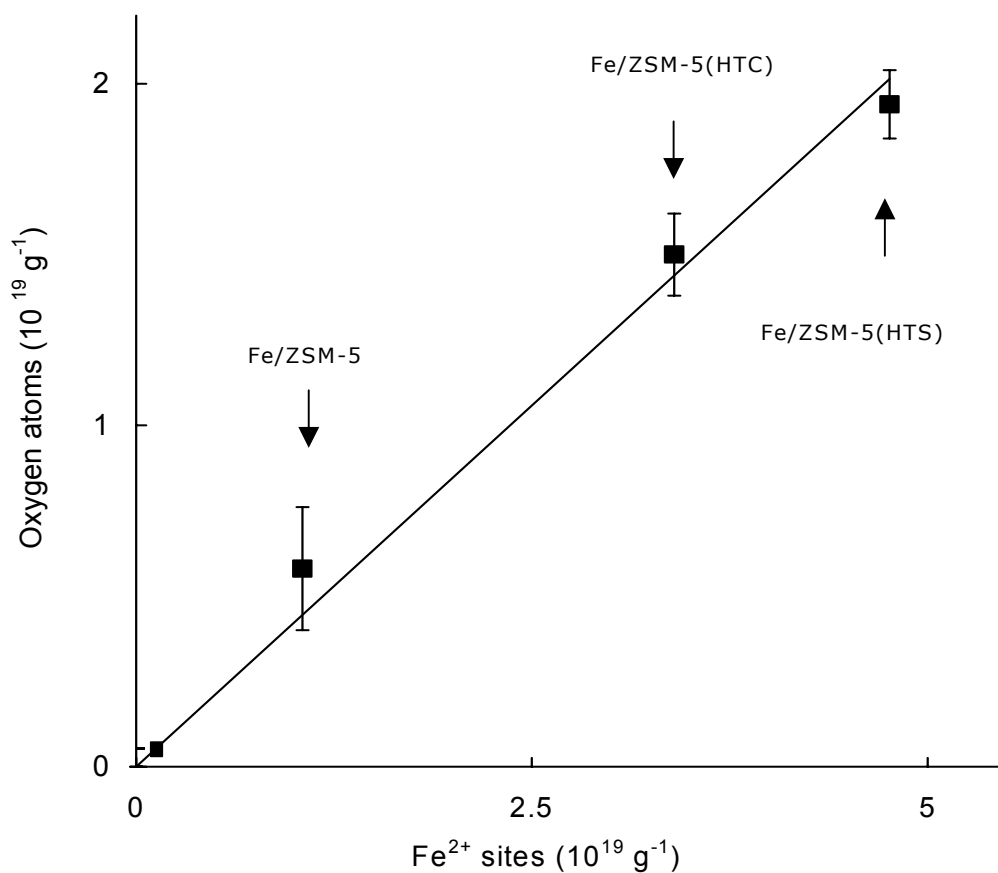
Figure 15: Relation between the amount of atoms deposited during low-temperature N_2O decomposition *versus* the amont of Fe^{2+} ions detected by ^{57}Fe Mössbauer spectroscopy

Since we expect that the redox properties of these catalysts are associated with the presence of Fe^{2+} species, we have plotted the number of deposited oxygen atoms as a function of the Fe^{2+} contribution as observed from Mössbauer spectroscopy. Indeed, a linear relation is found pointing to the relevance of these sites for the decomposition of nitrous oxide. For steamed Fe/ZSM-5(HTS), the amount of Fe^{2+} species was taken as the sum of the

two Fe^{2+} contributions observed by Mössbauer spectroscopy. Based on these data and the assumptions that the active sites are uniform and represented by the Fe^{2+} species identified by Mössbauer spectroscopy (C_{Fe2+}), we calculate the nuclearity of the active species defined as n = C_{Fe2+} /N_{N2O}. The values for n (1.8 for Fe/ZSM-5, 2.2 for Fe/ZSM-5(HTC) and 2.3 for Fe/ZSM-5(HTS)) appear to agree with the notion of a binuclear iron complex (22,23,66-70). Nevertheless, we stress the assumptions underlying the calculation of the nuclearity making it impossible to draw firm conclusions on the nuclearity. Most importantly, however, we can conclude that the fraction of iron species active in nitrous oxide decomposition is very low.

2.4.Discussion

Fe/ZSM-5 prepared by chemical vapor deposition of $FeCl_3$ followed by washing and calcination can be characterized various techniques. There are a variety of Fe species co-present. Most importantly, a predominant presence of iron oxide aggregates on the external surface was found. This primarily follows from a combination of TEM imaging and ^{57}Fe Mössbauer spectroscopy measurements. The latter technique shows a large contribution of iron oxide particles too large to be accommodated in the zeolite micropores. Conversely, structure analysis of Fe K-edge EXAFS data points to relatively low Fe-Fe coordination numbers (CN = 1.2). Both the TEM and ^{57}Fe Mössbauer results clearly show that this can not be explained by the predominant presence of binuclear clusters. The relatively low values for the hyperfine field of the iron oxide phase identified by ^{57}Fe Mössbauer spectroscopy in this sample indicate that we are dealing with a highly disordered iron oxide/hydroxide phase. The low Fe-Fe coordination number is thus due to the disordered nature of these iron oxide particles. This interpretation contrasts the conclusions reached by the groups of Prins (43,44) and Koningsberger (45,47) who attributed the Fe-Fe coordination number close to unity to a large fraction of binuclear Fe clusters occluded in the micropores. Battiston *et al.*(47) have carefully determined that a slow heating rate during calcination after washing results in a well –dispersed iron oxide phase. TEM imaging indeed showed that most of the iron species are located in the zeolite micropores. Moreover, the UV-Vis spectrum of the sample prepared by similar methods shows a lower fraction of larger clusters to be present than in our case. Also, the fraction of nanocrystalline iron oxide as determined by Mössbauer spectroscopy is lower in their case. On the other hand, the amount of Fe^{2+} in that sample is close to the amount identified for the present Fe/ZSM-5 determined under exactly the same experimental

conditions, giving some indication that the amount of active sites for nitrous oxide decomposition should be equally small for both samples. These findings stress that the iron distribution in sublimed catalysts is critically dependent on the exact pretreatment and most probably also on the nature of ZSM-5 zeolite. This renders it troublesome to directly compare results from various studies. An important finding, however, is that only a small fraction of Fe sites is involved in the decomposition of nitrous oxide at low temperature for Fe/ZSM-5 prepared by chemical vapor deposition of $FeCl_3$.

Further high-temperature treatment of Fe/ZSM-5 results in considerable changes of the intrazeolite Fe species. High-temperature calcination results in the replacement of charge–compensating protons by cationic Fe complexes. ^{27}Al NMR measurements confirm the closer proximity of Al nuclei and paramagnetic Fe ions after high-temperature treatment. Moreover, a qualitative interpretation of nitrogen adsorption data indicates large changes in the structure of the micropores due to changes in the size of the occluded species. The increased Fe-Fe coordination number for this sample is attributable to further ordering and/or growth of the iron oxide aggregates on the external surface.

A steaming treatment at 923 K results in a further redistribution of iron species. The fraction of large iron oxide aggregates slightly increases at the expense of the Fe^{3+} component with a QS of 1.53 mm·s^{-1}, to be tentatively explained by a higher mobility of iron oxide species in the presence of water. This increased ordering of the majority of iron species is also reflected in the EXAFS fit parameters for Fe/ZSM-5(HTS) and a contribution of larger iron oxide particles (TEM). Concomitantly, an increase of Fe^{2+} species is also observed by the Mössbauer spectroscopy. Careful analysis suggests that the contribution of the Fe^{2+} component with QS = 3.42 mm·s^{-1} and IS = 1.82 mm·s^{-1} remains constant while a new Fe^{2+} appears with QS = 3.55 mm·s^{-1} and IS = 1.40 mm·s^{-1}. The binuclear nature of the active species is suggested by the observation that approximately one oxygen atom is deposited from nitrous oxide per two Fe^{2+} sites. Finally, low-temperature nitrous oxide decomposition of a steamed HZSM-5 zeolite with a Fe content of 0.024 wt.% shows that an amount of 0.0083 wt.% iron is involved in the activation of nitrous oxide. This amount is considerably lower than in the sublimed samples, where active site concentrations in the range of 0.01-0.043 wt.% were found. This excludes the possibility that the increase of the number of active sites in Fe/ZSM-5(HTC) and Fe/ZSM-5(HTS) compared to Fe/ZSM-5 only derives from dislodgement of the Fe contamination in the starting zeolite material. In short, we take this observation as an indication that removal of Al from framework positions may play a role in the formation of the active sites.

2.5 Conclusion

FeZSM-5, prepared by sublimation method of $FeCl_3$ followed by washing and calcination, contains a large variety of Fe species. Iron oxide particles on the external zeolite surface are dominating, while neutral iron oxide nanoparticles and charge-compensating iron complexes are located in the micropores. High-temperature induces the growth and ordering of the iron oxide aggregates next to the protolysis between occluded neutral iron oxide nanoparticles and Brønsted acid sites. These effects are more pronounced in the case of steaming at 973K, a treatment additionally leading to dealumination. Relatively low Fe-Fe coordination numbers were derived from Fe K-edge EXAFS measurements. This should be taken as an indication of the disordered nature of the abundantly present iron oxide aggregates rather than as evidence for the predominant presence of binuclear clusters. More importantly from the catalysis point of view, we conclude that high-temperature treatments lead to a larger number of sites able to decompose nitrous oxide at relatively low temperature. The number of such active sites, however, is quite small and constitutes only a small fraction of the total iron content. Moreover, the amount of active sites correlates with the amount of Fe^{2+} as probed by ^{57}Fe Mössbauer spectroscopy at 4.2 K. Tentatively, the observation that approximately one oxygen atom is deposited per two Fe^{2+} atoms agrees with the binuclear active sites.

References

1. Catalysis by Unique Metal Ion Structures in Solid Matrices, G. Centi, B. Wichterlova and A.T. Bell, (Eds.), NATO Science Series, Kluwer Acadamic, Dordrecht, 2001.
2. A. Corma, J. Catal. 216 (2003) 298.
3. G.I. Panov, CatTech 4 (2000) 18.
4. A.K. Uriarte, M.A. Rodkin, M.J. Gross, A.S. Kharithonov, G.I. Panov, Stud. Surf. Sci. Catal. 110 (1997) 857.
5. G. Centi and F. Vazzana, Catal. Today 53 (1999) 683.
6. El-M. El Malki, R.A. van Santen and W.M.H. Sachtler, Microporous Mesoporous Mat. 35-36 (2000) 235.
7. El-M. El-Malki, R.A. van Santen and W.M.H. Sachtler, J. Catal. 196 (2000) 212.
8. J. Pérez-Ramírez, F. Kapteijn, G. Mul, X. Xu and J.A. Moulijn, Catal. Today 76 (2002) 55.

9. Q. Zhu, B.L. Mojet, R.A.J. Janssen, E.J.M. Hensen, J. van Grondelle, P.C.M.M. Magusin and R.A. van Santen, Catal. Lett. 81 (2002) 205.

10. Q. Zhu, E.J.M. Hensen, B.L. Mojet, J.H.M.C. van Wolput and R.A. van Santen, Chem. Commun. (2002) 1232.

11. R.Q. Long and R.T. Yang, J. Catal. 207 (2002) 224.

12. X. Feng and W.K. Hall, Catal. Lett. 41 (1996) 45.

13. X. Feng and W.K. Hall, J. Catal. 166 (1997) 368.

14. L.J. Lobree, I.-C. Hwang, J.A. Reimer and A.T. Bell, Catal. Lett. 63 (1999) 233.

15. H.-Y. Chen, T. Voskoboinikov and W.M.H. Sachtler, Catal. Today, 54 (1999) 483.

16. E. Suzuki, K. Nakashiro and Y. Ono, Chem. Lett. (1988) 953.

17. R. Burch and C. Howitt, Appl. Catal. A 103, (1993) 135.

18. V.L. Zholobenko, I.N. Senchenya, L.M. Kustov and V.B. Kazansky, Kinet. Catal. 32 (1991) 151.

19. L.M. Kustov, A.L. Tarasov, V.I. Bogdan, A.A. Tyrlov and J.W. Fulmer, Catal. Today 61 (2000) 123.

20. J.L. Motz, H. Heinrichen and W.F. Hölderich, J. Mol. Catal. 136 (1998) 175.

21. A.S. Kharitonov, G.A. Sheveleva, G.I. Panov, V.I. Sobolev, Y.A. Paukshits and V.N. Romannikov, Appl. Catal. A 98 (1993) 33.

22. G.I. Panov, V.I. Sobolev and A.S. Kharitonov, J. Mol. Catal. 85 (1990) 61.

23. G.I. Panov, G.A. Sheveleva, A.S. Kharitonov, V.N. Romannikov and L.A. Vostrikova, Appl. Catal. A 82 (1992) 31.

24. P. Notté, Top. Catal. 13 (2000) 387.

25. P. Kubánek, B. Wichterlová and Z. Sobalík, J. Catal. 211 (2002) 109.

26. G. Berlier, A. Zecchina, G. Spoto, G. Ricchiardi, S. Bordiga and C. Lamberti, J. Catal. 215 (2003) 264.

27. D. Meloni, R. Monaci, V. Solinas, G. Berlier, S. Bordiga, I. Rossetti, C. Oliva and L. Forni, J. Catal. 214 (2003) 169.

28. P. Ratnasamy and R. Kumar, Catal. Today 9 (1991) 329.

29. S.A. Axon, K.K. Fox, S.W. Carr and J. Klinowski, Chem. Phys. Lett. 189 (1992) 1.

30. V.I. Sobolev, G.I. Panov, A.S. Kharitonov, V.N. Romannikov, A.M. Volodin and K.G. Ione, J. Catal. 139 (1993) 435.

31. D.W. Lewis, R.A. Catlow, J. Sankar and S.W. Carr, J. Phys. Chem. 99 (1995) 2377.

32. S. Bordiga, R. Buzzoni, F. Geobaldo, C. Lamberti, E. Giamello, A. Zecchina, G. Leofanti, G. Petrini, G. Tozzola and G. Vlaic, J. Catal. 158 (1996) 486.

33. A. Ribera, I.W.C.E. Arends, S. de Vries, J. Pérez-Ramírez and R.A. Sheldon, J. Catal. 195 (2000) 287.

34. G. Spoto, A. Zecchina, G. Berlier, S. Bordiga, M.G. Clerici and L. Basini, J. Mol. Catal. A 158 (2000) 107.

35. G. Berlier, G. Spoto, S. Bordiga, G. Ricchiardi, P. Fisicaro, A. Zecchina, I. Rossetti, E. Selli, L. Forni, E. Giamello and C. Lamberti, J. Catal. 208 (2002) 64.

36. A.M. Ferretti, C. Oliva, L. Forni, G. Berlier, A. Zecchina and C. Lamberti, J. Catal. 208 (2002) 83.

37. L.V. Pirutko, V.S. Chernyavsky, A.K. Uriarte and G.I. Panov, Appl. Catal. A 227, (2002) 143.

38. A. Dubkov, N.S. Ovanesyan, A.A. Shteinman, K.A. Dubkov, V.I. Sobolov and G.I. Panov, Kinet. Catal. 39 (1998) 792.

39. H.-Y. Chen and W.M.H. Sachtler, Catal. Today 42 (1998) 73.

40. R. Joyner and M. Stockenhuber, J. Phys. Chem. B 103 (1999) 5963.

41. M. Kögel, R. Mönning, W. Schwieger, A. Tissler and T. Turek, J. Catal. 182 (1999) 470.

42. P. Marturano, A. Kogelbauer and R. Prins, J. Catal. 190 (2000) 460.

43. P. Marturano, L. Drozdová, A. Kogelbauer and R. Prins, J. Catal. 192, (2000) 236.

44. P. Marturano, L. Drozdová, A. Kogelbauer and R. Prins, Stud. Surf. Sci. Catal. 135 (2001) 1627.

45. A.A. Battiston, J.H. Bitter and D.C. Koningsberger, Catal. Lett. 66 (2000) 75.

46. F. Heinrich, C. Schmidt, E. Löffler, M. Menzel and W. Grünert, J. Catal. 212 (2002) 157.

47. A.A. Battiston, J.H. Bitter, F.M.F. de Groot, A.R. Overweg, O. Stephan, J.A. van Bokhoven, P.J. Kooyman, C. van der Spek, G. Vankó and D.C. Koningsberger, J. Catal. 213 (2003) 251.

48. A.Reitzmann, H. Friedrich, E. Klemm, M. Haefele and G. Emig, Proc. Polish-German Zeolite Colloquium 3rd, M. Rozwadoski (Eds.). Nicholas Copernicus Unversity Press, Torún, 1998, p. 239

49. T. Voskoboinikov, H-.Y. Chen and W.M.H. Sachtler, Appl. Catal. B 19 (1998) 279.

50. F.A. Cotton, G. Wilkinson, C.A. Murillo and M. Bochmam, In: Advanced Inorganic Chemistry, John Wiley & Sons, New York, 1999, p. 778

51. J. Dĕdeček, D. Kaucký and B. Wichterlová. Chem. Commun. (2001) 970.

52. S.C. van der Linde, Application of Positron Emission Profiling in n Catalysis, Ph.D.Thesis, 1999, Delft University of Technology, Delft.

53. D.P. Sobczyk, Positron Emission Profiling Study of Ammonia Oxidation on Platinum, Ph.D. Thesis, 2003, Eindhoven University of Technology, Eindhoven.

54. M. Vaarkamp, J.C. Linders and D.C. Koningsberger, Phys. B (1995) 209.

55. D.C. Koningsberger, B.L. Mojet, G.E. van Dorssen and D.E. Ramaker, Top. Catal. 143 (2000) 10.

56. T.J. Gricus Kofke, R.J. Gorte and W.E. Fameth, J. Catal. 114 (1988) 34.

57. K.A. Dubkov, V.I. Sobolev and G.I. Panov, Kinet. Katal. 39 (1998) 79.

58. K.A. Dubkov, N.S. Ovanesyan, A.A. Shteinman, E.V. Starokon and G.I. Panov, J. Catal. 207 (2002) 341.

59. P.A. Webb and C. Orr, Analytical Methods in Fine Particles Technology, Micromeritics Instrument Corp., Norcross, USA, 1997, p. 59.

60. G. Centi, F. Fazzini, J.L.G. Fierro, M. Lopèz Granados, R. Sanz and D. Serrano, Preparation of catalysts VII B. Delmon *et al.* (Eds), 1998, p.577.

61. L.J.Lobree, I. -C. Hwang , J.A. Reimer and A.T. Bell, J. Catal. 186 (1999) 242.

62. D. Goldfarb, M. Bernardo, K.G. Strohmaier, D.E.W. Vaughan and H. Thomann, J. Am. Chem. Soc. 116 (1994) 6344.

63. A. Brückner, In Spectroscopy of Transition Metal Ions on Surfaces B.M.Weckhuysen, P.Van Der Voort and G.Catana (Eds.), Leuven University Press.Belgium,1990, p.69.

64. J. Pérez-Ramírez, G. Mul, F. Kapteijn, J.A. Moulijn, A.R. Overweg, A. Doménech, A. Ribera and I.W.C.E. Arends, J. Catal. 207 (2002) 113.

65. G. Calas and J. Petiau, J. Solid State Commun. 48 (1983) 625.

66. K. Lázar, A.N. Kotasthane and R. Fejes, Catal. Lett. 57 (1999) 171.

67. M. Mauvezin, G. Delahay, B. Coq, S. Kieger, J.C. Jumas and J. Oliver-Fourcade, J. Phys. Chem. B 105 (2001) 928.

68. G.I. Panov, A.K. Uriarte, M.A. Rodkin and V.I. Sobolev, Catal. Today 41 (1998) 365.

69. G.I. Panov, V.I. Sobolev, K.A. Dubkov, V.N. Parmon, N.S. Ovanesyan, A.E. Shilov and A.A. Shteinman, React. Kinet. Catal. Lett. 61 (1997) 251.

70. G.I. Panov, V.I. Sobolev, K.A. Dubkov and A.S. Kharitonov, Stud. Surf. Sci. Catal. 101 (1996) 493.

Chapter 3

Nitrous oxide decomposition, selective oxidation of benzene to phenol by nitrous oxide and NO reduction over Fe/ZSM-5-prepared by chemical vapor deposition of FeCl$_3$

Abstract

The reactivity of Fe/ZSM-5 prepared by the chemical vapor deposition of FeCl$_3$ in the decomposition of nitrous oxide, the selective oxidation of benzene to phenol with nitrous oxide and reduction of NO with iso-butane was investigated. Further calcination or steaming treatment (973 K) of the precursor increased the decomposition rate of N$_2$O compared to conventional calcination (773 K). The strong initial deactivation in the N$_2$O decomposition reaction is related to reoxidation of Fe^{2+} species generated by auto-reduction of Fe$_2$O$_3$-like species at high temperatures. The catalytic activity depends strongly on the nature of Fe species. In the oxidation of benzene, only steamed Fe/ZSM-5 produces phenol with high selectivity. We forward that extra-framework Al sites are involved in the formation of active sites in addition to extra-framework Fe sites, providing an explanation for the necessity of the widely reported severe activation treatments. NO reduction by iso-butane does not require active sites with the property to activate nitrous oxide at low temperature and dispersed iron oxide nanoparticles appear to be more important. This explains the decrease in activity with increasing severity of treatment.

3.1. Introduction

Iron-containing zeolite materials with the MFI topology have been identified as potential catalysts for an increasing number of environmentally benign processes. Foremost, the reduction of nitrogen oxides by hydrocarbons or ammonia by these materials (1-8) has been an important topic in the field of environmental catalysis, because it may provide a technology for NO_x abatement with diesel and lean-burn Otto engines. The high activity in the decomposition of nitrous oxide has also been noted and is of potential value to the abatement of this notorious greenhouse gas in the tail-gas of nitric acid plants (5,9-15). The high selectivity to phenol in the selective oxidation of benzene using nitrous oxide as oxidant is well-known (16-19) and might be an alternative to the existing cumene process (20). Other interesting reactions include isomerization and dehydrogenation of alkanes (21) and selective ammonia oxidation (22).

The two most important preparation routes to active iron-containing MFI catalysts, *i.e,* isomorphous substitution of Fe in the MFI framework followed by activation and post-synthesis addition of Fe, have been studied thoroughly (16, 19, 23-27). One interesting application concerning these iron-loaded MFI zeolites is the selective oxidation of hydrocarbons with N_2O as the oxidant due to its successful application of benzene hydroxylation to phenol (19). Fe/ZSM-5 materials for this selective oxidation reaction are generally synthesized by isomorphous substitution of the MFI framework by Fe^{3+} and Al^{3+} followed by thermal treatments to remove Fe from framework to extra-framework positions. An alternative preparation route is the sublimation of $FeCl_3$ into the micropore space of HZSM-5 (4,10,11,14, 15,28). In our view, it appears that Fe/ZSM-5 prepared by sublimation of $FeCl_3$ followed by washing and calcination produces a quite heterogeneous material with a wide variety of iron species (chapter 2). While the exact distribution of Fe species clearly depends on the pre-treatment procedure (29-36), we have addressed the changes upon severe high temperature (973 K) treatments. For sublimed Fe/ZSM-5, the largest fraction of iron is located on the external surface as Fe_2O_3 aggregates, the remaining fraction being retained in the micropore space as neutral iron oxide nano-particles and as charge-compensating complexes. In our case, a combination of [57]Fe Mössbauer spectroscopy and low-temperature nitrous oxide decomposition indicated that the number of sites active in nitrous oxide activation is quite low and appears to relate to Fe^{2+} centers obtained after exposure to high-vacuum conditions at room temperature (chapter 2). Severe treatment of Fe/ZSM-5 results in an increase of such centers. Moreover, a crude analysis shows that about one oxygen atom

from nitrous oxide is deposited per two Fe^{2+} centers, providing some further clue to the binuclear nature of these active sites. The sintering of the prevailing iron oxide phase under such conditions is nevertheless observed by TEM and corroborated by EXAFS measurements which show that these phases become more ordered. This stresses our conclusion that only a minor fraction of iron is active in nitrous oxide activation.

This chapter includes the decomposition of nitrous oxide on various catalysts and aims to correlate the structure of the active sites with the catalytic performances. Since the ability to activate nitrous oxide has been related to the selective conversion of benzene to phenol (19), we also want to compare the catalytic activities of the present set of sublimed catalysts for this reaction. Commercially available HZSM-5, intensively used to study the selective oxidation to phenol in the literature and in our case with an iron content of 240 ppm, is also employed for the sake of comparison in calcined and steamed form. Finally, in view of the intense debate on the active sites and the speculations that for NO reduction also binuclear clusters are important, we also studied the catalysts prepared by sublimation for the catalytic reduction of NO with iso-butane.

3.2 Experimental

The experimental setup for evaluating catalyst activity in the decomposition of nitrous oxide, benzene oxidation by N_2O to phenol and selective catalytic reduction of NO by iso-butane is schematically shown by figure1. It consists of a gas mixing section, a reactor and a gas analysis section.
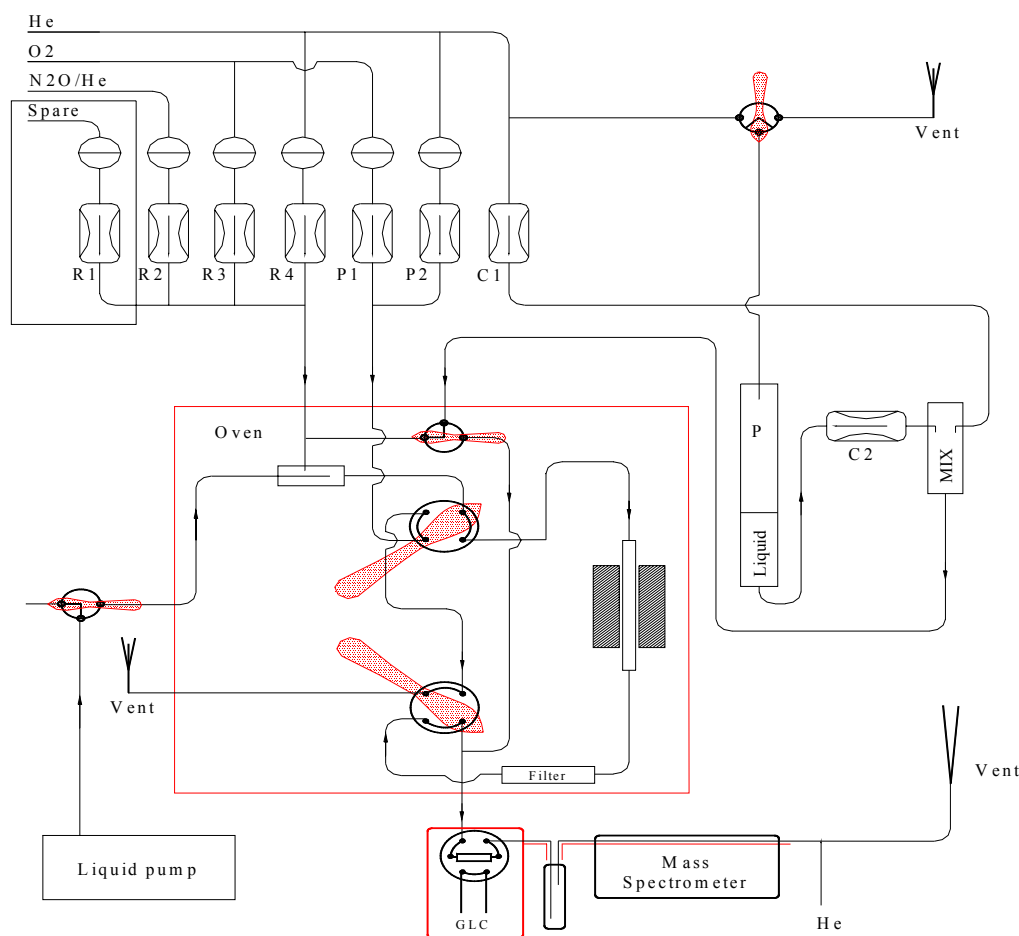
Figure 1: Schematic layout of the setup for the various reactions.

Reactant gas flow rates were controlled by mass flow controllers. The catalyst bed was located in the middle part of a quartz tube reactor with inner diameter of 4 mm and was held in place with quartz wool. A certain amount of Fe/ZSM-5, typically 0.04 g - 0.1 g (sieve fraction 125 μm –425 μm), was diluted with SiC to fulfil plug flow requirements. SiC did not show any activity for the indicated reactions. The total pressure in the reactor was near atmospheric and partial pressures of the reactants were varied by changing the individual flow rates. An extra thermocouple is located in the middle of the catalyst bed to calibrate the real reaction temperature.

N_2O decomposition

Reaction data were collected using a plug flow reactor and a well-calibrated online quadrupole mass spectrometer (MS, Balzers TPG215) was applied as the analyzing equipment. Typically, 3500 ppm or 5000 ppm N_2O/He was used as feed gas. A bypass

allowed the measurement of both feed gas and outlet products, using $m/e = 44$ for N_2O, $m/e = 28$ for N_2, $m/e = 32$ for O_2, $m/e = 4$ for He. Additionally, $m/e = 30$ for NO and $m/e = 46$ for NO_2 were applied and all the fragmentations were fully considered.

Benzene oxidation to phenol with N_2O as oxidant

Benzene was fed to the reaction feed mixture by a liquid mass flow controller (Bronkhorst). The final feed mixture contained 1 vol.% benzene, 4 vol.% nitrous oxide in He. at a total flow rate of 100 ml.min^{-1}. The gas hourly space velocity was 30000 h^{-1}. The tubing of the reaction system was heated to avoid condensation of heavy product molecules to guarantee their detection. The gas phase composition was determined by a combination of on-line gas chromatography (Hewlett-Packard GC-5890equipped with an OV1 column, FID) and a mass spectrometer system (Balzers TPG-420). The products included benzene, phenol, water, carbon monoxide and carbon dioxide. We calculated the nitrous oxide and benzene conversions, the nitrous oxide selectivity (the fraction of oxygen atoms from nitrous oxide incorporated in phenol), the benzene selectivity (the fraction of benzene converted to phenol) and the phenol productivity. The carbon and nitrogen mass balances closed at 98% and 99%, respectively.

SCR of NO by iso-butane

Reduction of NO by iso-butane was carried out by feeding a mixture of 0.2 vol.% NO, 0.2 vol.% iso-butane, 3 vol.% O_2 in He to the catalytic reactor. The total volumetric flow rate was 200 ml·min^{-1}, while a gas space hourly velocity of 42000 h^{-1} was adopted to compare the results with other groups (2,4). The temperature dependence of the reaction was tested in the following manner: a typical reaction was performed for 4 h while analyzing the reactor effluent continuously by MS and every 10 min by GC analysis. Subsequently, the catalyst was cooled to room temperature under a helium flow. The catalyst was recalcined by the O_2/He at 823K and tested again. During the calcination of spent catalyst, carbon monoxide, carbon dioxide and water were detected. Repetitive activity experiments at 673 K ensured that this procedure led to the regeneration of the initial catalyst.

3.3 Results

Decomposition of nitrous oxide
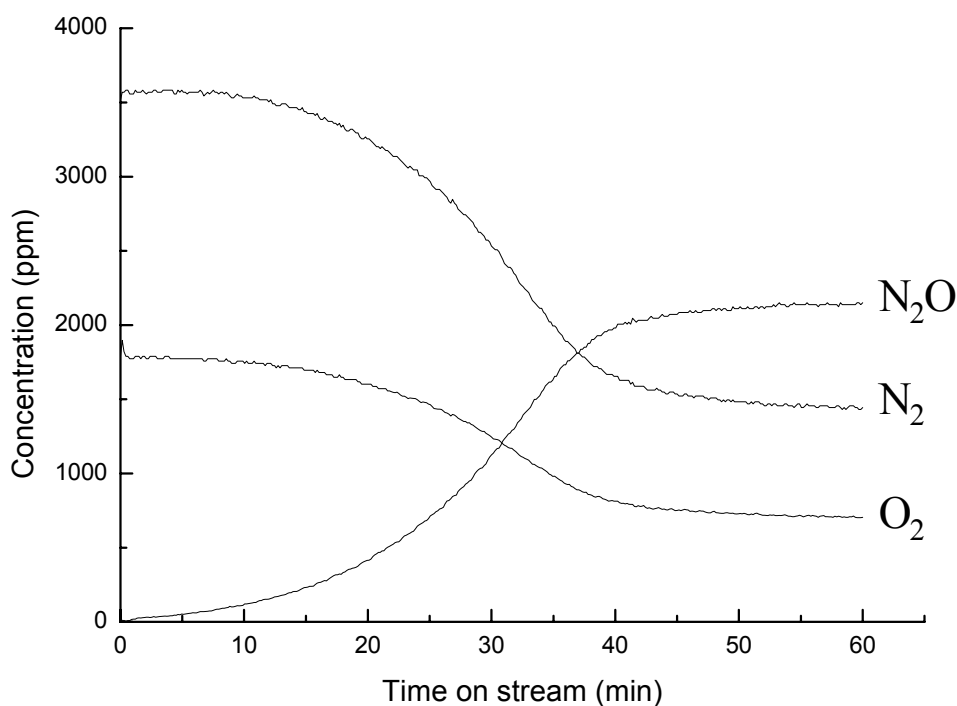
Figure 2: Concentration of N_2O, N_2 and O_2 during N_2O decomposition over Fe/ZSM-5

We observed that there is a strong initial deactivation of the N_2O decomposition activity over the sublimed catalysts. Figure 2 displays the gas-phase concentrations as a function of time-on-stream for a typical reaction over Fe/ZSM-5. The reaction temperature is 698 K, while the feed concentration is 3500 ppm at a GHSV of 24000 h^{-1}. The catalyst is treated in He at 698 K for 30 min prior to reaction. Clearly, a strong decrease is observed followed by a steady-state regime after approximately 0.7 h. Whereas the decomposition of nitrous oxide results in the stoichiometric production of molecular nitrogen and oxygen of 2:1 in the reaction process, the intial deactivation suggests the presence of highly active species in the initial stage. It was ascertained that neither NO nor NO_2 was produced. Thus, it follows that the deactivation is related to the irreversible deposition of oxygen from nitrous oxide on the iron oxide phase. The amount of oxygen deposited strongly depends on the reaction temperature and generally an increase with reaction temperature was found. Note that such a deactivation phenomenon is a common observation for all the Fe/ZSM-5 prepared by the

sublimation method regardless of the pre-treatments (high-temperature calcination or steaming).
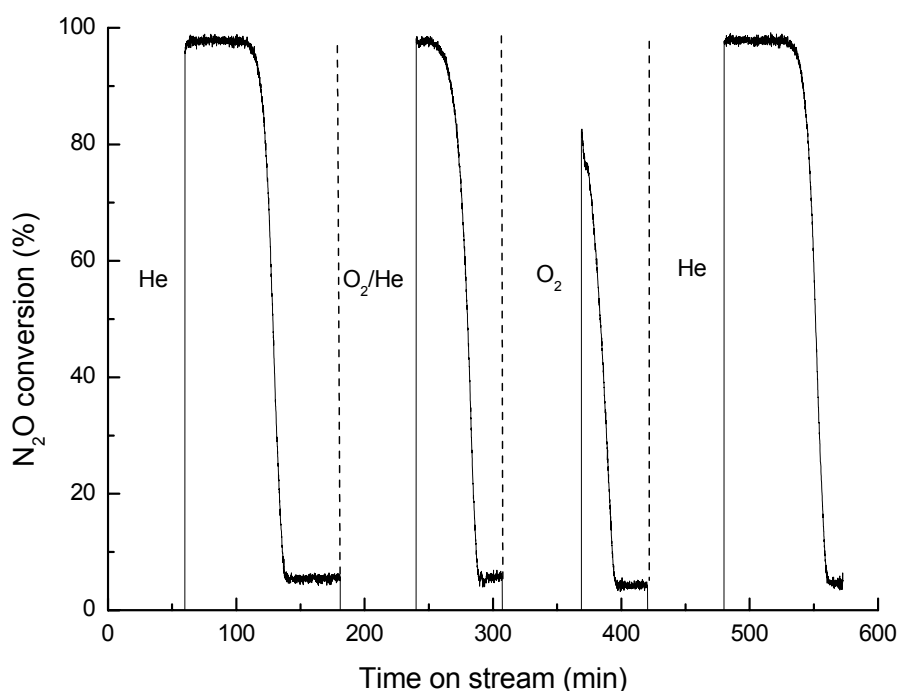
Figure 3: Deactivation of Fe/ZSM-5(HTS) with various intermittent regeneration procedures. Regeneration was carried out at the reaction temperatures of 658 K by exposure to a flow (100 ml·min^{-1}) of the indicated gases.

To obtain further insight into this deactivation, Fe/ZSM-5(HTS) was exposed to a He flow of 100 ml.min^{-1} for 1 h at 823 K prior to the reaction. The reaction was carried out at 658 K, the initial N$_2$O concentration is 5000 ppm at a GHSV of 30000 h^{-1}. Figure 3 shows the resulting activities as a function of time. Similar to figure 2, a deactivation process is observed for about 80 min before the reaction reaches the steady-state condition when the catalyst is pre-treated in He atmosphere. However, after the catalyst was treated in 20vol.% O$_2$/He (100 ml·min^{-1}) for 1 h at the reaction temperature and subsequently exposed to the reactant, deactivation takes place for *ca.* 50 min. When the catalyst is treated in pure O$_2$ (100 ml·min^{-1}) instead of O$_2$/He, the deactivation time is reduced to 30 min, although the final steady conversions are the same in all cases. In addition, after the catalyst is exposed to He (100 ml·min^{-1}) again for 1 h, the initial deactivation is completely reproduced to *ca.* 80 min. We conclude that this deactivation is related to the oxidation state of certain Fe species and that this strongly depends on the pre-treatment procedure.
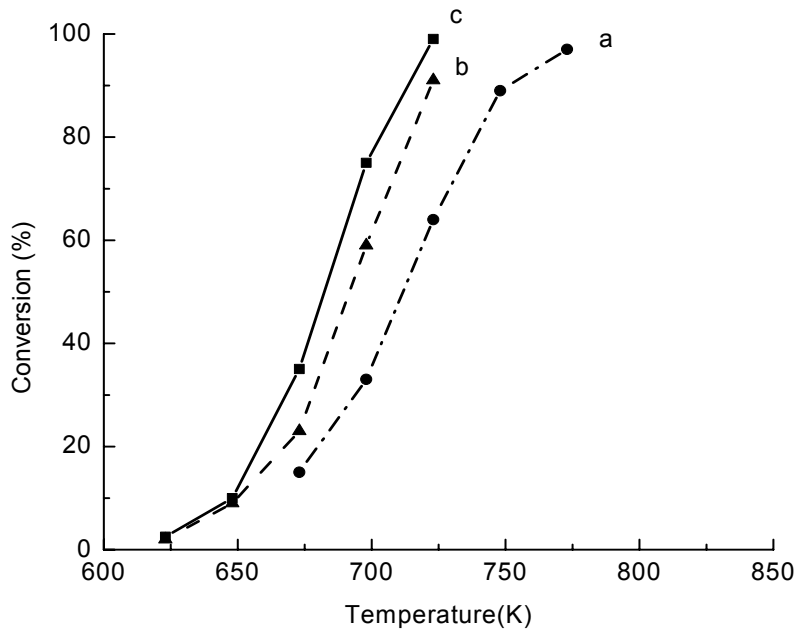
Figure 4: N_2O decomposition over Fe/ZSM-5.Feed concentration: 3500 ppm N_2O, GHSV=24000 h^{-1} (a)Fe/ZSM-5, (b) Fe/ZSM-5(HTC), (c) Fe/ZSM-5(HTS).

Figures 4 shows the steady-state conversion of N_2O decomposition over various Fe/ZSM-5 catalysts as a function of temperature. The conversion increases with increasing temperature. For Fe/ZSM-5, the conversion reaches 100% at 773 K. Further treatment (high-temperature calcination or steaming) increases the catalytic activity. For Fe/ZSM-5 (HTS) the N_2O decomposition starts at around 623K and full conversion is found at 723 K. Similar effects of high-temperature calcination or steaming was observed for Fe/ZSM-5 with Si to Al ratio of 30 (not shown).

The rate of N_2O decomposition can be written as

$$r = kP_{N_2O}{}^n = Ae^{-\frac{E_a}{RT}}P_{N_2O}{}^n$$

Our results (not shown) and other investigators' results indicate that the N_2O decomposition is first order in N_2O (n = 1) (37). Arrhenius plots for the N_2O decomposition over Fe/ZSM-5 are shown in figure 5. The apparent activation energies and ln A (apparent pre-exponential factor) for various catalysts given in table 1.
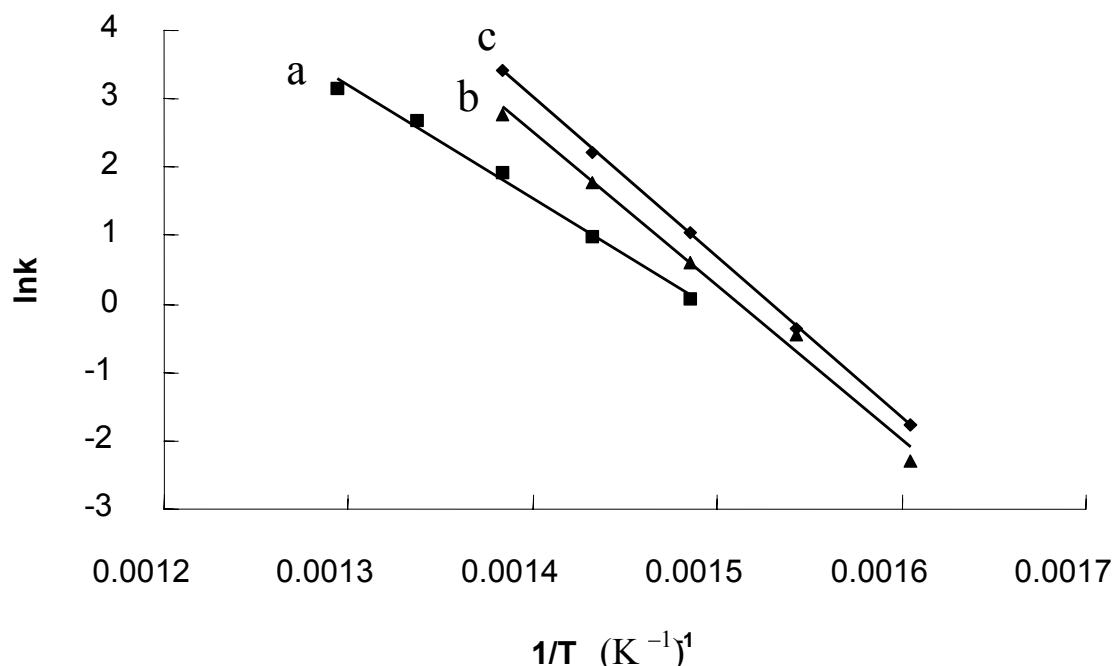
Figure 5: Arrhenius plot of N_2O decomposition over various Fe/ZSM-5,
(a) Fe/ZSM-5, (b) Fe/ZSM-5(HTC) and (c) Fe/ZSM-5(HTS).

The apparent activation energy of the Fe/ZSM-5 catalyst is approximately 136 kJ/mol. However, after high-temperature calcination or steaming, the apparent energies increase to 186 and 213 kJ/mol, respectively. Simultaneously, the apparent pre-exponential factor increases in the order of around 10^4-10^5. The higher activity is thus explained by the compensation effect, resulting from an increase of pre-exponential factor. It is worth pointing out that the apparent activation energy includes the contribution of all the elemental reaction steps involved in the N_2O decomposition.

Table 1: Kinetic parameters for N_2O decomposition in the various Fe/ZSM-5

	Fe/ZSM-5	*Fe/ZSM-5(HTC)*	Fe/ZSM-5(HTS)
Ln A (A: s^{-1})	24.5	33.8	35.8
E_a (kJ/mol)	136	186	205

In addition to the influence of high-temperature pre-treatment on the catalytic performance of Fe/ZSM-5 in the decomposition of nitrous oxide, the impact of water vapor on the Fe

species was studied. Figure 6 shows the nitrous oxide conversion over Fe/ZSM-5 as a function of various pre-treatment procedures.. Calcination at relatively high temperature (973 K) of the original Fe/ZSM-5 material efficiently increases the activity in N_2O decomposition as shown in figure 6. Exposure to 10% water vapor at 773 K lowers the catalytic activity substantially. Repeated treatments show that the behavior is reversible although a small, but significant increase in activity is noted (15).
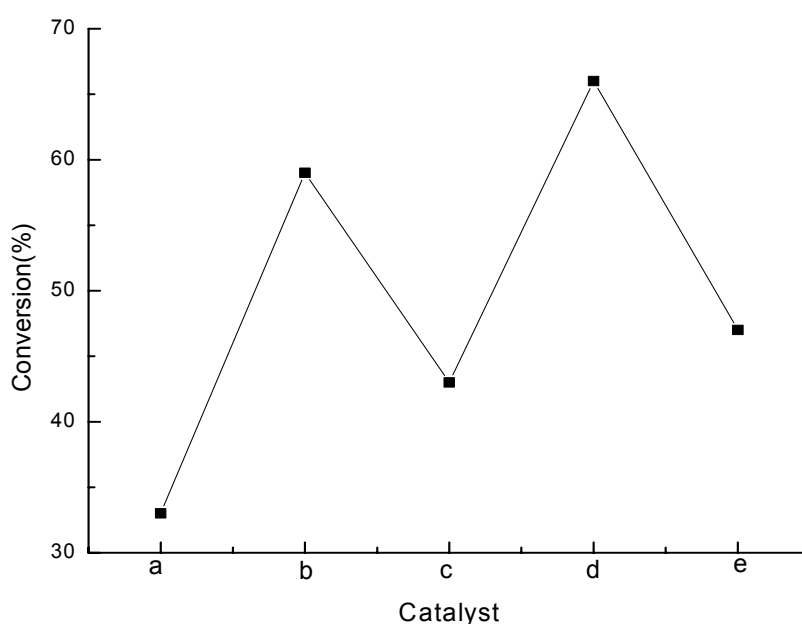
Figure 6: N_2O decomposition over various Fe/ZSM-5 catalysts, (3500 ppm N_2O at GHSV of 24000 h^{-1}, 698 K): (a) Fe/ZSM-5, (B) after calcination at 973 K (20% O_2 in He), (c) after treatment in water vapor at 773 K (10% H_2O/He), (d) after calcination at 973 K (20% O_2 in He), (E) D after treatment in water vapor at 773 K (10%H_2O/He).

Infrared spectra of the various Fe/ZSM-5 catalysts are presented in figure 7. The band at 3613 cm^{-1} is the stretching vibration of the Brønsted hydroxyl groups, while the band at 3745 cm^{-1} relates to the vibrations of terminal Si-OH groups. Generally, the band at 3665 cm^{-1} is assigned to the hydroxyl groups connected to extra-framework aluminium. After preparation of original Fe/ZSM-5, about 55% Brønsted acid sites of the parent zeolite (chapter 2) are replaced by cationic Fe species. After high-temperature calcination, only around 10% of the Brønsted acid sites remain. After the first water treatment, the Brønsted acid sites are restored to about 25%. Further high-temperature calcination and further water vapor treatment lead to similar disappearance and reappearance of Brønsted acid sites, although we note that the activity after both types of treatment appears to increase.

The disappearance of Brønsted acid sites might be caused by the removal of framework aluminum. After water vapor treatment, we indeed observe a very small increase of the hydroxyl group that is associated with the extra-framework aluminium (band at 3665 cm^{-1}). This is in line with our earlier observation that significant framework aluminium extraction is only induced by high temperature water treatment (chapter 2). Moreover, high-temperature calcination of the parent zeolite HZSM-5 only shows a slight decrease (5%) of Brønsted hydroxyl groups. The recovery of Brønsted acid sites strongly indicates that dealumination is not of overriding importance. We conclude that the drastic decrease of the number of zeolite protons is induced by the reaction with Fe-oxide species occluded in the zeolite micropores.
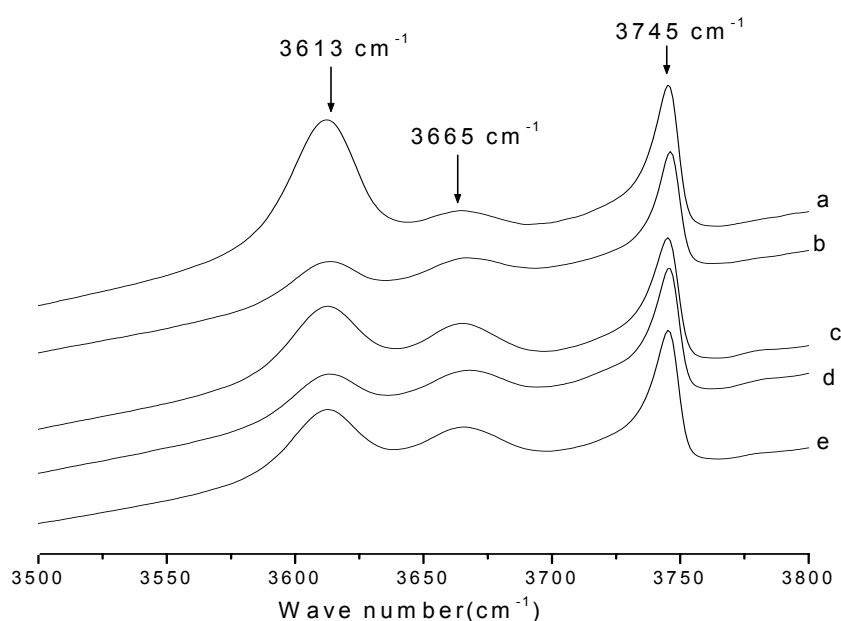
Figure 7: IR spectra of various Fe/ZSM-5 catalysts: (a) Fe/ZSM-5, (B) after calcination at 973 K (20% O$_2$ in He), (c) after treatment in water vapor at 773 K (10% H$_2$O/He), (d) after calcination at 973 K (20% O$_2$ in He), (E) D after treatment in water vapor at 773 K (10%H$_2$O/He).

The applied preparation method excludes the possibility of Fe at framework positions. Fe species are either present as cationic species counterbalancing the negative charge of zeolite framework or as Fe-oxide clusters. These latter clusters may present themselves as agglomerates at the external surface and as occluded nano-clusters. We capture the present data in an oversimplified reaction mechanism (14,15),

$$Fe_xO_y + 2(y-x)\ H \underset{773\ K}{\overset{973\ K}{\rightleftharpoons}} x\ [FeO]^+ + (y-x)H_2O$$
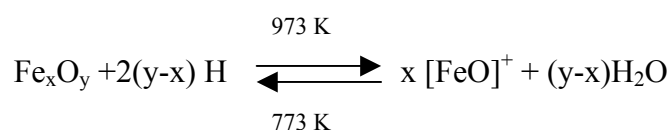
where neutral Fe-oxide clusters can react at elevated temperatures with zeolitic protons to cationic Fe species. The specific nature of the proposed species remains to be determined. Upon water treatment cationic Fe species are transformed again in Fe-oxide species, thus explaining the reappearance of Brønsted acid sites. In essence, our results indicate that such cationic species are more active in the decomposition of nitrous oxide. Moreover, the small amount of extraction of Al from the framework in the high-temperature treatments or water treatments might also play a role the enhancements of the N_2O decomposition rate. It is noteworthy that the Fe-oxide cluster not only reacts with the bridging hydroxyl groups, but also with the hydroxyl group that is associated with the extra-framework aluminum, displaying similar reversible chemistry.
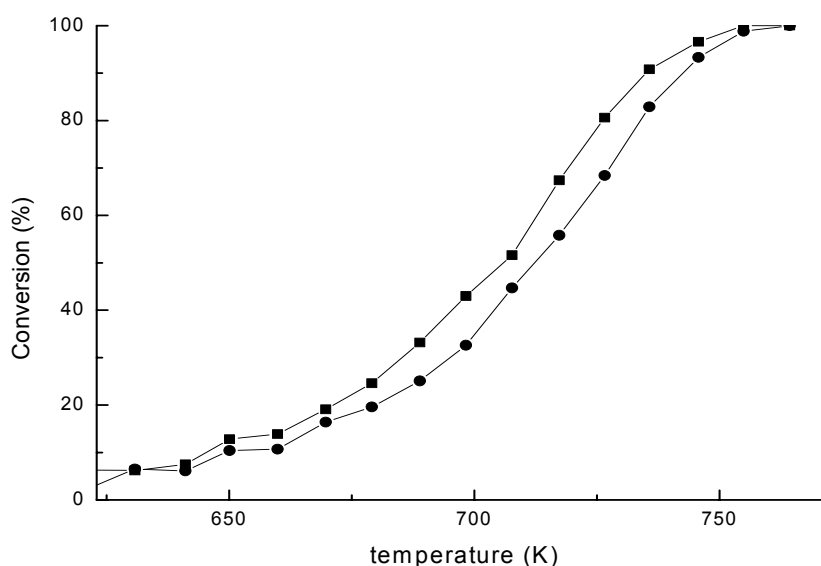
Figure 8: N_2O decomposition over Fe/ZSM-5, performed in using an industrial feed for (●) Fe/ZSM-5, (■) Fe/ZSM-5(HTS).

To evaluate whether the beneficial effect of steaming on the performance of Fe/ZSM-5 is retained under conditions which are relevant to the removal of nitrous oxide from tail gases of nitric acid plants, Fe/ZSM-5 and Fe/ZSM-5(HTS) were tested in nitrous oxide decomposition in the presence of nitrogen oxide, water and oxygen (simulated tail gas). These experiments were carried out at ECN (Energieonderzoek Centrum Nederland). To this end, 190 mg of catalyst was exposed to a reaction feed mixture (1500 ppm N_2O, 200 ppm NO, 0.5 vol.% H_2O, 2.5 vol.% O_2 and balance N_2) at a flow rate of 150 ml·min^{-1}. The reaction data (figure 8) show a substantial increase of the activity although the effect is less pronounced compared to the case where the feed does not contain water, oxygen and NO

(figure 4). While it has been suggested that NO facilitates the decomposition of N_2O, the presence of water which competitively adsorbs on the active centers with nitrous oxide can explain the lower activity (38). Moreover, based on the model derived from figure 6 the conversion of the highly active iron cationic species to less active centers by hydrolysis may also play a role. This is further exemplified in figure 9 showing the strongly negative effect of water addition to the nitrous oxide feed. In this case, we observed quantitative conversion of nitrous oxide at 773 K. Addition of 10 vol.% water vapor clearly results in a strong decrease of the activity.
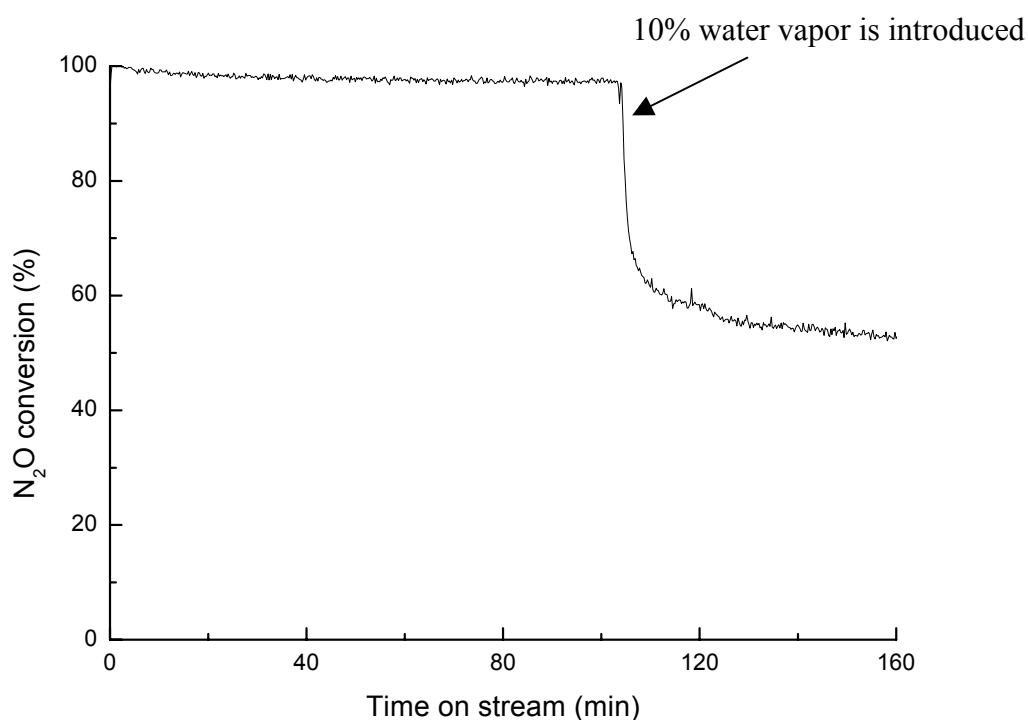
Figure 9: N_2O decomposition over Fe/ZSM-5, reaction temperature: 773 K, feed concentration: 3500 ppm N_2O in He, GHSV: 24000 h^{-1}
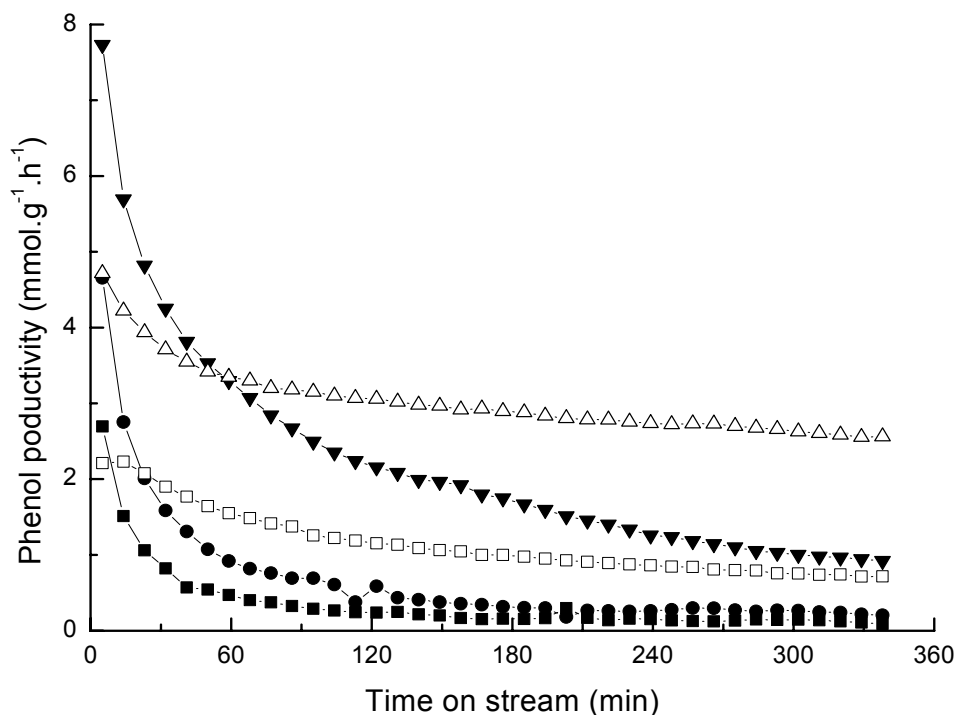
Figure 10: Oxidation of benzene to phenol with N_2O over various catalysts, Reaction temperature: 623 K, Gas composition: 1% benzene, 4% N_2O, 95% He, GHSV: 30000 h^{-1}, (■) Fe/ZSM-5, (●) Fe/ZSM-5(HTC), (▼)Fe/ZSM-5(HTS), (□)HZSM-5, (Δ)HZSM-5(HTS).

The phenol productivities as a function of the time-on-stream for the Fe/ZSM-5 catalysts,the parent HZSM-5 and HZSM-5(HTS) are shown in figure 10. Benzene was not found to be consumed in the absence of N_2O. Clearly, the initial activity is highest for the steamed material, Fe/ZSM-5(HTS). The initial activities amongst the sublimed catalysts decrease in the order: Fe/ZSM-5(HTS) > Fe/ZSM-5(HTC) > Fe/ZSM-5. The deactivation is relatively strong for these catalysts. HZSM-5(HTS) shows a somewhat lower initial activity than Fe/ZSM-5(HTS), but it exhibits the highest phenol productivity after prolonged reaction times. Moreover, HZSM-5 displays similar catalytic behaviour as HZSM-5(HTS) although both the initial catalytic activity and the steady-state activity are lower. Note that the zeolites to which with Fe has been added show higher initial activities than their HZSM-5 counterparts which proves the Fe presence is essential for the active sites. Deactivation is due to coke formation as indicated by the black color of the sample after reaction and more importantly, by the fact that its initial activity can be restored by oxidation with oxygen under the formation of CO_x and water. Although HZSM-5(HTS) shows an initial phenol

productivity similar to Fe/ZSM-5(HTC) after a reaction time of 5 min, the difference in deactivation rates suggests that the initial activity of the latter catalyst is much higher. A tentative explanation for the difference in deactivation behaviour relates to the overoxidation of the initially formed products in samples with a higher number of active sites resulting in the formation of condensed (multi) ring systems (39).

Table 2: Benzene conversion and selectivity to phenol with oxidant N_2O at 623K, Component: 4% N_2O, 1% benzene diluted in He, GHSV: 30000 h^{-1}.

	Conversion(%)				Selectivity(%)			
	5 min	1 h	3 h	5h	5 min	1 h	3 h	5h
Fe/ZSM-5	23	11	11	10	47	18	6	6
Fe/ZSM-5(HTC)	32	14	12	13	60	27	10	9
Fe/ZSM-5(HTS)	35	15	7	6	87	93	94	98
HZSM-5	17	7	4	4	53	90	98	97
HZSM-5(HTS)	20	13	10	9	>98	>98	>98	>98
Fe/SiO$_2$	0	0	0	0	0	0	0	0

Table 3: N_2O conversion and selectivity to phenol with oxidant N_2O at 623K. Component: 4% N_2O, 1% benzene diluted in He .GHSV: 30000 h^{-1}

	Conversion(%)				Selectivity(%)			
	5 min	1 h	3 h	5h	5 min	1 h	3 h	5h
Fe/ZSM-5	34	28	34	35	8	2	0.5	0.4
Fe/ZSM-5(HTC)	35	42	45	51	14	2	0.7	0.5
Fe/ZSM-5(HTS)	20	6	3	3	40	58	60	60
HZSM-5	4	2	2	2	57	82	57	35
HZSM-5(HTS)	5	3	3	2	>98	>98	>98	>98
Fe/SiO$_2$	0	0	0	0	0	0	0	0

Table 2 and 3 list the benzene and nitrous oxide conversions and selectivities, respectively. The results for the conversion and selectivity of nitrous oxide (measured by mass spectrometer analysis) corroborate well with those of benzene and phenol (measured by gas chromatography analysis). The initial benzene conversion for Fe/ZSM-5(HTS) is around 35% with a benzene selectivity around 90%. In contrast to HZSM-5(HTS), the nitrous oxide selectivity to phenol of Fe/ZSM-5(HTS) is relatively low and considerable amounts of CO, CO_2 and H_2O are detected. With increasing reaction time, phenol is almost selectively produced from benzene for this catalyst, although the remaining phenol productivity is only 1.0 mmol.g^{-1}.h^{-1}. Interestingly, large differences in benzene selectivities to phenol are observed between the various catalysts. HZSM-5 exhibits an initial benzene selectivity around 50% which increases to nearly 90% within 1 h while HZSM-5(HTS) has an initial selectivity close to 100%. Most importantly, the steaming enhances the selectivity of benzene

to phenol over Fe/ZSM-5(HTS) whereas the conversion of benzene does not increase. Indeed, the conversion of benzene is even lower that that of unsteamed Fe/ZSM-5 counterparts. The efficiency of steaming is thus mainly attributed to the enhancement of selectivity. On the other hand, the nitrous oxide selectivity towards phenol is below 60% after 1 h for the Fe/ZSM-5 catalysts implying that the build-up of some coke products on the catalyst surface. The absence of carbon monoxide, carbon dioxide and water at the start of the reaction confirms this suggestion. At higher reaction times, especially Fe/ZSM-5 and Fe/ZSM-5(HTC) produce large a amounts of combustion products. We observed no activity for Fe/SiO$_2$.
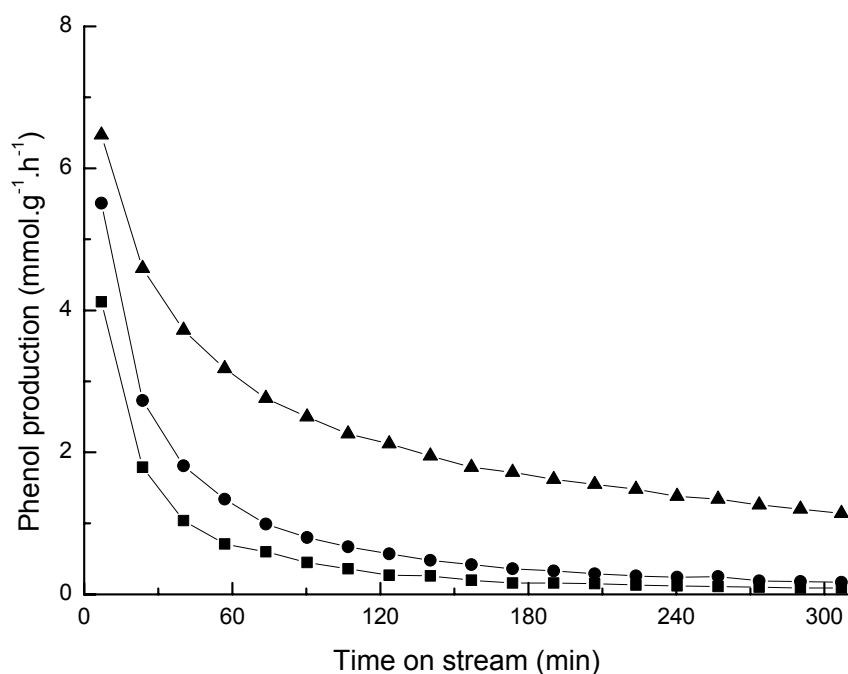
Figure 11: Oxidation of benzene to phenol with N$_2$O as oxidant over various catalysts. Reaction temperature: 633 K, Gas composition: 6.5% benzene, 0.065% N$_2$O, 93.3% He, GHSV: 30000 h^{-1}, (■)Fe/ZSM-5, (●) Fe/ZSM-5(HTC), (▲)Fe/ZSM-5(HTS).

The benzene hydroxylation to phenol was also carried out over various catalysts in the group of Panov (Novosibirsk, Russia). The feed components adopted are excess benzene content (6.5 %) and relatively low N$_2$O concentration (0.065 %) balanced by He. The reaction temperature is 633 K. Figure 11 shows the phenol yield as a function of time on stream over various catalysts. Compared with figure 10, the activity sequence is the same, i.e. Fe/ZSM-5(HTS) > Fe/ZSM-5(HTC) > FeZSM-5. The main difference between the two sets

of experiments is that the stable activities of the Fe/ZSM-5 studied in excess benzene are slightly higher than those in excess N_2O. Interestingly, although the reactant mixture varies from excess benzene to excess N_2O, the initial productivities are found to be similar.

SCR of NO by iso-butane
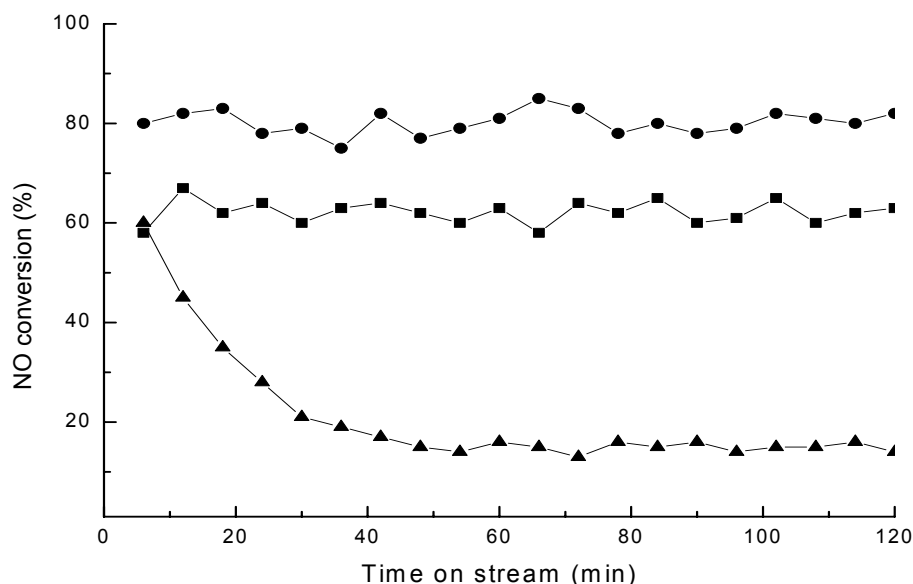
Figure 12: NO conversion as function of time on stream. Reaction temperature: 623 K, Gas composition: 0.2%NO; 3% O_2; 0.2%C_4H_8; GHSV: 42000 h^{-1}, (■)Fe/ZSM-5, (●)Fe/ZSM-5(HTC), (▲)Fe/ZSM-5(HTS).

The conversion of NO versus the time-on-stream for the various catalysts at a reaction temperature of 623 K is plotted in figure 12. For Fe/ZSM-5, we observe a stable conversion as a function of the time-on-stream. Also for Fe/ZSM-5(HTC), a stable NO conversion is obtained. The high-temperature calcined sample has a somewhat higher activity. Interestingly, the steamed material shows a strong deactivation with time-on-stream. Whereas the initial conversion is close to that for Fe/ZSM-5, a stable activity is obtained after 40 min with a remaining conversion of about 20%, considerably lower than those of the other catalysts.

Figure 13: NO conversion as function of temperature over various Fe/ZSM-5.
Gas composition: 0.2 % NO ; 3 % O_2; 0.2 % C_4H_8; GHSV: 42000 h^{-1} (■)Fe/ZSM-5, (●)Fe/ZSM-5(HTC), (▲)Fe/ZSM-5(HTS).

The temperature dependence of the conversion of NO and *i*-butane into N_2, H_2O and CO_2 for the various catalysts is plotted in figure 13 and figure 14, respectively. The light-off temperature of the NO reduction is around 523 K. With increasing temperature, the NO conversion increases and a maximum is found for all three catalysts. This is largely in accordance with the results reported by the group of Sachtler (4,30,40-45), although we find a somewhat lower maximum NO conversion for Fe/ZSM-5. Amongst the sublimed catalysts in this study, the maximum in activity is identified at a temperature of 623 K for the high-temperature calcined Fe/ZSM-5. At this temperature, the steamed sample has the lowest activity. On the other hand, the steamed sample has its maximum in activity around 673 K where it is the most active catalyst. At low temperature at 523 K, the activities decrease in the order: Fe/ZSM-5 > Fe/ZSM-5(HTC) > Fe/ZSM-5(HTS). Remarkable differences were observed at relatively high temperature of 623 K where the Fe/ZSM-5(HTC) shows the best catalytic performance. The activities all decrease drastically as the reaction temperature is increased to 723 K.
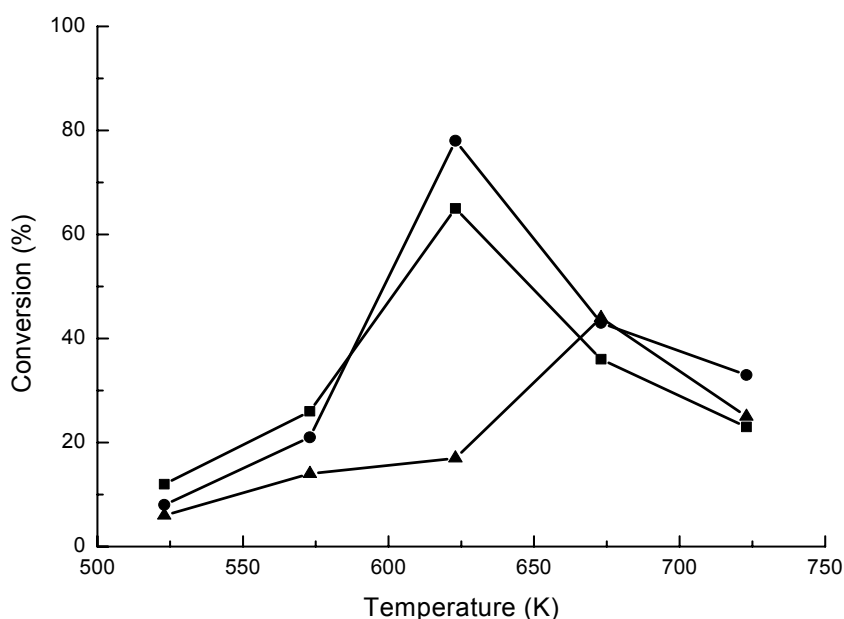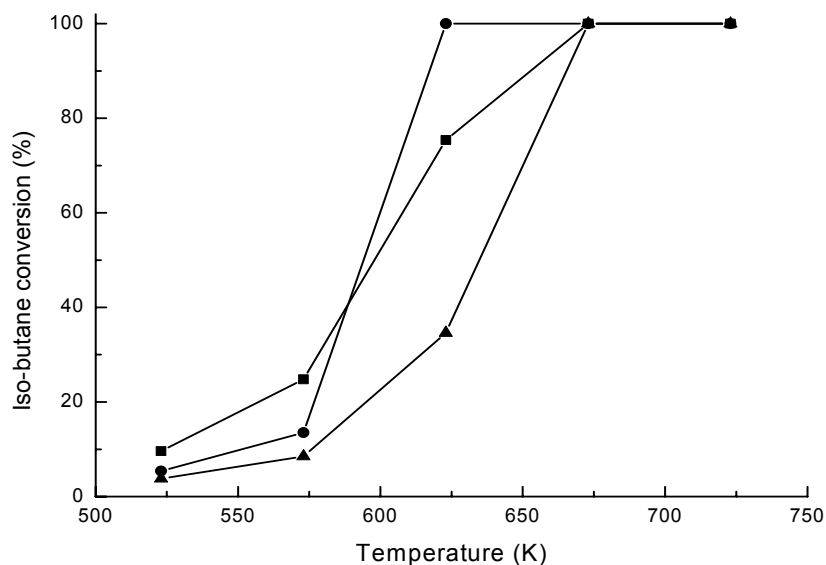
Figure 14: Iso-butane conversion as function of temperature over various Fe/ZSM-5. Gas composition: 0.2 % NO ; 3 % O_2; 0.2 % C_4H_8; GHSV: 42000h^{-1}. (■)Fe/ZSM-5, (●)Fe/ZSM-5(HTC), (▲)Fe/ZSM-5(HTS).

Figure 14 can be used to interpret the oxidation of iso-butane over various Fe/ZSM-5. The selective catalytic reduction of NO and the combustion of iso-butane by O_2 take place simultaneously. The latter reaction is probably not relevant at relatively low temperatures because we observe that the order of conversion of iso-butane corresponds to order for the NO conversion. This indicates that the SCR reaction is dominant in this temperature range. Whereas Fe/ZSM-5 is most active at relatively low temperature, the situation is different above 623 K. The NO conversion goes through a maximum and at higher temperatures oxidation of iso-butane by molecular oxygen prevails. Clearly, the activity of Fe/ZSM-5(HTC) is highest in this regime. Although the SCR of the NO still contributes to the consumption of iso-butane, full conversion of hydrocarbons over all catalysts clearly points to the oxidation of the iso-butane by O_2.

3.4 Discussion

The present activity data for nitrous oxide decomposition, benzene oxidation and selective reduction of NO by iso-butane clearly show the influence of the pre-treatment of Fe/ZSM-5 as well as the choice of reactants. These materials have been extensively characterized

(chapter 2). We have concluded that Fe/ZSM-5 prepared by sublimation method and its counterparts treated by high-temperature calcination or steaming result in various iron oxide species, underpinning the heterogeneous nature of these samples. In our opinion, there are at least two kinds of transformations of Fe species: (i) the protolysis of neutral Fe nanoparticles in the micropores of zeolites at high temperature treatment; (ii) the formation of Fe-Al-O clusters with dislodged Al (chapter 4 and 5). We forward that these cationic species and Fe-Al-O clusters are both active in the decomposition of nitrous oxide. The mechanism on these two sites may be different which is underlined by the large changes in apparent activation energy and pre-exponential factor comparing calcined, high-temperature calcined and high-temperature steamed catalysts. The number of cationic species is increased by a protolysis reaction between small-occluded iron oxide particles and Brønsted acid sites. This reaction is reversible under hydrothermal conditions at relatively low temperature, leading to the hydrolysis of the cationic species and regeneration of the charge-compensating protons. We surmise that repetitive high-temperature calcination/hydrolysis treatments will lead to extraction of some Al species. This process is not reversible. These extra-framework Al species can further react with extra-framework Fe-Al-O species which appear to be active in the nitrous oxide decomposition also. Steaming of Fe/ZSM-5 results in a considerable loss of framework Al which then forms active Fe-Al-O species.

Notably, we observe a strong deactivation process in the nitrous oxide decomposition experiments over the Fe/ZSM-5 materials. This deactivation is related to Fe species that are readily oxidized by molecular oxygen as derived from the dependence of their number on the oxygen partial pressure during pretreatment (figure 3). The amounts of oxygen deposited from nitrous oxide in this deactivation period are much larger than the values reported for low-temperature nitrous oxide decomposition (chapter 2). Moreover, the group of Panov forwarded that Fe^{2+} centers created upon high-temperature activation in FeZSM-5 and active in catalytic nitrous oxide decomposition can not be reoxidized by molecular oxygen, possibly due to structural relaxation after the initial loss of molecular oxygen (23-27). We strongly believe that the deactivating species are Fe^{2+} centers resulting from auto-reduction of iron oxide particles. These are present as small nanometric oxide particles in the micropores and as aggregates on the external surface. The deactivation thus leads to the irreversible deposition of oxygen atoms under oxidative conditions. The steady-state activities pertain to the catalytic centers that are able to decompose nitrous oxide. These include cationic species and extra-framework Fe-Al-O species wheareas it is reported N_2O also decomposes into N_2 and O_2 over Fe-silicalite (46).   Our study confirms that sublimation of $FeCl_3$ onto HZSM-5

zeolite is not the preferred preparation method for effective catalysts for benzene oxidation to phenol.   In contrast to the conclusion that both cationic Fe species and Fe-Al-O are responsible for the N_2O decomposition, the significant increase of the phenol productivity and the increase of the selectivity to nearly 100% for Fe/ZSM-5(HTS) indicate there is a strong synergistic effect between the Fe and extra-framework Al dislodged from framework during steaming. As will be extensively outlined in chapters 4 and 5, this leads to the extensive formation of Fe-Al-O species which are thought to be the sites capable of converting benzene and nitrous oxide selectively to phenol. The higher contribution of the full combustion route in Fe/ZSM-5 and Fe/ZSM-5(HTC) most probably relates to the higher fraction of cationic Fe species and/or small iron oxide particles.   HZSM-5 and HZSM-5(HTS) show similar catalytic behavior. The activity is related to the presence of about 0.024 wt.% Fe in the zeolite starting material, rather than to Brønsted acid sites or extra-framework Al sites. This proposal will be further elucidated in chapter 4. Part of the Fe impurity is located at extra-framework positions (chapter 2) and it is argued that this leads together with a small fraction of dislodged Al to a small number of Fe-Al-O species. The higher activity of the steamed sample is related to additional extraction of Fe and Al from framework positions. We surmise that the extraction of Al is more important in this process. The higher initial activity of Fe/ZSM-5(HTS) compared to that of HZSM-5 (HTS) points to the importance of iron as a component in the active sites. The better stability of HZSM-5 compared to the most active steamed material is noted. A very simple model indicates that overoxidation of phenol leads to multiply hydroxylated compounds and/or multiring products that cannot desorb from the zeolite micropores (39). A higher amount of active sites thus leads to a higher initial activity but also induces a higher coke make and deactivation rate.   The activity order for the selective reduction of NO by *iso*-butane is totally different from the order of nitrous oxide decomposition and benzene-to-phenol transformation. This strongly suggests that the active sites for nitrous oxide activation are different from those for NO reduction. This is not too surprising in view of the proposed mechanism for the latter reaction (4,30,40-45). The first step consists of the conversion of NO to NO_2 by O_2, followed by the reaction of nitrogen dioxide with carbonaceous deposits when hydrocarbons are the reductants and with NH_4^+ when ammonia is. Although it has been forwarded that this step takes place over cationic iron complexes, we expect that NO_2 formation is not a very structure-sensitive reaction and proceeds over various types of iron species. This appears to agree with the fact that the NO SCR reaction proceeds over a wide range of oxides. The activity order for the present set of catalysts points to the importance of the iron oxide phase dispersion for a high activity in NO

reduction. The growth of these occluded iron oxide particles and migration from the micropores upon severe treatment reduces the number of active sites for NO_2 formation. We surmise that the low activity in the steamed catalyst is due to an imbalance between the formation of carbonaceous deposits and the generation of NO_2 to remove them. This explains the relatively high initial activity which decreases strongly when deposits fill up the pores and block the active sites. Alternatively, the role of Brønsted acid sites may be important since their removal by steaming as shown here or treatment with NaOH strongly decreases the activity for the SCR reaction. The preference for the steamed sample at elevated temperatures, combustion of the hydrocarbon by molecular oxygen being dominant, is probably due to the more open pore architecture of this sample.

3.5 Conclusion

Further calcination or steaming treatment (973 K) of Fe/ZSM-5 prepared by the sublimation method increases the decomposition rate of N_2O. The strong initial deactivation is due to reoxidation of Fe^{2+} centers, generated by auto-reduction of iron oxides at elevated temperatures. Kinetic and characterization data indicate that two species are important for the nitrous oxide decomposition (i) cationic species that can be generated by a protolysis reaction between occluded iron oxide particles and Brønsted acid sites and (ii) extra-framework Fe species that interaction with extra-framework Al sites (Fe-Al-O species). The first species can be transformed back into Brønsted acid sites and iron oxide particles by hydrothermal treatment at relatively low temperature (773 K), while similar treatments at more elevated temperatures lead to the (irreversible) extraction of Al from the framework and the formation of active Fe-Al-O species. Fe/ZSM-5 and Fe/ZSM-5(HTC) exhibit relatively low phenol selecitivies due to significant hydrocarbon combustion. Only the steamed Fe/ZSM-5 produces phenol with high selectivity. The stability of the sublimed samples is relatively low due to the relatively large coke make. Commercial HZSM-5 with an iron content of 0.024 wt.% and its steamed counterpart are also active and provide a higher stability, the latter one exhibiting the highest stable activity. We forward that extra-framework Al sites are involved in the formation of active sites in addition to extra-framework Fe sites, providing an explanation for the necessity of widely reported severe activation treatments. NO reduction by *iso*-butane does not require those sites with the property to activate nitrous oxide at low temperature and dispersed iron oxide nanoparticles appear to be more important, which explains the decrease in activity with increasing severity of treatment.

Reference

1. X. Feng and W.K. Hall, Catal. Lett. 41 (1996) 45.
2. X. Feng and W.K. Hall, J. Catal. 166 (1997) 368.
3. L.J. Lobree, I.-C. Hwang, J.A. Reimer and A.T. Bell, Catal. Lett. 63 (1999) 233.
4. H.-Y. Chen, T. Voskoboinikov and W.M.H. Sachtler, Catal. Today 54 (1999) 483.
5. G. Centi and F. Vazzana, Catal. Today 53 (1999) 683.
6. R.Q. Long and R.T. Yang, J. Am. Chem. Soc. 121 (1999) 5595.
7. R.Q. Long and R.T. Yang, J. Catal. 207 (2002) 224.
8. F. Heinrich, C. Schmidt, E. Löffler, M. Menzel and W. Grünert, J. Catal. 212, (2002) 157.
9. M. Rauscher, K. Kesore, R. Mönning, W. Schweiger, A. Tissler and T. Turek, Appl. Catal. A 184 (1999) 249.
10. El-M. El Malki, R.A. van Santen and W.M.H. Sachtler, Microporous Mesoporous Mat.35-36 (2000) 235.
11. El-M. El-Malki, R.A. van Santen and W.M.H. Sachtler, J. Catal.196 (2000) 212.
12. J. Pérez-Ramírez, F. Kapteijn, G. Mul, X. Xu and J.A. Moulijn, Catal. Today 76 (2002) 55.
13. J. Pérez-Ramírez, F. Kapteijn, G. Mul and J.A. Moulijn, Chem. Commun. (2001) 693.
14. Q. Zhu, B.L. Mojet, R.A.J. Janssen, E.J.M. Hensen, J. Van Grondelle, P.C.M.M. Magusin and R.A. van Santen, Catal. Lett. 81 (2002) 205.
15. Q. Zhu, E.J.M. Hensen, B.L. Mojet, J.H.M.C. van Wolput and R.A. van Santen, Chem. Commun. (2002) 1232.
16. V.I. Sobolev, K.A. Dubkov, E.A. Paukshtis, L.V. Pirutko, M.A. Rodkin, A.S. Kharitonov and G.I. Panov., Appl Catal A 141 (1996) 185.
17. A. Ribera, I.W.C.E. Arends, S. de Vries, J. Pérez-Ramírez and R.A. Sheldon, J. Catal. 195 (2000) 287.
18. P. Kubánek, B. Wichterlová and Z. Sobalík J.Catal. 211 (2002) 109.
19. G.I. Panov, CatTech 4 (2000) 18.
20. A.K. Uriarte, M.A. Rodkin, M.J. Gross, A.S. Kharithonov, G.I. Panov, Stud. Surf. Sci. Catal. 857 (1997) 110.
21. P.B. Venuto, Microporous Mat. 2 (1994) 297.
22. R.Q. Long and R.T. Yang, Chem. Commun. (2000) 1651.
23. G.I. Panov, V.I. Sobolev, K.A. Dubkov, V.N. Parmon, N. S. Ovanesyan, A.E. Shilov and A.A. Shteinman, React.Kinet.Catal.Lett. 61 (1997) 251
24. K.A. Dubkov, V.I. Sobolev, E.P. Talsi, M.A. Rodkin, N.H. Watkins, A.A. Shteinman and G.I. Panov, J. Mol. Catal. 123 (1997) 155
25. G.I. Panov, V.I. Sobolev, K.A. Dubkov and A.S. Kharitonov, Stud. Surf. Sci. Catal. 101 (1996) 493.
26. A.K. Uriarte, M.A. Rodkin, M.J. Gross, A.S. Kharitonov, G.I. Panov, Stud. Surf. Sci. Catal. 110 (1996) 857.
27. G.I. Panov, A.K. Uriarte, M.A. Rodkin, V.I. Sobolev, Catal.Today., 41 (1998) 365.

28. E.J.M. Hensen, Q. Zhu, M.M.R.M. Hendrix, A.R. Overweg, P.J. Kooyman, M.V. Sychev, R.A. van Santen, submitted.

29. A. Dubkov, N.S. Ovanesyan, A.A. Shteinman, K.A. Dubkov, V.I. Sobolov and G.I. Panov, Kinet. Catal. 39 (1998) 792.

30. H.-Y. Chen and W.M.H. Sachtler, Catal. Today 42 (1998) 73.

31. R. Joyner and M. Stockenhuber, J. Phys. Chem. B 103 (1999) 5963.

32. M. Kögel, R. Mönning, W. Schwieger, A. Tissler and T. Turek, J. Catal. 182 (1999) 470.

33. P. Marturano, A. Kogelbauer and R. Prins, J. Catal. 190 (2000) 460.

34. P. Marturano, L. Drozdová, A. Kogelbauer and R. Prins, J. Catal. 192 (2000) 236.

35. A.A. Battiston, J.H. Bitter and D.C. Kongingsberger, Catal. Lett. 66 (2000) 75.

36. A.A. Battiston, J.H. Bitter, F.M.F. de Groot, A.R. Overweg, O. Stephan, J.A. van Bokhoven, P.J. Kooyman, C. van der Spek, G. Vankó and D.C. Koningsberger, J. Catal. 213 (2003) 251.

37. F.Kapteijn, G. Marbán, J.RodrÍguez-Mirasol and J.A.Moulijn, J.Catal. 167 (1997) 256.

38. A.L.Yakovlev, G.M. Zhidomirov and R.A. van Santen, Catal.Lett. 75 (2001) 45.

39. D. Meloni, R. Monaci, V. Solinas, G. Berlier, S. Bordiga, I. Rossetti, C. Oliva and L. Forni, J. Catal. 214 (2003) 169.

40. H.-Y. Chen, T. Voskoboinikov and W.M.H. Sachtler, J. Catal. 180 (1998) 171.

41. H.-Y. Chen, X. Wang and W.M.H. Sachtler, PCCP 2 (2000) 3083.

42. Q. Sun, Z.-X. Gao, H.-Y. Chen and W.M.H. Sachtler, J. Catal. 201 (1998) 89.

43. T.V. Voskoboinikov, H.-Y. Chen and W.M.H. Sachtler, Appl. Catal. B. 19 (1998) 279.

44. H.-Y Chen, El-M. El-Malki, X. Wang, R.A. van Santen and W.M.H. Sachtler, J. Mol. Catal. 162 (2000) 159.

45. J. Jia, B. Wen and W.M.H. Sachtler, J. Catal. 210 (2002) 453.

46. J. Pérez-Ramírez, F. Kapteijn and A. Brückner, J. Catal. 218 (2002) 234.

Chapter 4

Characterization and reactivity of
iron- and aluminum-substituted MFI zeolites

Abstract

Iron- and aluminum-containing MFI zeolites were synthesized by hydrothermal synthesis starting from tetraethylorthosilicate. Various characterization techniques were employed to identify the Fe and Al species incorporated into the zeolites. Particular attention is paid to the evolution of these species during template removal by calcination and subsequent steaming activation. Directly after synthesis, Fe and Al appear to be both incorporated to a large extent in the zeolite framework. Removal of the template leads to the extensive removal of Fe from the framework, while only a small part of Al is removed. Steaming results in further removal of aluminum from framework positions. Extensive characterization (^{27}Al NMR and IR spectroscopy of adsorbed NO) show the close interactions between extra-framework Fe and Al species. This effect is more pronounced after steaming. While zeolites containing exclusively Fe or Al as hetero-atoms are inactive, MFI zeolite containing both Fe and Al at extra-framework positions shows good activity in nitrous oxide activation and phenol production from benzene. Our results suggest that both the presence of extra-framework Fe and Al play an essential role in these reactions, resulting in a synergistic effect. The formation of a certain kind of species of Fe-Al-O is speculated to be responsible for the activation of nitrous oxide. The results indicate that the controversy about active sites of commercial ZSM-5 zeolites in benzene hydroxylation to phenol is most probably due to trace amounts of iron. The notion that extra-framework Al is required for active catalysts explains various aspects regarding catalyst preparation and activation.

4.1 Introduction

Zeolites are porous aluminosilicates made up from corner and edge-sharing SiO_4 and AlO_4 tetrahedra (1). The incorporation of transition metal into the framework of the aluminosilicates has drawn consistent interest in the past years due to their potential catalytic properties (2). Already in the early 70's, it was established that iron impurities can occupy tetrahedral framework positions in faujasite zeolites (3). Isomorphous substitution of Si^{4+} in the zeolites framework with Fe^{3+} results in ferrialuminosilicates (with Al in the framework) or ferrisilicates (without Al in the framework). The incorporation of iron into MFI zeolite, one of the most important zeolites currently used in industry, was first reported in 1985 (4). This type of catalyst can carry out acid-catalyzed, dehydrogenation and redox reactions. In the last decade, much research effort has been focused on the unique property of iron-containing MFI zeolites to hydroxylate alkanes, most notably benzene, with nitrous oxide as oxidizing agent (5-15).

The direct conversion of benzene to phenol with N_2O as oxidant was first reported by Iwamoto *et al.* over a vanadia catalyst (16). Later, it was found that MFI zeolite is also a promising catalyst for this reaction (5,7,8) and an industrial process based on iron-containing MFI was recently claimed (17-18). It provides a practical heterogeneously catalyzed one-step conversion of benzene to phenol. The reported selective conversion of methane to methanol at ambient temperatures may point to further applications in view of the challenge for cleaner oxidation processes (19). As to the nature of active sites, inspired by an analogy with the binuclear active Fe center in enzyme methane monooxygenase (MMO), Panov has proposed a binuclear Fe cluster, denoted as α-sites with Fe valence state of +2 and compensating the negative framework charge of the zeolite, to be responsible for the catalysis (5,9,10, 20). Consequently, Fe/ZSM-5 catalysts have been termed biomimetic, although an important difference remains the need to apply nitrous oxide in the zeolite case instead of molecular oxygen. This binuclear cluster is proposed to dissociate N_2O into an adsorbed oxygen atom and gaseous dinitrogen. The deposited oxygen atom subsequently reacts with a further nitrous oxide molecule to molecular oxygen and nitrogen (nitrous oxide decomposition) or inserts into C-H bonds of hydrocarbons (selective oxidation). First-principles DFT calculations relating to the reaction mechanism of benzene hydroxylation over Fe centers were carried out and arene oxide was suggested to be the reaction intermediate for the conversion of benzene to phenol (21). However, despite the strong indications supporting this model, the exact nature and structure of the active sites remain a topic of intense debate in literature. Burch *et*

al. (14) concluded that Brønsted acid sites and a particular internal structure are required to produce phenol, while Notté recently showed that in addition to the Brønsted acidity, a specific (extra-framework) Fe site is necessary for the reaction (22). Contrasting these proposals stressing the importance of Brønsted acidity, Motz *et al.* measured the catalytic activity of dealuminated HZSM-5 and demonstrated that the activity is determined by Lewis acidic extra-framework aluminium created by steaming (15). Nevertheless, it is claimed recently that there is no correlation between the phenol productivity and Brønsted acidity or Lewis acidity (12). Also, there are indications that Fe-silicalite is capable of converting benzene selectively to phenol with nitrous oxide (13, 23,24).

The most important questions pertaining to the active sites for nitrous oxide decomposition and benzene oxidation to phenol relate to (i) the necessity of the presence of Fe and (ii) the necessity of the presence of Al, if at all, and the required location (framework or extra-framework). It is interesting to note that in most of the research listed above, commercial zeolites or industrially adapted synthesis method were used to prepare catalysts in which either Fe or Al impurities are unavoidable. Thus, one may obtain important information comparing pure aluminosilicates, ferrosilicates and ferroaluminosilicates.

In this chapter, a number of zeolites with the MFI topology, containing either iron or aluminum or a combination of both were synthesized. A variety of characterization techniques including UV-Vis spectroscopy, ^{27}Al NMR, ESR, IR with NO as a probe molecule and XAS, were employed to identify the resulting Fe and Al species. Finally, reactions involving the activation of nitrous oxide (N_2O decomposition and selective oxidation to phenol) were performed to correlate the characterization data to the catalytic performance. This research was initiated by the observation in chapter 2 and 3 that the presence of extra-framework Al, induced by steaming in Fe/ZSM-5, leads to increase of catalytic activity of N_2O decomposition and higher yields of phenol in the hydroxylation of benzene. It is thus of the utmost importance to prepare highly pure [Fe]-MFI and [Al]-MFI samples in an attempt to separate the catalytic roles of Fe and Al.

4.2 Experimental

Three MFI-type zeolites were prepared by hydrothermal synthesis (11,25). In principle, ZSM-5 refers to aluminosilicates with the MFI topology. The materials in this chapter include iron-substituted silicalite and therefore the zeolites are designated by the MFI instead of ZSM-5. Thus, [Fe]-MFI (iron-substituted silicalite), [Al]-MFI (HZSM-5) and [Fe,Al]-MFI

(iron-substituted ZSM-5) were synthesized. To this end, 102.4 g tetraethylorthosilicate (TEOS, Acros, 98 %), was added to 150 g organic template tetrapropylammonium hydroxide (Fluka, 20 % in water) with good mixing overnight. Then, appropriate amounts of solutions of iron nitrate ($Fe(NO_3)_3 \cdot 9H_2O$, Merck, 98%) and/or aluminium nitrate(($Al(NO_3)_3 \cdot 9H_2O$, Janssen, 99%) were added dropwise to the solution of the silica source under vigorous stirring. The mixture was kept in a teflon autoclave at 443 K for five days. After filtration and drying at 383 K overnight, the organic template was carefully removed by the following calcination procedure: (1) 0.2 g zeolite was treated in 100 ml·min^{-1} N_2 whilst heating to 823 K at a ramp rate of 1 K·min^{-1} and kept at this temperature for 8 h, (2) the material was further treated in 100 ml·min^{-1} 20 vol.% O_2 in N_2 at 823 K for another 4 h. To study the evolution of Al and Fe species during these calcination steps, several zeolite samples were taken out for further characterization at different stages of the calcination process. Steaming modification of the zeolitic materials was achieved by steaming 2 g zeolite in a flow of 100 ml·min^{-1} 20 vol. % O_2 in He with 10 % water vapor at 973 K for 3 h. The samples modified by steaming are designated by adding the postfix HTS.

Powder x-ray diffractograms were measured using a Rigaku difractometer. Typically, an XRD spectrum was recorded in the range $5^o < 2\theta < 50^o$ using Cu Kα radiation with a scanning speed of 0.01^o min^{-1}. UV-Vis spectra were recorded on Shimadzu UV-2401 PC spectrometer. $BaSO_4$ was used as a reference sample. Nitrogen adsorption at 77 K was carried out in a Micromeritics ASAP 2000 apparatus. Prior to nitrogen adsorption, samples were evacuated at 623 K for 16 h.

Infrared spectra of self-supporting 10 mg catalyst wafers were recorded at room temperature on a Bruker IFS-113v Fourier Transform IR spectrometer with a DTGS detector at a resolution of 4 cm^{-1}. Typically, a sample was pretreated *in situ* in oxygen at a temperature of 823 K for 1 h and cooled to room temperature *in vacuo* (pressure less than 10^{-6} mbar), followed by room temperature exposure to NO (purity > 99.9%, 10 mbar) for 30 minutes. Finally, the sample was evacuated and spectra were recorded at room temperature.

Solid-state ^{27}Al magic-angle spinning NMR spectra were obtained on a Bruker Ultrashield 500 spectrometer at a magnetic field of 11.7 T, equipped with a 4 mm MAS probe head. The Al resonance frequency at this field was 130 MHz. The sample rotation speed was 12.5 kHz. The ^{27}Al chemical shifts were referenced to a saturated $Al(NO_3)_3$ solution.

ESR experiments were carried out with a Bruker ESP 300E spectrometer, operating with an X-band standard cavity (9.44 GHz), an ER 035 M NMR Gauss meter, and a HP 5350B frequency counter. A 100 kHz modulation of 5 Gauss and 2 mW microwave power were used

to record the spectra. The field axis was corrected for the variations in frequency in different spectra. The spectra were recorded at 10 K with the use of an Oxford continuous flow cryostat and variable temperature unit.

Fe K-edge XAS measurements were performed at beamline 17C of the National Synchrotron Radiation Research Center in Hsinchu (Taiwan). The electron energy and ring current were 1.5 GeV and 160 mA, respectively. The spectra were recorded in fluorescence mode at ambient temperature in He atmosphere with sampling steps of 0.5 eV in the XANES region and of 1 to 2 eV in the EXAFS region. Prior to measurement, the samples were calcined at 673 K to remove physisorbed water. Fe K-edge spectra were recorded in transmission mode at ambient temperature in He atmosphere. EXAFS data were extracted from the measured absorption spectra with the XDAP code (26). The pre-edge was subtracted using a modified Victoreen curve, while the background was subtracted by using cubic spline routines. Finally, normalization took place by dividing the subtracted absorption spectra by the intensity of the absorption spectrum at 50 eV above the Fe K-edge.

Reaction data were collected using a plug flow reactor operating at atmospheric pressure. An amount of 0.1 g catalyst (sieve fraction 125 μm – 425 μm) was diluted with SiC to fulfil plug flow requirements. The reaction mixture contained 1 vol.% benzene and 4 vol.% N_2O in He at a GHSV of 30000 h^{-1}. For nitrous oxide decomposition, 80 mg of catalyst sample with sieve fraction (125 μm – 425 μm) was exposed to a gas mixture of 5000 ppm N_2O in He gas flow at a GHSV of 30000 h^{-1}. More details concerning the experimental setup and reaction conditions are given in chapter 3.

4.3 Results

XRD
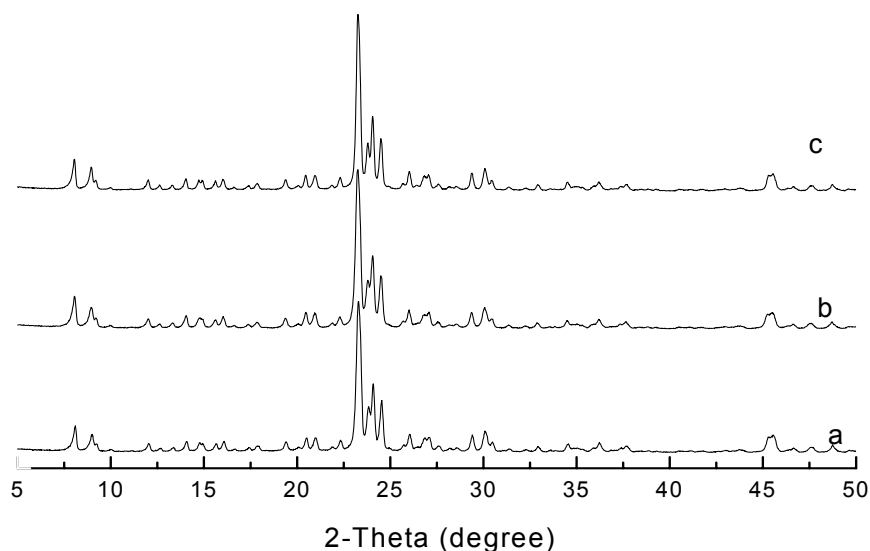
Figure 1: XRD spectra of synthesized samples: (a) [Al]-MFI, (b) [Fe]-MFI, (C) [Fe,Al]-MFI.

The XRD patterns of the synthesized materials are shown in figure 1. There are no significant discrepancies among the XRD spectrum of [Fe]-MFI, [Al]-MFI and [Fe,Al]-MFI. They all exhibit the characteristic pattern of the MFI topology. Expansion of the unit cell due to incorporation of iron is not observed, mainly due to the extraction of Fe during the calcination procedure (*vide infra*). No typical iron-oxide-type phases were detected.

Table 1: Elemental analysis of the various synthesized zeolites

	Al content (wt. %)	Fe content(wt. %)	Si/Al	Si/Fe
[Al]-MFI	0.88	<0.001	42	-
[Fe]-MFI	<0.005	0.55	-	143
[Al,Fe]-MFI	0.92	0.51	40	147

The elemental composition of the various materials is given in table 1. Compared with commercially available HZSM-5 materials that generally contain more than 0.01 wt.% Fe impurity, the use of TEOS as silica source reduces the Fe content to less than 0.001 wt.%. Moreover, the Al content in [Fe]-MFI is also negligible in contrast to commonly used

synthesis methods that result in aluminum contents of 0.01 - 0.04 wt.%. Since the iron and aluminum content of [Fe,Al]-MFI is close to the iron content in [Fe]-MFI and the aluminum content in [Al]-MFI, the zeolites can be directly compared

N$_2$ adsorption

As outlined earlier (chapter 2), BET analysis of nitrogen adsorption isotherms is not qualified for a quantitative analysis of the pore structure of MFI zeolites. The parameters from various other methods for the zeolitic samples are listed in table 2. Clearly, the synthesis of these materials under similar conditions results in three zeolites with very similar textural properties. The addition of Fe results in a slight increase of the surface area and micropore volume. The similar textural properties among these samples and also compared to those of a commercial HZSM-5 zeolite which has been extensively characterized in chapter 2 provide a possibility to compare the catalytic results of benzene hydroxylation to phenol among the various catalysts.

Table 2: The surface area (S_{Lang}) and micropore volume (V_{Lang}) derived from the Langmuir equation, the surface area (S_{D-R}) and micropore volume (V_{D-R}) calculated using the Dubinin-Radushkevich method and the Dubinin-Astakhov limiting micropore volume (V_{D-Ast}).

Sample	S_{Lang} (m^2.g^{-1})	V_{Lang} (cm^3.g^{-1})	S_{D-R} (m^2.g^{-1})	V_{D-R} (cm^3.g^{-1})	V_{D-Ast} (cm^3.g^{-1})
[Al]-MFI	441	0.157	397	0.141	0.157
[Fe]-MFI	470	0.167	409	0.146	0.163
[Fe,Al]-MFI	465	0.165	401	0.143	0.162

Electron Spin Resonance

Whereas, in principle, ESR is known to be a suitable technique for characterization of Fe sites in zeolites where the weak ligand field of the possible ligands (water, hydroxide, framework oxygen atoms) results in high-spin ferric states, the interpretation of the resulting spectra is far from ambiguous due to complications associated with inhomogeneous broadening and overlapping signals. To study the evolution of Fe species during zeolite activation at elevated temperatures, ESR spectra, recorded at 10 K, of [Fe]-MFI are shown in

figure 2. These spectra are quite similar with minor, but distinct differences. They all consist of two main features at g-values of 2.0 and 4.4 and a broad band centered on g-value of 3.1. In earlier reports, the signal at 4.4 has been assigned to Fe^{3+} incorporated in the framework of zeolite (27). However, it was later suggested that the signal at g-value of 4.4 does not necessarily indicate the location of Fe in the framework but points to tetrahedral coordination of Fe (28). In general, the band at a g-value of 2.0, with a zero splitting field of zero, is attributed to Fe^{3+} in a octahedral coordination state (29). Therefore, it is often assigned to Fe at extra-framework locations. Compared to the other two signals, the broad band centered at g-value of 3.1 is less discussed although it has been observed before. Recently, Bordiga *et al.* (30) proposed that this signal might relate to small extra-framework Fe-O clusters or to very small ferric oxide particles exhibiting superparamagnetic or even ferromagnetic behaviour. Nevertheless, we point out that such a broad band might constitute the contribution of several signals as suggested by a similar report which describes a broad "hump" at g-values of 2.4 or $g = 2.6$ (31).

Although the assignment of the band at $g = 4.4$ is not conclusive, the broad band centered on $g = 3.1$ and the presence of the band at $g = 2.0$ indicate that not all Fe is located in tetrahedral framework positions directly after synthesis. After calcination at 823 K and especially after steaming of [Fe]-MFI, the signal at $g = 2.0$ increases which points to the further removal of framework Fe to clustered extra-framework species with octahedral coordination.
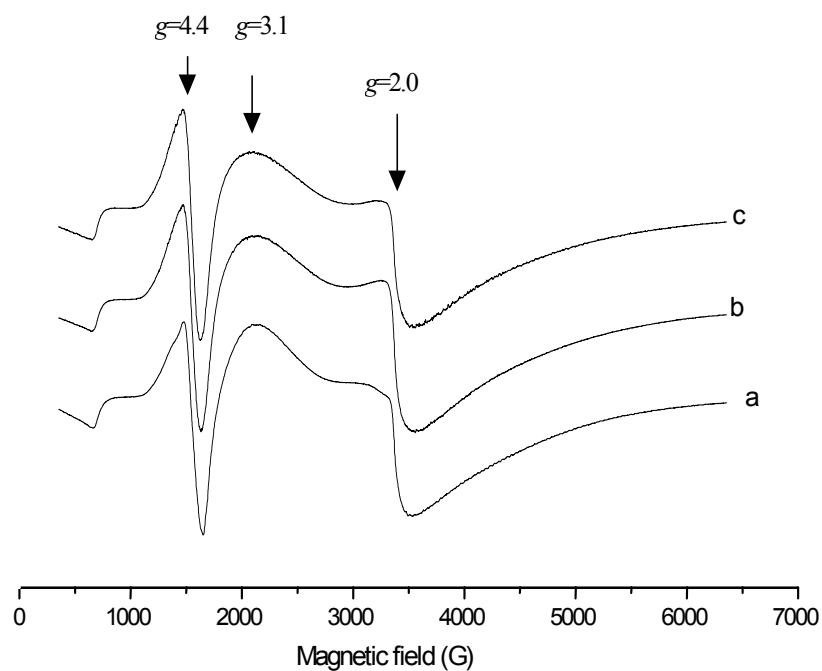
Figure 2: ESR spectra of various [Fe]-MFI, (a) [Fe] as-prepared, (b)[Fe]-MFI calcined at 823K, (C)[Fe]-MFI steamed at 973K.

ESR spectra of calcined and steamed [Fe,Al]-MFI are displayed in figure 3. For [Fe,Al]-MFI calcined at 823K (figure 3 a), compared to its counterpart of [Fe]-MFI spectra in figure 2 b, the broad line centered at $g = 3.1$ is almost absent whereas the signal at g-values of 2.0 and 4.4 still remain. This might indicate that the iron-oxide phase in [Fe,Al]-MFI is better defined and/or consists of smaller particles than in [Fe]-MFI. The ESR spectrum undergoes some changes after steaming. We observe a small increase of both the signal centered at a g-value of 3.1, and a signal of $g = 2.0$ (figure 3 b). This could indicate that more iron is removed from the framework under more severe conditions. Nevertheless, we note that the signals due to clustered iron-oxide species ($g = 2.0$ and 3.1) are smaller in [Fe,Al]-MFI than in [Fe]-MFI indicating that the presence of Al prevents extensive clustering of Fe in some way. Alternatively, a larger part of Fe might be present as Fe^{2+} which is not be detected by ESR.
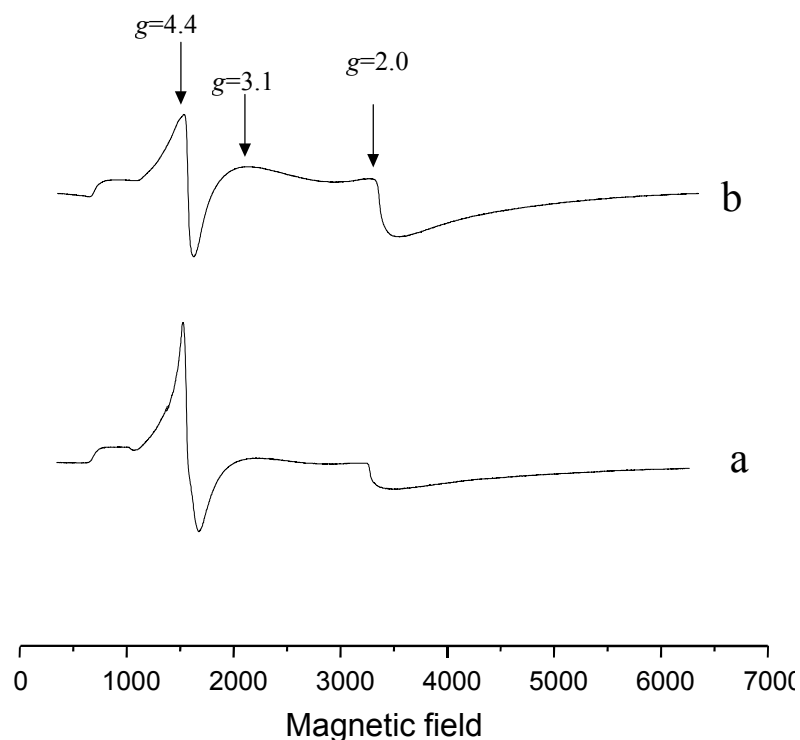
Figure 3: ESR spectra of [Fe,Al]-MFI, (a)[Fe,Al]-MFI calcined at 823K, (b)[Fe,Al]-MFI steamed at 973K

UV-Vis spectroscopy

The coordination states of Fe in the iron-containing samples and its evolution in subsequent activation steps are investigated by UV-Vis spectroscopy. The measurements were carried out in diffuse reflectance mode. The main disadvantage of the technique is that the spectra usually encompass several broad and overlapping bands that make the interpretation difficult. This is obviously reflected in our samples. However, valuable information concerning the transition metal ions in zeolites can be obtained which is complementary to the other techniques like ESR.

The UV-visible spectra of the iron-containing samples all contain two characteristic maxima around 217 and 245 nm (not shown here) which are ligand to Fe^{3+} charge transfer bands indicative for the presence of tetrahedral Fe^{3+}.

Figure 4: UV-Vis spectra of [Fe]-MFI treated under different conditions,(a) As prepared, (b) calcined at 823 K at O_2/N_2 for 8 h, (c) steamed at 973 K in 10 vol. % water for 3 h.

Figure 4 and 5 display the electronic spectra in the region of the *d-d* transitions for [Fe]-MFI and [Fe,Al]-MFI. Spectra are presented of the as-prepared materials with template, the materials after template removal and after steaming activation. These weak transitions are due to forbidden *d-d* transition and are indicative of the tetrahedral environment of Fe^{3+} in the zeolite framework (32-34). These bands are partially masked by the tail of one of the CT bands. Therefore, no full quantitative analysis of the Racah parameters could be performed (25). Nevertheless, we observe that upon calcination approximately 80% of Fe is removed from tetrahedral framework positions in [Fe]-MFI. Steaming activation leads to additional removal of Fe from the framework and we estimate that finally about 90% of the framework Fe is removed. Comparing the spectra of as-prepared [Fe]-MFI and [Fe,Al]-MFI, we can conclude that a small, but significant portion of Fe (~ 25%) has not been built into the zeolite framework of [Fe,Al]-MFI and must be present at extra-framework positions. After calcination, virtually all Fe is removed from framework positions as can be deduced from the absence of the band at 412 nm. The spectrum of this region for steamed [Fe,Al]-MFI is expectedly similar.

The removal of Fe from framework positions is underpinned by the broadening of the charge transfer band around 217 nm and the shift towards higher wavelength of the band around 245 nm (not shown). Moreover, we observe the formation of an asymmetric peak around 277 nm. This latter feature, which is found to be more pronounced for [Fe,Al]-MFI than for [Fe]-MFI, points to the presence of octahdral Fe^{3+} species present in small clusters. As we did not observe larger iron oxide aggregates, $i.e.$ Fe_2O_3 which produces a characteristic band around 500 nm, we assume that the larger part of the extra-framework Fe species have ended up in small clustered species.
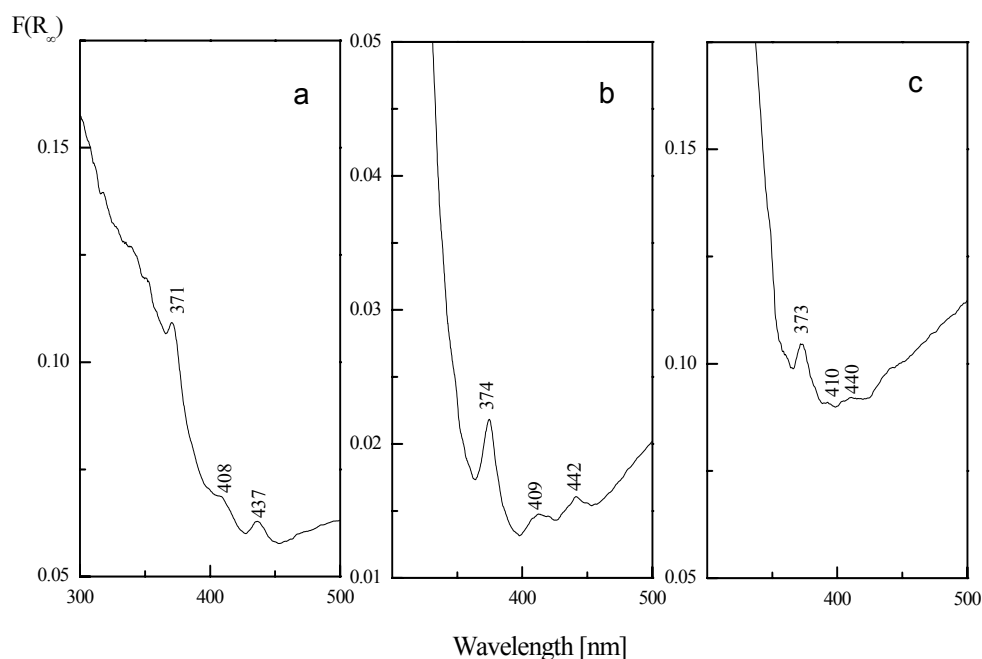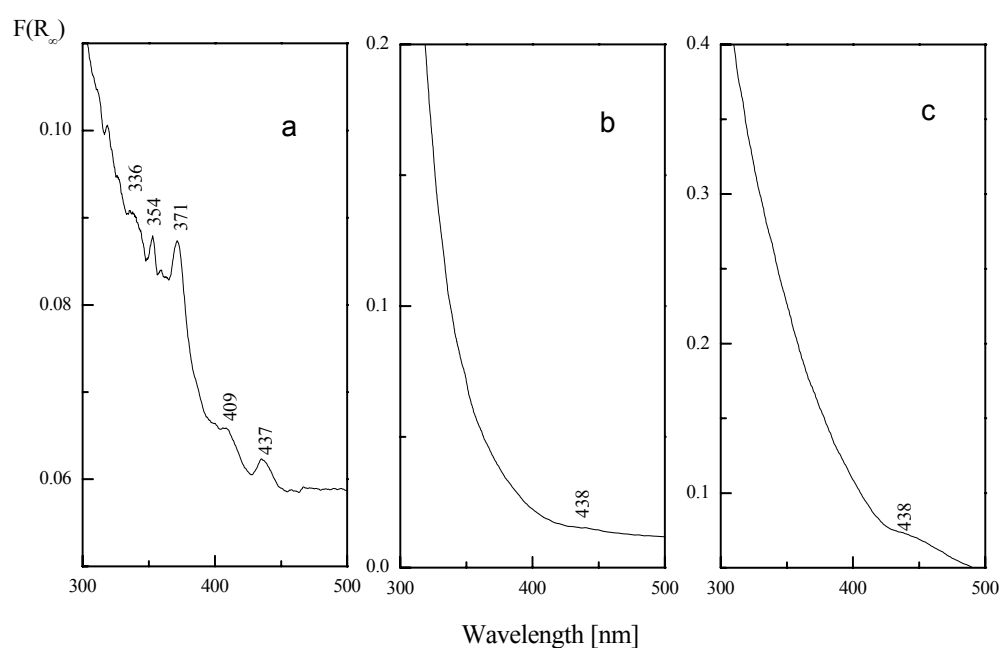

Figure 5: UV-Vis spectra of [Fe,Al]-MFI treated under different conditions,(a) As prepared, (b) calcined at 823 K at O_2/N_2 for 8 h, (c) steamed at 973 K in 10 vol. % water for 3 h.
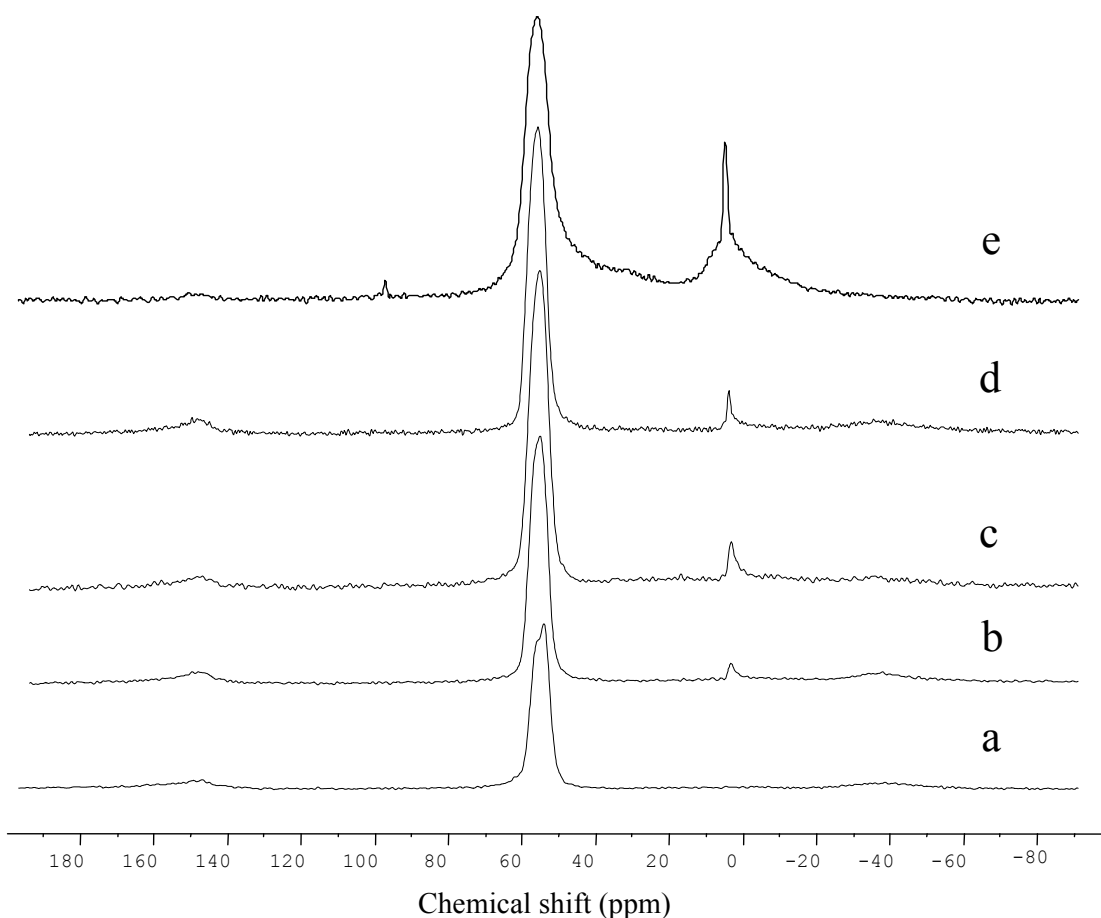
Figure 6: ^{27}Al NMR spectra of [Al]-MFI after various treatments: (a) As prepared, (b) calcination in N$_2$ at 473 K, (c) calcination in N$_2$ at 673 K, (d) calcination at 823 K in an artificial air mixture for 8 h, (e) steaming at 973 K in 10 vol. % water for 3 h.

^{27}Al NMR provides a very powerful tool to study Al species in aluminosilicates. The evolution of ^{27}Al NMR spectra in [Al]-MFI during progressive calcination is presented in figure 6. Quantitative data are collected in table 3. As outlined in chapter 2, the band at 52 ppm is generally assigned to tetrahedral framework Al species, while a chemical shift of 0 ppm is commonly assigned to octahedral Al in extra-framework positions. When the template is still in the zeolite sample (figure 6 a), the spectrum shows one dominant resonance at 52 ppm that we take as proof that Al is fully incorporated in the framework. The asymmetry of this feature might point to the presence of at least two crystallographically distinct Al sites in the zeolite framework as proposed in the literature (35). The very weak side bands at 150 and -50 ppm are due to the small but noticeable presence of Fe (36). After the sample is treated in N$_2$ at 473 K in the calcination process, a small but distinct peak at 0 ppm appears (figure 6 b). This indicates the presence of extra-framework Al which is dislodged from zeolite framework

positions after partial removal of the template. Increasing severity of calcination result in an increase of the feature at 0 ppm (figure 6 c and d). Quantitative analysis (table 3) shows that approximately 5% of Al is dislodged from framework positions after complete removal of the organic template (figure 6 d). It is indeed difficult to obtain MFI zeolites totally free from defects, even when careful procedures for the removal of template are applied. Further steaming activation of [Al]-MFI results in further dislodging of aluminum from the framework (*ca*. 35%). Moreover, a new broad peak around 38 ppm appears to be visible which is usually referred to as pentahedrally-coordinated Al or distorted tetrahedral Al (15).

Table 3: Quantitative analysis of ^{27}Al NMR spectra of [Al]-MFI and [Fe,Al]-MFI corresponding to figures 6 and 7, respectively. All signals are normalized to the resonant signal of the as-prepared [Al]-MFI.

	Treatment	Al_{tet} (%)	Al_{oct} (%)
[Al]-MFI	as prepared	100	0
figure 6	N_2, 473 K	97	3
	N_2, 673 K	97	3
	O_2/N_2,823 K	95	5
	steaming, 973 K	65	35
[Fe,Al]-MFI	As prepared	90	0
figure 7	N_2, 473 K	78	1
	N_2, 673 K	55	1
	O_2/N_2,823 K	37	1
	Steaming, 973 K	33	8

Figure 7 shows the ^{27}Al NMR spectra of [Fe,Al]-MFI after various activation treatments. The corresponding quantitative data are also listed in table 3. The side bands centered at -50 and 150 ppm of the ^{27}Al NMR spectra are a direct consequence of the paramagnetic nature of iron nuclei present in [Fe,Al]-MFI. Therefore, part of the resonant signal is not observed. Nevertheless, we observe that the ^{27}Al NMR spectra of [Fe,Al]-MFI exhibit a similar pattern as those of its counterpart in [Al]-MFI, *i.e.* framework aluminum is progressively removed at elevated temperature and this dislodgement is more evident after steaming in [Fe,Al]-MFI(HTS). The quantitative data in table 3 further underline the loss of resonant signal and for instance, only 38% of the total resonant signal in [Al]-MFI remains in [Fe,Al]-MFI calcined at 823 K. Comparing the ratio of octahedral and tetrahedral Al ions in [Fe,Al]-MFI

and [Fe]-MFI, we observe that this is lower for the former zeolite. This implies that a larger part of the extra-framework Al nuclei present in [Fe,Al]-MFI become invisible due to the proximity of paramagnetic Fe centers. This is taken as an indication that Fe species are vicinal to Al centers. As outlined in chapter 2, the paramagnatism of the unpaired electron in the d-shell of Fe^{3+} reduces the amount of Al that can be detected by the ^{27}Al NMR. This notion is underlined by the observation that the resonance due to octahedrally coordinated Al is more broadened than the resonance due to tetrahedrally coordinated Al centers.
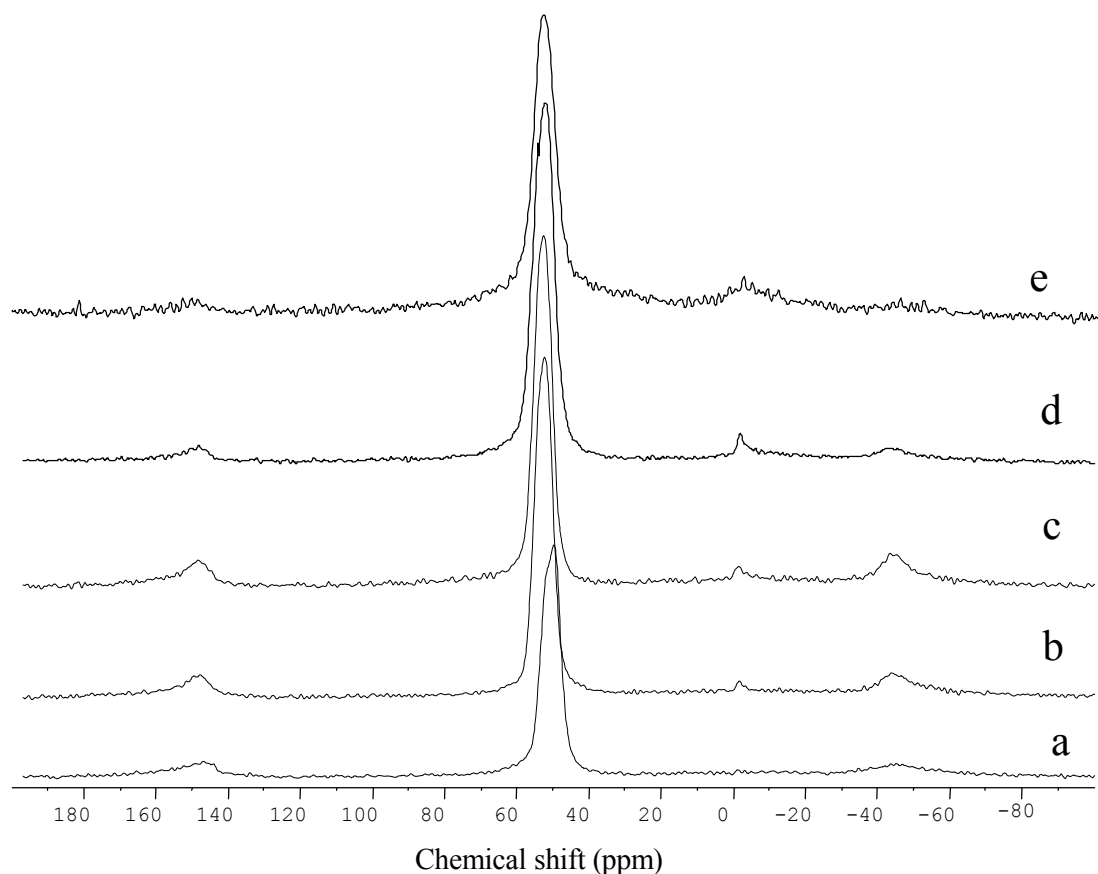
Figure 7: ^{27}Al NMR spectra of [Fe,Al]-MFI after various treatments: (a) As prepared, (b) calcination in N_2 at 473 K, (c) calcination in N_2 at 673 K, (d) calcination at 823 K in an artificial air mixture for 8 h, (e) steaming at 973 K in 10 vol. % water for 3 h.

The nature of the Al species including its location in the framework or in the micropores plays an essential role in the catalytic properties of zeolites. In contrast to the Brønsted acidity, the catalytic function of extra-framework Al sites (Lewis acidity) is less known partly due to the difficulty in identifying such species. Recent developments in 2D multiquantum NMR techniques provide potential applications in further details of the characteristics of Al species (35,37). Indeed, a successful study confirms a consistent speculation that Al is not randomly located in the zeolites, leading to non-equivalent Al species in the framework.

Encouraged by that finding, we applied the same method for the [Al]-MFI(HTS) to investigate if there are various extra-framework Al simultaneously present.
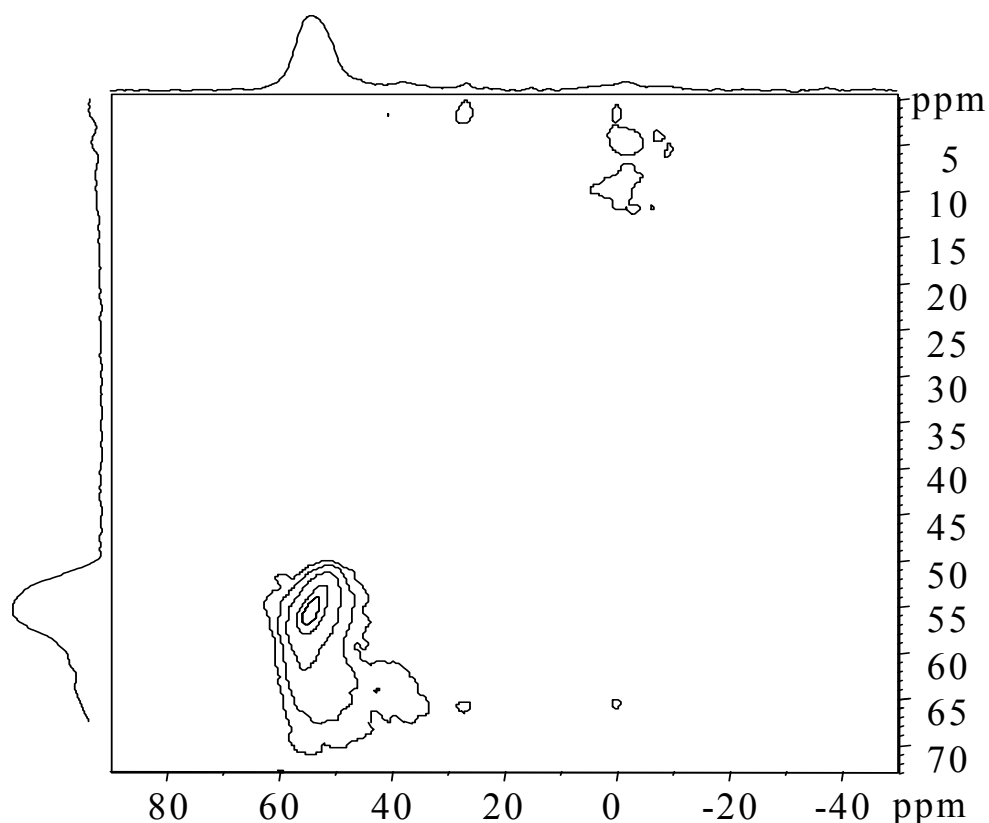
Figure 8: 2D ^{27}Al MQ MAS NMR of [Al]-MFI(HTS)

Figure 8 presents the 2D ^{27}Al MQ MAS NMR spectrum of the [Al]-MFI(HTS) . A close inspection of the contours and the projection of the isotropic axis confirms the presence of a band around 37 ppm. This band is due to a separate Al species and not due to the heterogeneity of the zeolite sample. This signal, assigned to distorted tetrahedral coordination or pentahedrally-coordinated Al, is not observed in HZSM-5 without steaming treatment in literature. Thus, we attribute the signal of 37 ppm to extra-framework Al species. It is concluded that there are at least two types of extra-framework Al present in [Al]-MFI(HTS) and most probably also in [Fe,Al]-MFI(HTS) as well.

IR spectroscopy of adsorbed NO

To obtain further insight into the nature of the extra-framework species, we performed an IR spectroscopic investigation of adsorbed NO (figure 9). We note that the characteristic bands of reversibly adsorbed NO around 1880 cm^{-1} and in some cases those around 2130 cm^{-1} were observed in the presence of gaseous NO but were absent after evacuation.
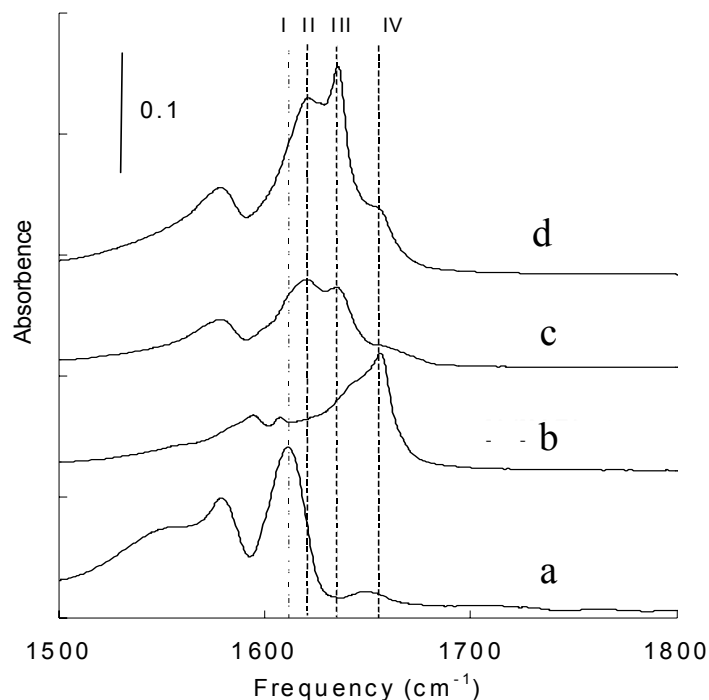
Figure 9: Infrared spectra of adsorbed NO, (a) [Fe]-MFI(HTS), (b) [Al]-MFI(HTS), (c) [Fe,Al]-MFI, (d)[Fe,Al]-MFI(HTS).

The observed bands between 1550 cm^{-1} to 1700 cm^{-1} are due to adsorption complexes of NO with extra framework oxygen atom, constituent of extra-framework metal-oxide species. This results in NO_2 (nitro and nitrito) groups and NO_3 (nitrate groups) (38-42). The spectrum of [Fe]-MFI(HTS) contains three bands. The bands below 1600 cm^{-1} are assigned to monodentate/bidentate nitrate groups and the strong band at 1613 cm^{-1} (band I) to NO_2 (the asymmetric stretch frequency of NO_2 is at 1610 cm^{-1}) on Fe ions. [Al]-MFI(HTS) contains a strong band at 1657 cm^{-1} (band IV) assigned to NO_2 in interaction with extra-framework Al species next to a shoulder at 1643 cm^{-1} and weaker feature around 1600 cm^{-1} (nitrate groups). The spectra for [Fe,Al]-MFI and [Fe,Al]-MFI(HTS) are more complex. While in both samples a band at ~1656 cm^{-1} similar to the one in [Al]-MFI(HTS) is visible with lower intensity, the band corresponding to NO_2 on extra-framework Fe is only weakly found in the calcined [Fe,Al]-MFI. More importantly, the spectrum contains two new bands around 1620 cm^{-1} (band II) and 1635 cm^{-1} (band III). These bands have been before observed for Fe/ZSM-5 samples. Mul. *et al.* (39) attributed the latter band to Fe-Al-O nanoparticles in the zeolite micropores . This agrees with our findings that the bands are only observed in [Fe,Al]-MFI and that steaming increases the intensity of the band at 1635 cm^{-1}. Although we can not identify those two bands with certainty -possibly nitro or/and nitrito groups on Fe-Al-O

species – the present data point to the formation of a new type of extra-framework species in [Fe,Al]-MFI.

X-ray absorption spectra
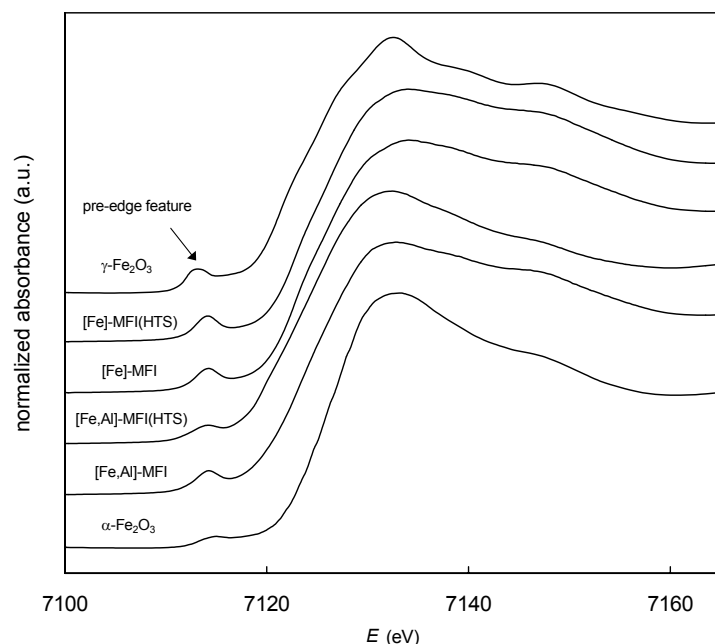
Figure 10: XANES spectra of calcined and steamed [Fe]-MFI and [Fe,Al]-MFI. The XANES spectra of α - Fe_2O_3 , γ - Fe_2O_3.

Figure 10 shows the XANES region of calcined and steamed [Fe]-MFI and [Fe,Al]-MFI. The corresponding near-edge regions of the X-ray absorption spectra of α - Fe_2O_3, γ - Fe_2O_3 are included for the sake of comparison. All spectra show the pre-edge feature which derives from 1s → 3d transitions in iron in tetrahedral and distorted octahedral symmetries. This is particularly evident for α-Fe_2O_3 which contains 50% of tetrahedral Fe^{3+}. The pre-edge feature in the zeolite materials appears to be sensitive to the pre-treatment (calcination or steaming) and the presence of Al in the zeolite. From figure 10, it is evident that its intensity is smaller for steamed [Fe,Al]-MFI than for the other materials. This points to a lower amount of tetrahedral Fe^{3+} in [Fe,Al]-MFI(HTS). Such tetrahedral Fe^{3+} species could be transformed into octahedral Fe^{3+} or into Fe^{2+} species. Close inspection of the spectra discloses that the main absorption maximum for [Fe,Al]-MFI(HTS) lies at a lower energy than for the zeolites that have been substituted only by Fe.
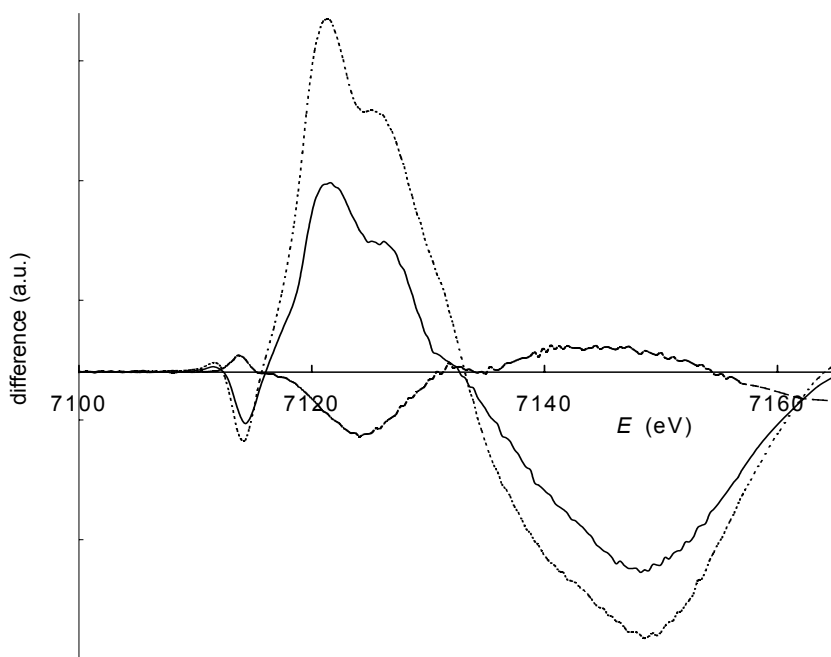
Figure 11: Difference spectra of the XANES regions of [Fe]-MFI with [Fe,Al]-MFI (full line), [Fe]-MFI(HTS) (dashed line) and [Fe,Al]-MFI(HTS) (dotted line).

The difference spectra in figure 11 show that [Fe,Al]-MFI(HTS) exhibits a significantly stronger absorption below the maximum than [Fe]-MFI(HTS). This indicates a more reduced state of Fe in [Fe,Al]-MFI(HTS) which is in line with the relatively strong decrease of the Fe^{3+} pre-edge feature. The transformation to Fe^{2+} species in the aluminum-containing zeolites is further indicated by the appearance of a small pre-edge peak around 7112 eV which corresponds to Fe^{2+} (43). A similar effect is observed when comparing [Fe,Al]-MFI(HTS) and [Fe,Al]-MFI. The steamed catalyst contains a larger fraction of reduced states than [Fe,Al]-MFI which is reflected by a stronger absorption at energies below the maximum and a smaller Fe^{3+} pre-edge feature. Moreover, we observe that the scattering features above the edge for [Fe,Al]-MFI(HTS) are different from those of the other isomorphously substituted samples. Finally, the difference between [Fe]-MFI and [Fe]-MFI(HTS) is very small. Steaming results in a small increase of the pre-edge feature in [Fe]-MFI(HTS). Bordiga *et al*. (30) have investigated Fe-silicalite and found a decrease of the pre-edge feature upon higher pre-treatment temperatures comparing activation at 773 K and 973 K. Our deviant results may be explained by the observation that already a large fraction of Fe has been removed from the framework in [Fe]-MFI. While the remainder is removed upon steaming in [Fe]-

MFI(HTS), concomitantly the iron oxide aggregates grow and form phases with structural parameters more close to α - Fe_2O_3. This leads to an increase of the pre-edge peak.
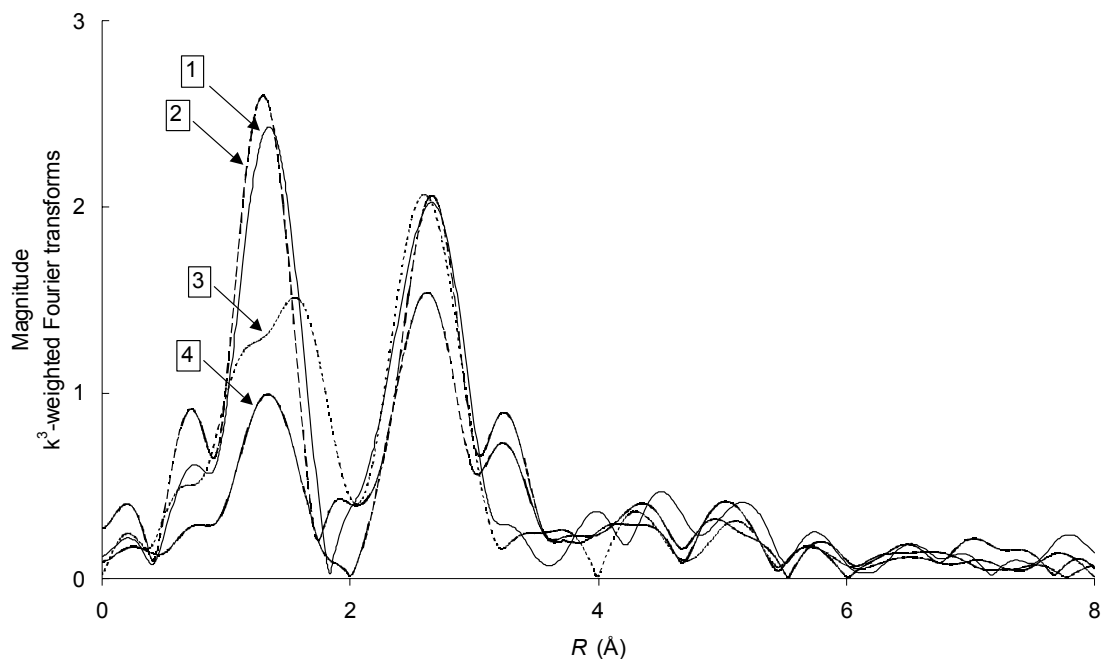
Figure 12: Magnitude of k^3-weighted Fourier transforms of [Fe,Al]-MFI (1), [Fe,Al]-MFI(HTS) (2), [Fe]-MFI (3) and [Fe]-MFI(HTS) (4).

In figure 12, the k^3-weighted Fourier transforms are shown. The samples show similar peak positions, although it is evident that [Fe,Al]-MFI(HTS) shows a different first coordination shell than the other samples. Moreover, the [Fe]-MFI samples appear to be better ordered because we observe a peak around 3.3 Å. Importantly, we note that the steamed samples exhibit decreased intensities. This was noted before by Bordiga *et al.* (30) who pointed out that this must be due to the heterogeneous nature of the Fe phase in these materials. Similar to our spectra, the Fe species tend to become more heterogeneous after more severe treatment. Thus, it is difficult to perform a detailed structural analysis of these samples and therefore we decided to leave it out altogether.

N2O decomposition
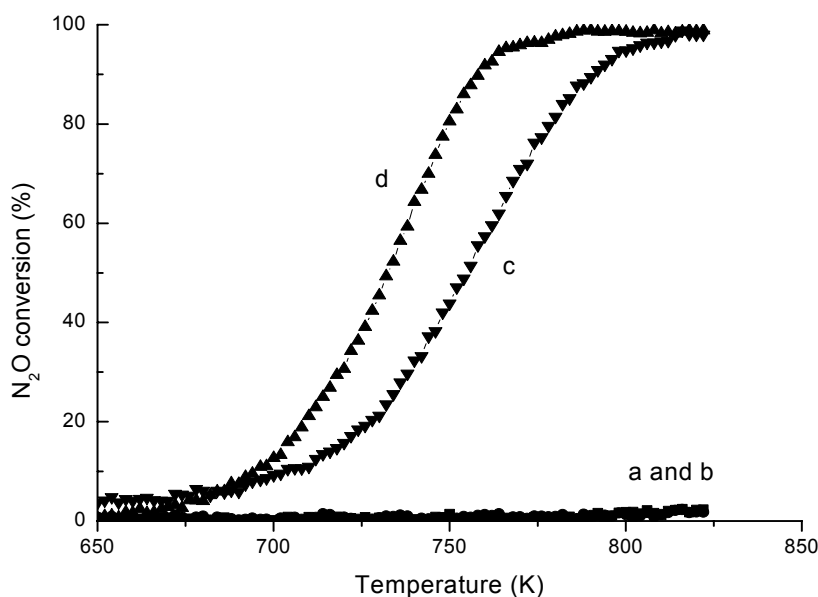
Figure 13: Temperature programmed decomposition of N_2O over (a and ■) [Al]-MFI(HTS), (b and ●)[Fe]-MFI(HTS), (c and ▼)[Fe,Al]-MFI, (d and ▲) [Fe,Al]-MFI(HTS) (feed composition: 0.5vol.% N_2O in balance He at GHSV of 30000 h^{-1}).

Figure 13 shows the temperature programmed decomposition of nitrous oxide over [Al]-MFI(HTS), Fe-[MFI](HTS), [Fe,Al]MFI and [Fe,Al]-MFI(HTS). The nitrous oxide decomposition rates for [Al]-MFI(HTS) and [Fe]-MFI(HTS) are very low and conversions are below 3% at 800 K. The activities of the corresponding calcined materials were even lower. [Fe,Al]-MFI(HTS), on the other hand, exhibits a significant higher reaction rate. The catalytic decomposition of N_2O starts at approximately 650 K and 100% conversion is reached at 775 K whereas its calcined counterpart [Fe,Al]-MFI shows relatively lower catalytic performance. Compared to a steamed Fe/ZSM-5 catalyst prepared by sublimation method and extensively described in chapter 3, [Fe,Al]-MFI(HTS) has a considerably lower activity. However, taking into account that the Fe content in Fe/ZSM-5 is six times higher than in [Fe,Al]-MFI, we conclude that the turnover frequency over [Fe,Al]-MFI(HTS) is higher. This suits well with the earlier notion that a large part of the Fe species in Fe/ZSM-5 prepared by sublimation are not active (chapter 3). Assuming that Fe^{2+} found in Fe/ZSM-5 is responsible for the catalysis and the active sites in these two catalysts are similar, a crude analysis comparing the nitrous oxide decomposition rates at 723 K indicates that about 10%

of the total Fe content in [Fe,Al]-MFI(HTS), corresponding to 0.05 wt.%, is involved in the active sites. It also indicates that only a fraction of Fe in [Fe,Al]-MFI(HTS) is active.
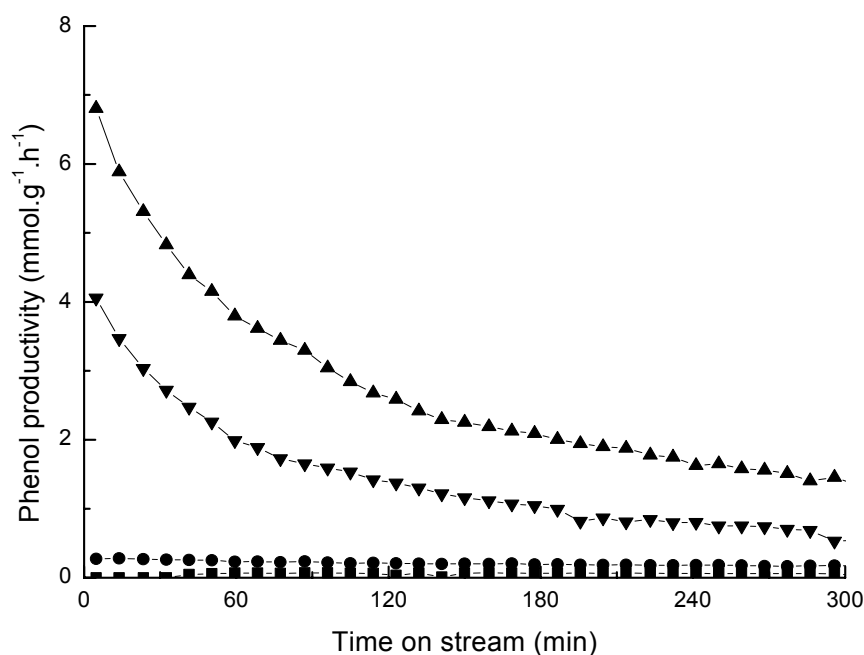
Figure 14: Benzene hydroxylation to phenol using N_2O as oxidant over various catalysts. Reaction temperature: 623 K, Gas composition: 1% benzene, 4% N_2O, 95% He, GHSV: 30000 h^{-1}, (■)[Al]-MFI(HTS), (●)[Fe]-MFI(HTS), (▼)[Fe,Al]-MFI, (▲)[Fe,Al]-MFI(HTS).

Figure 14 shows the rate of phenol productivity at 623 K as a function of the time-on-stream for the various catalysts. In contrast to the report that steamed [Al]-MFI is an active catalyst (15), the present [Al]-MFI(HTS) shows negligible activity while its calcined [Al]-MFI counterpart (not shown) is also not active. Moreover, the zeolite containing only iron, [Fe]-MFI(HTS), exhibits somewhat higher, but still almost negligible catalytic activity, *i.e.* it produces trace amount of phenol (0.1-0.2 mmol·g^{-1}·h^{-1}) at 623 K. Strikingly, the performance of [Fe,Al]-MFI(HTS) is very high and a high initial productivity of phenol is observed. The deactivation of this latter material is pronounced and relative stable activities are obtained after approximately 3 h. Moreover, we observe that the activity of [Fe,Al]-MFI(HTS) is higher than its untreated counterpart.

Further reaction parameters (benzene and nitrous oxide conversions and their selectivities towards phenol) are listed in table 4. The initial selectivity (after 5 minutes) of benzene to phenol over [Fe,Al]-MFI is approximately 70% indicating that part of the benzene is converted into products different from phenol. These include not only high molecular-weight

coking products but also carbon dioxide and water. Although the conversion of benzene decreases to 7% after 1 h, the selectivity remarkably increases to values close to 100% This is accompanied with a large decrease in the production of water and carbon dioxide. While the benzene selectivity remains close to 100% during the reaction, the nitrous oxide selectivity is clearly lower. These results are explained by the oxidation of coke products that are initially deposited on the catalyst surface. Whether this oxidation occurs directly by nitrous oxide or by molecular oxygen produced by nitrous oxide decomposition is not clear. [Fe,Al]-MFI(HTS) shows a similar reaction pattern as [Fe,Al]-MFI, however, with higher conversion of benzene, resulting in a higher yield of phenol (figure 14). Nevertheless, the nitrous oxide selectivities are somewhat lower suggesting that the process over the calcined zeolite is less efficient.

Table 4: Conversion (X) and selectivity (S) for benzene hydroxylation to phenol (reaction temperature: 623 K, gas composition: 1% benzene, 4% N_2O, 95% He, GHSV: 30000h^{-1}).

	5 min				1 h			
	Benzene		N_2O		benzene		N_2O	
	X	S	X	S	X	S	X	S
	(%)	(%)	(%)	(%)	(%)	(%)	(%)	(%)
[Fe,Al]-MFI	22	69	10	36	7	>98	3	59
[Fe,Al]-MFI(HTS)	38	68	16	42	14	>98	5	71
	3 h				5 h			
	Benzene		N_2O		Benzene		N_2O	
	X	S	X	S	X	S	X	S
	(%)	(%)	(%)	(%)	(%)	(%)	(%)	(%)
[Fe,Al]-MFI	4	>98	3	31	2	>98	4	14
[Fe,Al]-MFI(HTS)	7	>98	3	63	6	>98	3	52

4.4 Discussion

Characterization

[Fe]-MFI, [Al]-MFI and [Fe,Al]-MFI were successfully synthesized via hydrothermal synthesis. The XRD patterns of the calcined materials (figure 1) show the presence of MFI structure. The evolution of the Fe and Al species in these zeolites was studied by various techniques. UV-Vis spectra point to the dispersed nature of Fe in the as-prepared [Fe]-MFI material. Calcination to remove the template leads to the migration of a large part of framework Fe (~ 80%) to extra-framework positions. This result is corroborated by ESR spectra which show a strong increase of the signal at $g = 2.0$. Subsequent steaming further extracts iron from framework positions and we estimate that in this material about 90% of the framework Fe atoms has migrated to extra-framework positions. This migration, however, did not lead to strong agglomeration of the iron oxide phase as derived from the UV-Vis spectra. While in [Al]-MFI virtually all Al atoms are incorporated in the framework of the MFI structure in the presence of the template, we clearly observe that thermal activation leads to the partial loss of Al from framework positions. Complete removal of the template results in the removal of about 5% of aluminum from the framework. After steaming activation about one third of the Al atoms is present at extra-framework positions. The lower stability of Fe at framework positions of the MFI framework agrees with its larger ionic radius (0.057 nm for Al^{3+} *vs.* 0.067 nm for Fe^{3+}).

The combination of both metals in the framework results in a further destabilization of the framework. This is already noted in the as-prepared material since the amount of Fe at framework positions has significantly decreased comparing [Fe,Al]-MFI and [Fe]-MFI. After calcination and complete removal of the template almost all Fe atoms have migrated to extra-framework positions. It is more difficult to draw conclusions on the removal of Al from framework positions for [Fe,Al]-MFI samples because the presence of paramagnetic Fe leads to broadening of part of the ^{27}Al NMR signal beyond detection. For instance, about 90% of the Al signal is detected in the as-synthesized [Fe,Al]-MFI zeolite. All Al atoms might still be at framework positions but a portion is perturbed by extra-framework Fe species leading to a decrease of the resonant signal at 52 ppm. On the other hand, it might also be that part of the Al atoms has migrated to the micropores close to Fe centers. This latter explanation is underpinned by the observation that in calcined and steamed [Fe,Al]-MFI the ratio of detectable octahedral and tetrahedral species is lower than in the [Al]-MFI zeolite. These

observations point to the close proximity of (extra-framework) Fe species to extra-framework Al species. A comparison of the ESR spectra of the [Fe,Al]-MFI and [Fe]-MFI zeolites shows that in the former sample the signal around $g = 3.1$ is smaller. Although the assignment of this signal is not clear, it has been suggested to relate to very small iron oxide clusters. It may thus very well be that the presence of Al prevents sintering of Fe oxide species to some degree or that part of the Fe^{3+} is not detected. Possibly, this is due to the presence of a larger fraction of Fe^{2+} in [Fe,Al]-MFI. The x-ray absorption data are in support of this latter surmise. Clearly, the pre-edge feature due to Fe^{3+} species is lower in the samples containing aluminum and a pre-edge feature due to Fe^{2+} presence. The stronger absorption at lower energies further points to the presence of a fraction of Fe in a lower oxidation state. Interestingly, it appears that [Fe,Al]-MFI(HTS) contains a larger fraction of such reduced Fe states than [Fe,Al]-MFI.

Reactivity

The present reactivity data show large differences in the nitrous oxide decomposition rates among the various catalysts. Before and after steaming, [Al]-MFI shows a negligible N_2O conversions up to temperatures of 800 K. This corresponds to recent data of Pérez-Ramirez *et al*. (44,45) who found that [Al]-MFI and [Ga]-MFI only exhibit significant activities above 800 K. A deviant result in the present work is the observation that [Fe]-MFI and [Fe]-MFI(HTS) are also not active up to temperatures of 800 K. Pérez-Ramirez *et al.* (44,45) reported relatively high activities for steam-activated [Fe]-MFI. The reason for the discrepancy is unclear at the moment.

The present results point to a strong synergy between Fe and Al in the nitrous oxide decomposition reaction. The activity of [Fe,Al]-MFI(HTS) is considerably higher than that of its calcined counterpart. The positive effect of steam treatment on the decomposition of nitrous oxide has been described before (44-46)**.** Although generally the beneficial effect of a hydrothermal treatment is attributed to additional extraction of Fe from framework positions, we have concluded that virtually all Fe is already extracted in the calcined sample. Therefore, it is unlikely that the increase in activity obtained after steaming, *i.e.* [Fe,Al]-MFI(HTS) ,is due to changes in the distribution of framework and extra-framework Fe species.

A comparison of the activities in the selective oxidation of benzene to phenol shows similar differences. The samples containing one hetero-atom, either [Al]-MFI or [Fe]-MFI, produce almost negligible amounts of phenol, whereas [Fe,Al]-MFI exhibits high phenol

productivities. The absence of phenol production for [Al]-MFI proves that strong Brønsted acid sites (14) cannot be the active sites. Our data also contrast earlier claims that Al Lewis sites obtained by dehydroxylation of zeolite Si-O-Al groups are the active sites. Steam-activated [Al]-MFI ([Al]-MFI(HTS)) in which about one third of the Al is located at extra-framework positions has a negligible activity. The deviant conclusions of earlier reports most probably derive from the presence of considerable amounts of iron in the zeolitic starting materials. This is exemplified by the good performance of a steam-activated commercial HZSM-5 zeolite (chapter 3) with an iron content of 0.024 wt.%. On the other hand, the two [Fe]-MFI zeolites also exhibit a much lower activity than [Fe,Al]-MFI. Others have reported reasonable phenol productivities for [Fe]-MFI (23), the activities being generally somewhat lower compared to [Fe,Al]-MFI-type materials. While Selli *et al.* (23) prepared [Fe]-MFI from sodium silicate which often contains an Al admixture (25), other authors have reported the presence of considerable amounts of Al (~ 0.03 wt.%) in their samples (47). We thus interpret the present finding, *i.e.* the almost negligible activity of Fe-[MFI](HTS) with an Al content below 0.005 wt.%, as a strong indication that aluminum is a required element for the selective benzene oxidation with nitrous oxide. This finding is further corroborated by the observation that the addition of Al via reaction with trimethylaluminum followed by calcination or steaming results in a catalyst with similar phenol productivities as [Fe,Al]-MFI (chapter 5). Comparing [Fe,Al]-MFI and [Fe,Al]-MFI(HTS) we note that the latter catalyst shows a significantly higher phenol productivity. The reaction parameters for both catalysts are almost similar suggesting that the difference is mainly due to a larger amount of active sites in the steamed catalyst.

Active sites in [Fe,Al]-MFI zeolites

The present data thus provide very strong indications for the proposal that Fe and Al are both important in the generation of catalytic sites for the oxidation of benzene with nitrous oxide. Whereas it is more or less clear that Fe should be located at extra-framework positions, the preferred position of Al has not been elucidated yet. Stabilization of iron complexes of low nuclearity on cation-exchange positions has been proposed (5,25). A general finding is that steam activation at moderate or calcination at high temperatures is required to activate these catalysts. This has been described for [Fe,Al]-MFI, despite the observation that already a significant fraction of iron has migrated from framework positions during template removal. The present results also show that the largest fraction of Fe has been removed from

framework positions in calcined [Fe,Al]-MFI. Nevertheless, we observe that a subsequent steam treatment strongly improves the decomposition rate of nitrous oxide and the oxidation of benzene to phenol. Rather than extraction of Fe from the zeolite framework, it appears that the extraction of Al from the framework is a prerequisite for a more active material. We can thus propose an alternative description of the active sites, *i.e.* an extra-framework mixed iron-aluminum-oxide (Fe-Al-O) species. The importance of high-temperature treatments (calcination or steaming) is thus related to the extraction of Al, resulting in the formation of a larger amount of Fe-Al-O species (6,11,13,15). This tentative model explains various reports in the literature. For instance, Dubkov *et al.* (48) have shown that active materials can be obtained by impregnation of small amounts of $FeCl_3$ into HZSM-5 followed by high-temperature calcination or steaming. Obviously, the impregnation route results in extra-framework Fe species and the necessity of high-temperature treatments for the formation of active sites can be explained by the removal of Al from framework positions. Those data show that steaming activation can be carried out at lower temperatures than calcination to produce equivalent numbers of active sites and this perfectly corresponds to the general notion that zeolite Si-O-Al bonds are less stable under hydrothermal conditions. Our results in chapter 2 and 3 for sublimed catalysts can also be interpreted in these terms. While sublimation mainly leads to the deposition of Fe at extra-framework positions, high-temperature calcination and especially steaming results in a higher number of sites active in nitrous oxide decomposition and a higher activity in the decomposition of nitrous oxide and the oxidation of benzene to phenol.

This interpretation is further underpinned by the IR results of adsorbed NO. Spectra of steamed [Al]-MFI and [Fe]-MFI clearly show bands due to NO_2 complexes on extra-framework Al and Fe sites, respectively. These bands are less pronounced in [Fe,Al]-MFI with similar Fe and Al content. Additionally, strong additional bands are found around 1620 and 1635 cm^{-1}. We infer that these bands are related to an extra-framework mixed iron-aluminum-oxide species (Fe-Al-O) in line with the assignment of the band at 1635 cm^{-1} to such particles by Mul *et al*. (39). The observation that these signals increase after steam activation stresses their extra-framework nature.

The current findings warrant the conclusion that an extra-framework Fe-Al-O species stabilized in the zeolite micropores is the active component in the activation of nitrous oxide and the related benzene oxidation with nitrous oxide. We can only speculate on the structure of such species. Earlier, we concluded that the active sites in sublimed Fe/ZSM-5 may very well be made up of dimeric Fe^{2+} complexes (chapter 2). Instead of the proposed stabilization

of such Fe dimers on cationic exchange positions we surmise that extra-framework Al species may be involved. The importance of Fe^{2+} in active materials is also suggested by the present XANES observation that [Fe,Al]-MFI contains a higher amount of Fe^{2+} states than [Fe]-MFI, while steaming of [Fe,Al]-MFI leads to an even more reduced state. This evolution of the oxidation state of Fe corresponds to an increased presence of Al at extra-framework positions, an increased activity in nitrous oxide decomposition and an increased phenol productivity.

4.5 Conclusion

Fe and Al are incorporated into the framework of MFI zeolites by isomorphous substitution. During subsequent calcination or steaming steps, the hetero-atoms (Fe and Al) are removed from framework to extra-framework positions. There is a strong indication from the ^{27}Al NMR spectra and IR of adsorbed NO that Fe-Al-O clusters are formed at elevated temperature and such clusters are responsible to activate N_2O for the selective oxidation of benzene to phenol. Base on X-ray absorption spectra, we suggest that the Fe in the active sites is Fe^{2+} and stabilized by extra-framework Al. The controversial results in the literature are most probably caused by the impurities of iron or aluminum.

Reference

1. Catalysis: An Integrated Approach to Homogeneous, Heterogeneous and Industrial Catalysis, J.A. Moulijn, P.W.N.M. van Leeuwen and R.A. van Santen (Eds.), Elsevier, Amsterdam, 1993.
2. Catalysis and Zeolites Fundamentals and Applications, J. Weitkamp and L. Puppe (Eds.) chapter.5, Springer Press, NewYork, 1999.
3. B.D. Mcnicol and G.T. Pott, J. Catal. 25 (1972) 223.
4. P. Ratnasamy, R.B. Borade, S. Sivasanker,V.P. Shiralkar and S.G. Hegde, Acta, Phys. Chem. 31 (1985) 137.
5. G.I. Panov, CatTech 4 (2000) 18.
6. G.I.Panov, V.I. Sobolev and A.S. Kharitonov, J. Mol. Catal. 61 (1990) 85.
7. E. Suzui, K. Nakashiro and Y. Ono, Chem. Lett. (1988) 953.
8. M.H. Gubelmannand P.J. Tirel, Fr.Pat. 2630735 (1988).
9. V.I. Sobolev, G.I. Panov, A.S. Kharitonov, V.N. Romannikov, A.M. Volodin and K.G. Ione, J. Catal. 139 (1993) 435.

10. K.A. Dubkov, V.I. Sobolev, E.P. Talsi, M.A. Rodkin, N.H. Watkins, A.A. Shteinman and G.I. Panov, J. Mol. Catal. 123 (1997) 155.

11. A. Ribera, I.W.C.E. Arends, S.de Vries, J. Pérez-Ramírez and R.A. Sheldon, J. Catal. 195 (2000) 287.

12. P. Kubánek, B. Wichterlová and Z. Sobalík , J. Catal. 211 (2002) 109.

13. D. Meloni, R. Monaci, V. Solinas, G. Berlier, S. Bordiga, I. Rossetti, C. Oliva and L. Forni, J. Catal. 214 (2003) 169.

14. R. Burch and C. Howitt, Appl. Catal. A 103 (1993) 135.

15. J.L. Motz, H. Heinrichen and W.F. Hölderich, J. Mol. Catal. A. 136 (1998) 175.

16. M. Iwamoto, K. Matsukami and K. Kagawa, J. Phys. Chem. 87 (1983) 903

17. A.K. Uriarte, M.A. Rodkin, M.J. Gross, A.S. Kharithonov, G.I. Panov, Stud. Surf. Sci. Catal. 110 (1997) 857.

18. A.M. Thayer, C&Eng News, April 6th (1998) 21.

19. G. Centi, F. Cavani, F. Trifirò, Selective Oxidation by Heterogeneous Catalysis, Kluwer Academic, New York, 2001.

20. G.I. Panov, V.I. Sobolev, K.A. Dubkov, V.N. Parmon, N. S. Ovanesyan, A.E. Shilov and A.A. Shteinman, React. Kinet. Catal. Lett. 61 (1997) 251.

21. N.A. Kachurovskaya, G.M. Zhidomirov, E.J.M. Hensen and R.A. van Santen, Catal. Lett. 86.(2003) 25

22. P.Notté, Top.Catal. 13 (2000) 387.

23. E. Selli, A. Isernia and L. Forni, PCCP 2 (2002) 3301.

24. G. Berlier, A. Zecchina, G. Spoto, G. Ricchiardi., S. Bordiga, C. Lamberti, J. Catal. 215 (2003) 264.

25. P.Ratnasamy and R. Kumar, Catal. Today 9 (1991) 329.

26. M. Vaarkamp, J.C. Linders and D.C. Koningsberger, Phys. B (1995) 209.

27. G. Zi, T. Dake and Z. Ruiming, zeolites 8 (1988) 453.

28. D. Goldfarb, M. Bernardo, K.G. Strohmaier, D.E.W. Vaughan and H. Thomann, J. Am. Chem. Soc. 116 (1994) 6344

29. A. Brückner, In Spectroscopy of Transition Metal Ions on Surfaces B.M. Weckhuysen, P. Van Der Voort and G. Catana (Eds.), Leuven University Press.Belgium,1990, p.69.

30. G. Berlier, G. Spoto, S. Bordiga, G. Ricchiardi, P. Fisicaro, A. Zecchina, I. Rossetti, E. Selli, L. Forni, E. Giamello and C. Lamberti, J. Catal. 208 (2003) 64.

31. P. Fejes, I. Kiricsi, K. Lázár, I. Marsi, A. Rockenbauer, L. Korecz, J. B. Nagy, R. Aiello and F. Testa, Appl. Catal 242 (2003) 247.

32. D.H. Lin, G. Coudurier and J.C. Vedrine, Stud. Surf. Sci. Catal. 49 (1989) 1431.

33. Y. Han, X. Meng, H. Guan, Y. Yu, L. Zhao, X. Xu, X. Yang ,S. Wu, N. Li and F. Xiao, Micropor. Mesopor. Mater. 57 (2003) 191.

34. S. Bordiga, R. Buzzoni, F. Geobaldo, C. Lamberti, E. Giamello, A. Zecchnina, G. Leofanti, G. Petrini, G. Tozzola and G. Vlaic J. Catal. 158 (1996) 486.

35. O.H. Han, C.-S. Kim and S.B. Hong, Angew. Chem. Int. Ed. 41 (2002) 469.

36. P. Marturano, L. Drozdová, A. Kogelbauer and R. Prins, J. Catal. 192, (2000) 236.

37. P. Sarv, C. Fernandez, J.-P. Amourex, J. Phys. Chem. 100 (1996) 19223.

38. H.-Y Chen, El-M. El-Malki, X. Wang, R.A. van Santen and W.M.H. Sachtler, J. Mol. Catal. 162 (2000) 159.

39. G. Mul, J. Pérez-Ramírez, F. Kapteijn and J.A. Moulijn, Catal. Lett. 80 (2002) 129.

40. L.J. Lobree, I.-C. Hwang, J.A. Reimer and A.T. Bell, Catal. Lett. 63 (1999) 233.

41. K. Nakamoto, Infrared and Raman Spectra of Inorganic and Coordination Compounds, Wiley, New York, 1997.

42. H.-Y. Chen, T. Voskoboinikov and W.M.H. Sachtler, J. Catal. 180 (1998) 171.

43. A.A. Battiston, J.H. Bitter, F.M.F. de Groot, A.R. Overweg, O. Stephan, J.A. van Bokhoven, P.J. Kooyman, C. van der Spek, G. Vankó and D.C. Koningsberger, J. Catal. 213 (2003) 251.

44. J. Pérez-Ramírez, F. Kapteijn, G. Mul and J.A. Moulijn, Catal. Commun. 3 (2002) 19.

45. J. Pérez-Ramírez, F. Kapteijn and A. Brückner, J.Catal. 218 (2002) 234.

46. J. Pérez-Ramírez and E.V.Kondratenko, Chem.Commun (2003) 2152

47. V.I. Sobolev, K.A. Dubkov, E.A. Paukshtis, L.V. Pirutko, M.A. Rodkin, A.S. Kharitonov and G.I.Panov, Appl Catal A. 141 (1996) 185.

48. K.A. Dubkov, N.S. Ovansyan, A.A. Shteinman, E.V. Starokon and G.I. Panov, J. Catal., 207 (2002) 341.

Chapter 5

Design of active catalysts for the selective oxidation
of benzene to phenol by nitrous oxide

Abstract

A number of iron- and aluminum-containing MFI zeolites were synthesized by various methods. The active site content was evaluated by IR spectroscopy of adsorbed NO and correlated to the activity in the selective oxidation of benzene to phenol by nitrous oxide. Next to the known route via extraction of these elements from framework positions in isomorphously substituted FeZSM-5, post-synthesis dispersion of aluminum into iron-silicalite, of iron into HZSM-5 or iron and aluminum into silicalite-1 offer preparation routes to obtain active and selective catalysts. The results provide very strong evidence for the necessity of an extra-framework mixed iron-aluminum oxo complex in the activation of nitrous oxide and the selective formation of phenol from benzene with nitrous oxide. In addition to the removal of hetero-atoms from the framework, hydrothermal treatment at relatively high temperatures facilitates the formation of such active sites.

5.1 Introduction

Generally, studies in heterogeneous catalysis include the preparation of catalytic materials, characterization of active sites and catalytic test reactions. The final goal is to come to a fundamental understanding of the constitution of the active sites thus providing clues for the synthesis of catalysts that suit the demand most. This is particularly true for selective oxidation reactions where fine-tuning of the oxidation capability of catalysts is important for obtaining maximum yield of the oxygenated products and avoiding extensive combustion of the valuable product (1). The oxidation of benzene to phenol with nitrous oxide presents a special case where the reactant and product molecules are rather stable towards oxidation to carbon dioxide and water (2). However, overoxidation of phenol produces unwanted condensable products responsible for deactivation (3).

Characterization of the active sites in the Fe/ZSM-5 system for the activation of nitrous oxide and the subsequent oxidation of an aromatic is very challenging. This is partly due to the fact that only a small fraction of Fe participates in these reactions, an observation which is particularly true for samples with a higher Fe loading as for instance obtained by sublimation of $FeCl_3$ on HZSM-5 (chapter 2 and 3). Nevertheless, careful characterization of sublimed samples treated under different conditions and a comparison of the resulting reactivities pointed out that extra-framework Al species might play an important role in the formation of the active sites and to further study this, isomorphously substituted samples were prepared with lower Fe loading (chapter 4). These results provided strong evidence for the presence of an extra-framework Fe-Al-O species. The observed synergism between Fe and Al explains a large number of apparently contradictory observations in the recent literature (4-10). Foremost, the necessity to activate these materials at high temperature, preferably under hydrothermal conditions, tallies with our proposal that Al should be present at extra-framework positions.

It is obvious that these conclusions are more persuasive if one can use this knowledge to predict the catalytic performance of new preparation methods. The aim of this chapter is foremost to do so. The starting point for the design of catalytic materials for the selective oxidation of benzene is the conclusion that extra-framework Fe and Al species are required for the active site formation. Since [Fe]-MFI (iron-silicalite) is (almost) inactive in the benzene oxidation, incorporation of Al should result in an active material. Inspired by a recent report on the incorporation of trimethylgallium in the micropores of HZSM-5 (11), we attempt to incorporate trimethylaluminum, in the micropores of [Fe]-MFI. Conversely, we

attempted to incorporate iron into inactive [Al]-MFI via the sublimation method. Although this has been extensively described in chapters 2 and 3, it is worthwhile to revisit this method starting from an iron-free HZSM-5 material that is inactive in the selective oxidation of benzene to phenol with nitrous oxide. Both of the preparations involve the attachment of molecular species onto the surface via reaction with hydroxyl group Moreover, the impregnation of the nitrates of iron and aluminum into silicalite-1 was attempted. To obtain more insight into the efficiency of the formation of active sites, several [Fe,Al]-MFI samples were prepared with different Fe and Al content by isomorphous substitution. The materials are characterized by IR of adsorbed NO, giving insight into the amount of extra-framework Fe, Al and Fe-Al oxide species, which is correlated to the activity in selective oxidation of benzene.

5.2 Experimental

Catalyst preparation

Zeolites with the MFI topology and different Fe and Al contents were prepared by hydrothermal synthesis and optionally steamed as described before (chapter 4). The samples are designated as [Fe]-MFI, [Al]-MFI followed by the suffix '(HTS)' when the sample was steamed. The zeolites which were prepared by incorporating both Fe and Al in the lattice are designated as [Fe,Al]-MFI(x, y, HTS) where x stands for the weight percentage of iron, y for the Si/Al ratio and HTS optionally for steaming. Iron-silicalite, [Fe]-MFI, was used as a precursor to incorporate Al via the deposition of trimethylaluminum. To this end, an amount of well-dried [Fe]-MFI, either calcined or steamed, was mixed with excess of pure trimethylaluminum (Me$_3$Al, Aldrich) in a nitrogen-flushed glove box. The methyl groups of Me$_3$Al are reactive towards hydroxyl groups. After 24 h, excess Me$_3$Al was removed by evacuation and the sample was calcined at 823 K. Optionally, the samples were further modified by a steaming treatment at 973 K. The resulting materials are denoted as [Fe]-MFI+Me$_3$Al, [Fe]-MFI(HTS)+Me$_3$Al, [Fe]-MFI+Me$_3$Al(HTS) and [Fe]-MFI(HTS)+Me$_3$Al(HTS). Incorporation of Fe in [Al]-MFI was carried out by the sublimation method that was extensively described in chapter 2. Further modification was achieved by steaming, (973 K, 10% water vapor for 3 h). The catalysts are referred to by the suffix 'FeCl$_3$'. Silicalite-1 was synthesized by the indicated procedure (chapter 4) without addition of iron or aluminum to the synthesis gel. Fe and Al were introduced into silicalite-1 by pore volume impregnation of the corresponding nitrates (Fe(NO$_3$)$_3$·9H$_2$O, Merck,

98%Al(NO$_3$)$_3$·9H$_2$O, Janssen, 99%) at a pH of 4. The catalyst is referred to as Si-1+Imp(Fe,Al)

All materials show the typical diffraction pattern of zeolites with the MFI topology. Elemental analysis was carried out by ICP-OES and the elemental composition of the various materials are condensed in table 1.

Table 1: Elemental analysis for the various catalysts.

	Al content (wt. %)	Fe content (wt. %)	Si/Al
[Al]-MFI	0.88	<0.001	42
[Fe]-MFI	<0.005	0.55	-
[Fe,Al]-MFI	0.92	0.51	40
[Fe,Al]-MFI(0.015,40)	0.96	0.015	38
[Fe,Al]-MFI(0.092,40)	0.96	0.092	38
[Fe,Al]-MFI(0.45,40)	0.88	0.45	42
[Fe,Al]-MFI(0.013,80)	0.48	0.013	78
[Fe,Al]-MFI(0.089,80)	0.48	0.089	78
[Fe,Al]-MFI(0.46,80)	0.50	0.46	77
[Fe]-MFI+AlMe$_3$	1.4	0.55	27
[Al]-MFI+FeCl$_3$	0.88	2.63	42
Si-1+Imp(Fe,Al)	1.0	0.6	36

Infrared spectra of self-supporting 10 mg catalyst wafers were recorded at room temperature on a Bruker IFS-113v Fourier Transform IR spectrometer with a DTGS detector at a resolution of 4 cm^{-1}. Typically, a sample was pre-treated *in situ* in oxygen at a temperature of 823 K for 1 h and cooled to room temperature *in vacuo* (pressure less than 10^{-6} mbar), followed by room temperature exposure to NO (purity > 99.9%, 10 mbar) for 30 minutes. The sample was evacuated and a spectrum was recorded at 298 K. Subsequently, the sample was stepwise evacuated at various desorption temperatures (423 K, 473 K, 573 K, 673 K and 773 K). After each desorption, the sample was cooled to ambient temperature and a spectrum was recorded.

Reaction data were collected in a single-pass atmospheric plug flow reactor. Analysis was performed by a well-calibrated combination of GC and MS. Prior to reaction, the catalyst was pre-treated in a flow of 100 ml·min^{-1} O$_2$/He (20 vol.% O$_2$) whilst heating to 823 K at a rate of 1 K·min^{-1}. Benzene oxidation was carried out by feeding a mixture of C$_6$H$_6$/N$_2$O/He (volume

ratio = 1:4:96) at a flow rate of 100 ml·min^{-1} at a reaction temperature of 623 K. More details are given in chapter 3.

5.3 Results and discussion

Two series of zeolites were prepared with silicon-to-aluminum ratios of 40 and 80. We will first discuss the results for the aluminum-rich materials and then present a comparison with the data for the zeolites with a lower Al content. Figure 1 shows the phenol productivities of the zeolites with a Si/Al ratio of 40 and increasing Fe content. Note that all materials have been steam-treated. The corresponding reaction data are condensed in tables 2 and 3.
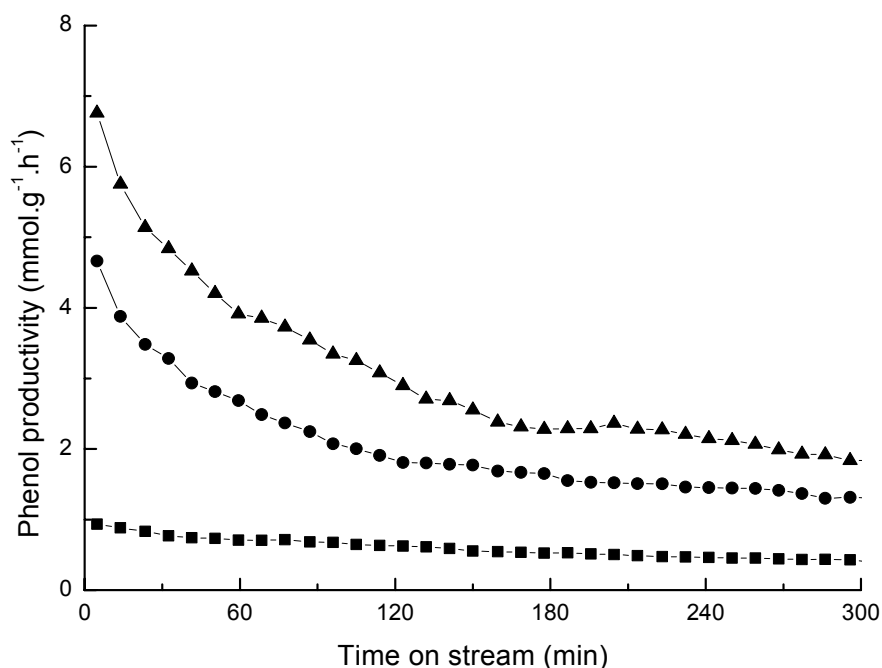
Figure 1: Phenol productivity as function of the reaction time in the oxidation of benzene with nitrous oxide (temperature: 623 K, feed composition: 1 vol.% C_6H_6, 4 vol.% N_2O, make-up He, GHSV = 30000 h^{-1}) for (■) [Fe,Al]-MFI(0.015, 40, HTS), (●) [Fe,Al]-MFI(0.092, 40, HTS), (▲) [Fe,Al]-MFI(0.45, 40, HTS).

All the catalysts show similar behavior in the sense that a high activity is followed by a strong deactivation and a plateau in activity after approximately 3 h. The deactivation is more pronounced for a higher Fe content. This stems from a higher degree of coke formation. The trend appears to correspond to the model where a higher content of active sites not only

results in a higher productivity of phenol but also to further condensable (over- oxidized) products. Moreover, we can conclude that the utilization of Fe in active sites decreases strongly with increasing Fe content. This point will be discussed in more detail below.

The reaction parameters clearly show that an increase of the Fe content primarily leads to an increase of the benzene conversion. Although the selectivities are close to 100% at higher reaction times, we find that a small part of the benzene feed is combusted at the initial stages. This is confirmed by the somewhat lower benzene and nitrous oxide selectivities (tables 2 and 3) and the concomitant production of carbon dioxide and water (not shown). The extent to which combustion contributes to the conversion of benzene increases with increasing Fe content and tentatively we attribute this to small iron oxide particles occluded in the micropores of the zeolites similar to the case in sublimed Fe/ZSM-5 catalysts (chapter 2 and 3).

Table 2: Benzene conversion and selectivity to phenol for the two series with Si/Al = 40 and 80 with varying iron content.

	Conversion (%)			Selectivity (%)		
	5 min	1 h	5 h	5 min	1h	5 h
[Fe,Al]-MFI(0.015, 40, HTS)	7	4	2	95	>98	>98
[Fe,Al]-MFI(0.092, 40, HTS)	20	10	5	90	>98	>98
[Fe,Al]-MFI(0.45, 40, HTS)	32	14	6	80	>98	>98
[Fe,Al]-MFI(0.013, 80, HTS)	4	2	1	96	>98	>98
[Fe,Al]-MFI(0.089, 80, HTS)	10	7	3	94	>98	>98
[Fe,Al]-MFI(0.46, 80, HTS)	29	14	7	73	96	>98

Table 3: Nitrous oxide conversion and selectivity to phenol for the two series with Si/Al = 40 and 80 with varying iron content.

	Conversion(%)			Selectivity(%)		
	5 min	1 h	5h	5 min	1 h	5 h
[Fe,Al]-MFI(0.015, 40, HTS)	2	1	<1	97	>98	>98
[Fe,Al]-MFI(0.092, 40, HTS)	6	2	1	73	>98	>98
[Fe,Al]-MFI(0.45, 40, HTS)	13	3	2	50	>98	>98
[Fe,Al]-MFI(0.013, 80, HTS)	1	<1	<1	>98	>98	>98
[Fe,Al]-MFI(0.089, 80, HTS)	3	2	1	84	>98	>98
[Fe,Al]-MFI(0.46, 80, HTS)	8	3	2	62	>98	>98

Figure 2 compares the nitrous oxide decomposition activities as a function of the temperatures for the zeolites with a Si/Al ratio of 40. Clearly, one observes that the trends in nitrous oxide decomposition are similar to those found in the selective oxidation of benzene to phenol, although the differences tend to be somewhat larger. Furthermore, we notice that the activity of the sample with the highest iron content is considerably lower than that of a sublimed Fe/ZSM-5(HTS) catalyst (chapter 3).
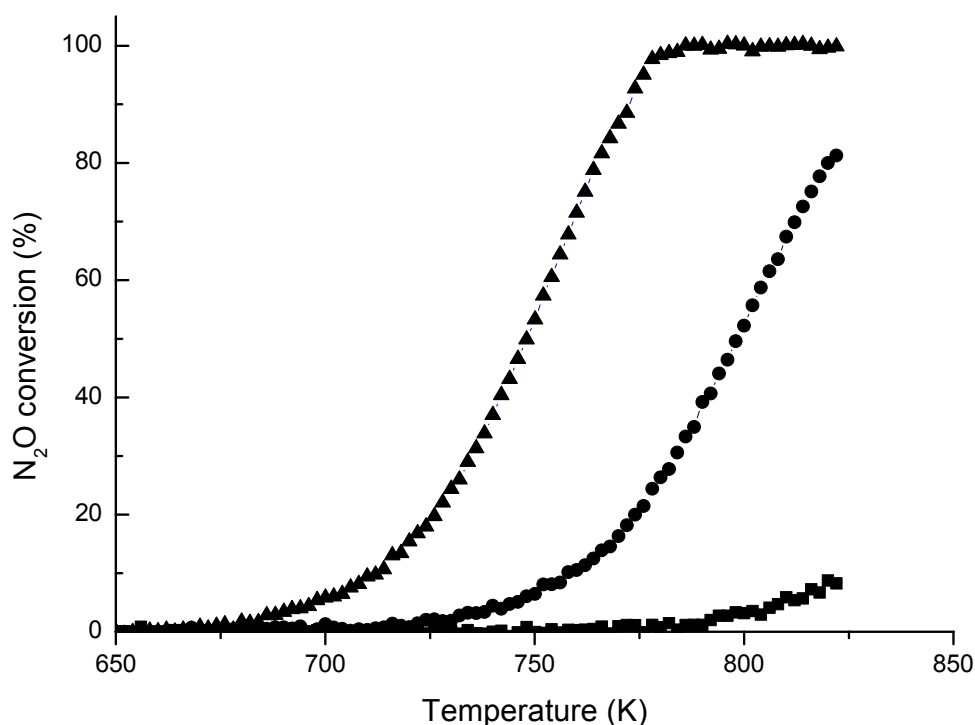

Figure 2: Temperature programmed decomposition of nitrous oxide (feed composition: 5000 ppm N_2O, make-up He, GHSV = 30000 h^{-1}) for (■) [Fe,Al]-MFI(0.015, 40, HTS), (●) [Fe,Al]-MFI(0.092, 40, HTS), (▲) [Fe,Al]-MFI(0.45, 40, HTS).

Figure 3 shows the IR spectra in the region of 1500 to 4000 cm^{-1} after adsorption of NO at room temperature. The spectra of the corresponding dehydrated zeolites have been subtracted. The interaction of NO with the Si(OH)Al bridging hydroxyl groups can be easily observed by the negative peak around 3610 cm^{-1}. The hydroxyl stretching mode is perturbed by adsorbed NO. Concomitantly, the signal due to positively charged NO at cationic positions of the zeolite framework appears around 2130 cm^{-1} (12,13). The stability of this complex is relatively low as derived from the disappearance of the bands around 2130 cm^{-1} upon evacuation (not shown). The calcined zeolites have similar Brønsted acidity except for the

zeolite with a higher Si/Al ratio. Steam activation results in a substantial decrease of the number of bridging hydroxyl groups. We also observe that the acidity is lowest for the steamed zeolite with a Si/Al ratio of 80.
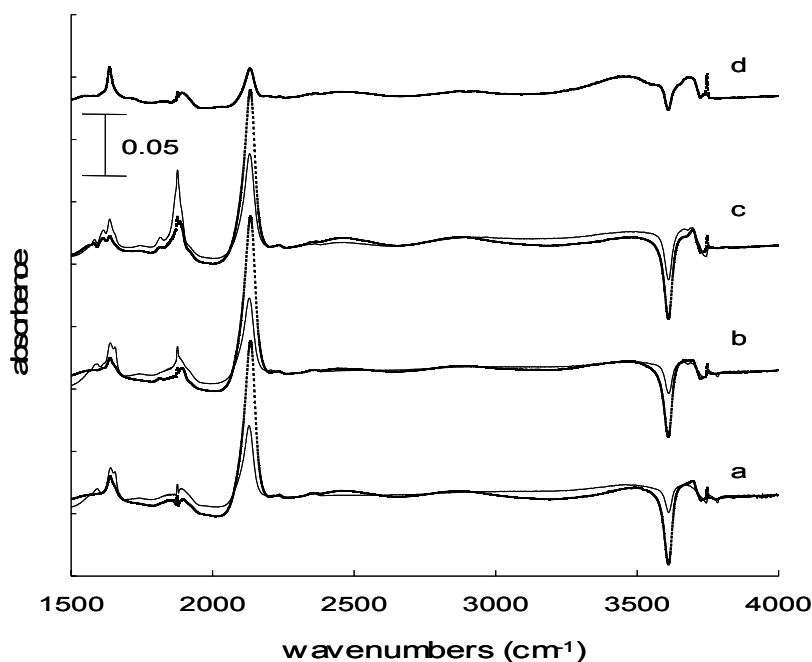

Figure 3: Room temperature IR spectra of adsorbed NO (5 mbar) on (a) [Fe,Al]-MFI(0.015, 40), (b) [Fe,Al]-MFI(0.092, 40), (c) [Fe,Al]-MFI(0.45, 40) and (d) [Fe,Al]-MFI(0.089, 80). Full and dotted lines correspond to steamed and calcined zeolites, respectively.

The spectra also present a strong feature around 1876 cm^{-1} superimposed on the gas-phase spectrum of NO. The intensity of this band increases with increasing iron content. This is in line with the assignment to NO adsorbed on Fe species and most frequently this band is attributed to mono-nitrosylic species associated with Fe^{2+} sites (14,15). On the contrary, Mul *et al*. (13) recently provided indications that this feature belongs to NO on Fe^{2+} species associated in FeAlO$_x$ nanoparticles. In the present investigations, we observe that this band increases with increasing iron content and is more pronounced after steaming. Whereas this would appear to cohere with the reported assignment of Mul *et al*. (13), we also identify this band in steamed [Al]-MFI suggesting that NO adsorbed on extra-framework Al species produces a similar signal. We thus surmise that the signal at 1876 cm^{-1} that is close to the gas-phase vibration of NO is due to weakly chemisorbed NO on coordinately unsaturated sites. Thus, NO also adsorbs on coordinatively unsaturated Al sites. This then explains the somewhat lower intensity of this band in [Fe,Al]-MFI(0.092, 80, HTS) than in [Fe,Al]-

MFI(0.089, 40, HTS). Whereas the materials with quite low Fe content contain one feature around 1876 cm^{-1}, this band exhibits a shoulder in [Fe,Al]-MFI(0.45, 40, HTS) at the low frequency side. The fact that we observe this band around 1865 cm^{-1} only for samples with a high Fe content agrees with the notion of extra-framework Fe species that are located on the external surface of the zeolite (13). The band at 1818 cm^{-1} which is observed weakly for the [Fe,Al]-MFI(0.092, 40) zeolites and more pronounced for the [Fe,Al]-MFI(0.45, 40) zeolites is usually assigned to a dinitrosyl adsorbed on isolated Fe^{2+} sites located in the accessible α-positions of the zeolite lattice (12,16). The finding that this feature is only observed for high Fe contents would suggest the contrary and we attribute this band tentatively to some form of aggregated iron oxide.
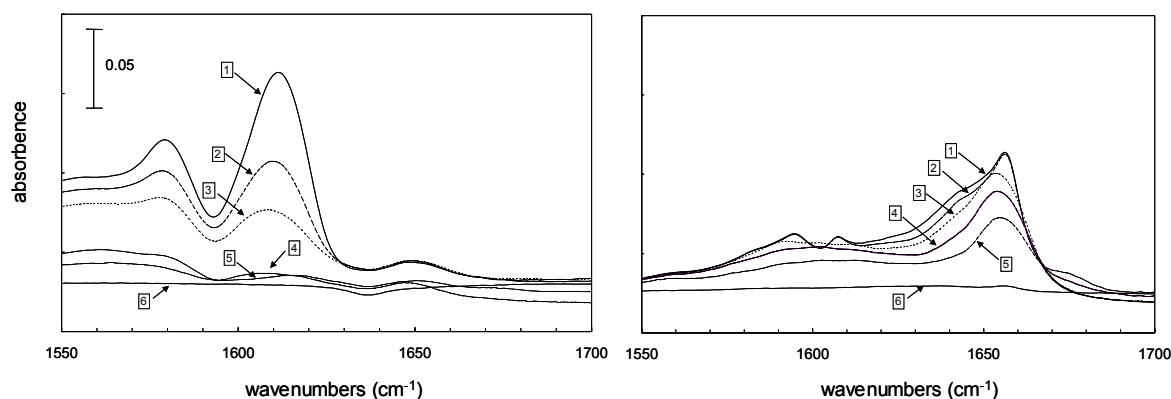

Figure 4: IR spectra after stepwise desorption of NO on (left) [Fe]-MFI(HTS) and (right) [Al]-MFI(HTS). The labels 1-6 refer to the desorption temperatures 273 K, 323 K, 373 K, 473 K, 573 K and 773 K.

Figure 4-7 compare IR spectra in the region of 1500-1700 cm^{-1} after stepwise temperature desorption of NO for the [Fe,Al]-MFI series with a Si/Al ratio of 40 with those of steam-activated [Fe]-MFI and [Al]-MFI (figure 4). These spectra allow us to study the evolution of the absorption bands in samples with Fe contents in the range of <0.001 wt.% to 0.45 wt.% Fe. Features between 1600 and 1700 cm^{-1} are usually attributed to NO_2 complexes in view of the fundamental of NO_2 at 1621 cm^{-1} (13,17, chapter 4). [Al]-MFI(HTS) presents bands around 1644 cm^{-1}, 1656 cm^{-1} and a band around 1673 cm^{-1} which only forms at higher temperatures. The bands at 1656 cm^{-1} and 1673 cm^{-1} exhibit a much lower intensity in calcined [Al]-MFI (not shown), while the band at 1644 cm^{-1} presents a similar intensity. We attribute the bands at 1656 cm^{-1} and 1673 cm^{-1} to NO_2 bands on extra-framework Al species extracted from lattice positions during the steaming treatment. The assignment of the band at 1644 cm^{-1} is not clear, but we observe this band also for [Fe]-MFI(HTS) and it thus may

relate to some structural defect of the zeolite not related to the presence of hetero-atoms.. The spectrum of [Fe]-MFI(HTS) clearly presents a band around 1610 cm^{-1} and this is attributed to extra-framework Fe-NO$_2$ species (chapter 4). The spectra of calcined [Fe,Al]MFI(0.015, 40) in figure 5 exhibit similar bands as [Al]-MFI(HTS) and their evolution with increasing desorption temperature is also alike. The band at 1656 cm^{-1} has a lower intensity as the corresponding band in [Al]-MFI(HTS) because the sample has not been steamed. In this case, we observe a very weak shoulder around 1635 cm^{-1} which we have identified as an extra-framework Fe-Al-O species (chapter 4). There might also be a very weak feature centered around 1615 cm^{-1} indicative of the presence of Fe-O species.

Figure 5: IR spectra after stepwise desorption of NO on calcined (left) and steamed (right) [Fe,Al]-MFI(0.015, 40). The labels 1-7 refer to the desorption temperatures 273 K, 323 K, 373 K, 473 K, 573 K, 673 K and 773 K.
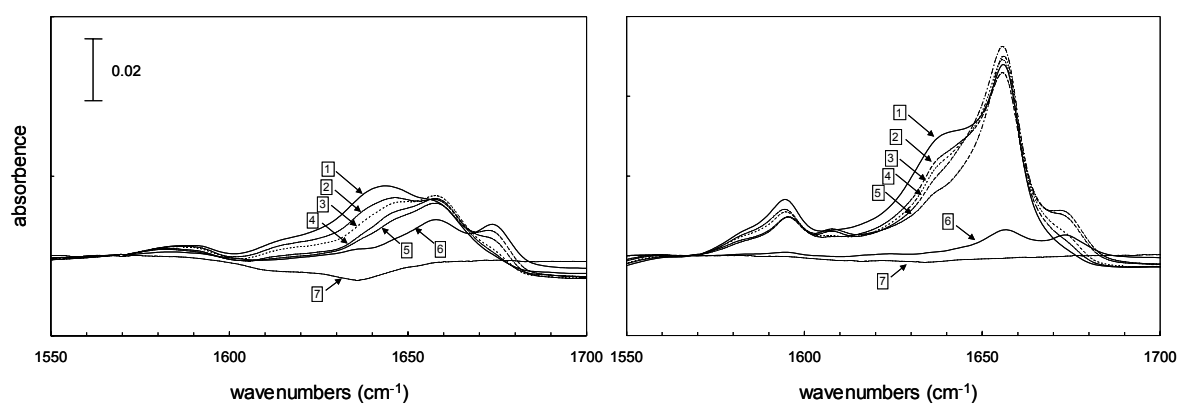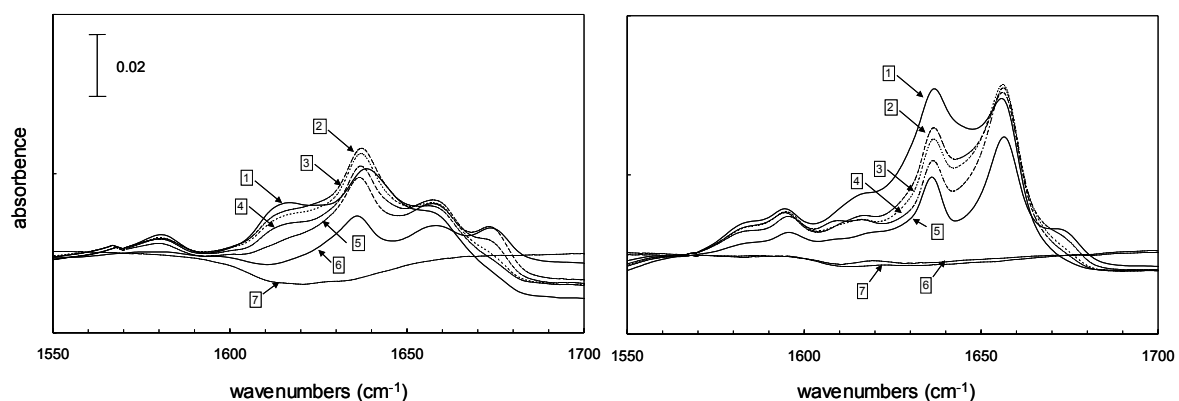

Figure 6: IR spectra after stepwise desorption of NO on calcined (left) and steamed (right) [Fe,Al]-MFI(0.092, 40). The labels 1-7 refer to the desorption temperatures 273 K, 323 K, 373 K, 473 K, 573 K, 673 K and 773 K.

Interestingly, we observe an isobestic point at 1668 cm^{-1} suggesting that the species belonging to the band at 1673 cm^{-1} derives from the complex associated with the band at 1656 cm^{-1}. It might very well be that we are dealing with nitrito groups (NO$_2$ coordinating to a metal center via oxygen atoms) which transform into nitro groups (NO$_2$ group coordinating to a metal center via a nitrogen atom) at elevated temperature.

The various bands become more pronounced after steam activation of this sample. The band at 1635 cm^{-1} is now clearly observed next to the weak band around 1610 cm^{-1}. More extensive removal of Al from the framework is underpinned by a strong increase of the signal at 1656 cm^{-1}. The weak bands below 1600 cm^{-1} are usually assigned to nitrate groups and their intensity appears to correlate to the occurrence of NO$_2$ groups. A further increase of the iron content to 0.092 wt.% results in a significant growth of the band at 1635 cm^{-1}. The band at 1644 cm^{-1} cannot be observed anymore. The band at 1635 cm^{-1} in [Fe,Al]-MFI(0.092, 40, HTS) is much more pronounced than in its calcined counterpart (figure 6). Moreover, the signal around 1656 cm^{-1} has decreased and this underpins our surmise that extra-framework Al atoms are involved in the occurrence of the band at 1636 cm^{-1}. While the intensity of the band around 1615 cm^{-1} due to NO$_2$ in interaction with Fe centers is low in these samples, it becomes more pronounced in [Fe,Al]-MFI(0.45, 40). We attribute this to the higher iron content allowing the formation of extra-framework Fe species in which no Al is present. The signal due to Fe-Al-O species around 1635 cm^{-1} has also increased. However, the signals due to NO$_2$ interacting with extra-framework Al species are hardly observed. The steamed sample shows a peculiar behavior. After room temperature adsorption the spectrum is dominated by two bands at 1615 cm^{-1} and 1635 cm^{-1} and a weak features around 1656 cm^{-1} and higher. Upon desorption at higher temperatures we observe that the band at 1615 cm^{-1} decreases and the band at 1635 cm^{-1} increases. The reason for this behaviour is not clear at the moment but it can be that NO$_2$ or NO species migrate from the extra-framework Fe species to the Fe-Al-O species. This could be taken as an indication that the Fe-Al-O species and Fe-O species are not too distant. In any case, it is clear that the sample with a higher Fe content is more heterogeneous in the sense that it contains both extra-framework Fe-O and Fe-Al-O species.
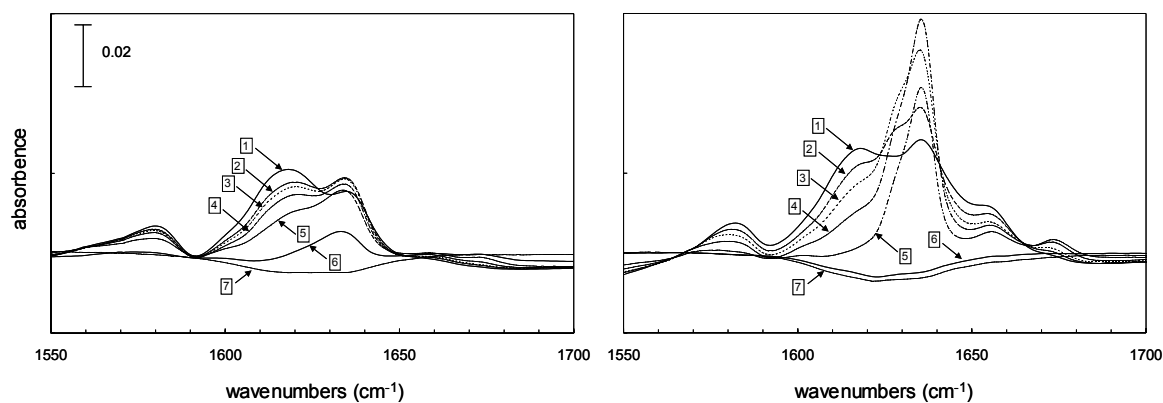
Figure 7: IR spectra after stepwise desorption of NO on calcined (left) and steamed (right) [Fe,Al]-MFI(0.45, 40). The labels 1-7 refer to the desorption temperatures 273 K, 323 K, 373 K, 473 K, 573 K, 673 K and 773 K.
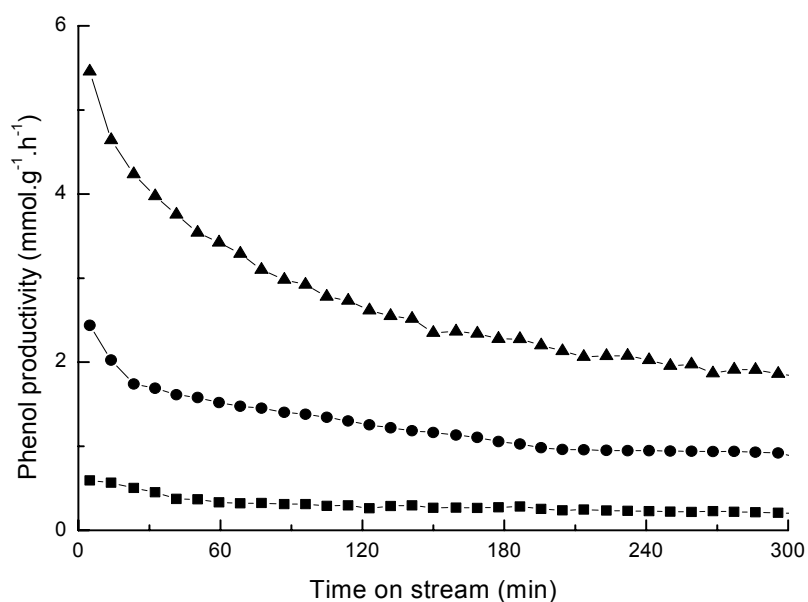
Figure 8: Phenol productivity as function of the reaction time in the oxidation of benzene with nitrous oxide (temperature: 623 K, feed composition: 1 vol.% C_6H_6, 4 vol.% N_2O, make-up He, GHSV = 30000 h^{-1}) for (■) [Fe,Al]-MFI(0.013, 80, HTS), (●) [Fe,Al]-MFI(0.089, 80, HTS), (▲) [Fe,Al]-MFI(0.46, 80, HTS).

Figure 8 collects the phenol productivities as a function of the reaction time for the materials with a lower Al content. The corresponding benzene and nitrous oxides conversion and selectivities were given already in tables 2 and 3. The trends in the various parameters are almost identical to the results for the catalysts with a Si/Al ratio of 40. We clearly observe

that the lower Al content primarily leads to a decrease of the conversion and this can be explained by a lower content of active sites.

This also has a positive influence on the relative stability and we observe lower deactivation rates for the silica-rich materials. Comparing the activities of [Fe,Al]-MFI(0.015, 40, HTS) and [Fe,Al]-MFI(0.013, 80, HTS) we note that the former is about two times more active than the sample with half the Al content. This shows that the phenol productivity correlates to the Al content in this range. On the other hand, this is valid to a lesser extent for the samples with a higher Fe content. However, we note that deactivation of these samples is more pronounced and it could very well be that the initial productivity for [Fe,Al]-MFI(0.45, 40, HTS) is much higher than for [Fe,Al]-MFI(0.46, 80, HTS). The IR spectrum of adsorbed NO is shown in figure 9 and clearly shows a lower intensity of the band due to extra-framework Al-O species. This corresponds to a lower Al content of the starting material. The almost complete absence of this band, however, seems to be in contrast with the possibility to further increase the activity upon increasing the iron content. Although not conclusive, we forward that an increase of the Fe content in the starting material will also further destabilize framework Al species and thus increase the extra-framework Fe-Al-O species.

Figure 9: IR spectra after stepwise desorption of NO on [Fe,Al]-MFI(0.089, 80, HTS). The labels 1-7 refer to the desorption temperatues 273 K, 323 K, 373 K, 473 K, 573 K, 673 K and 773 K.

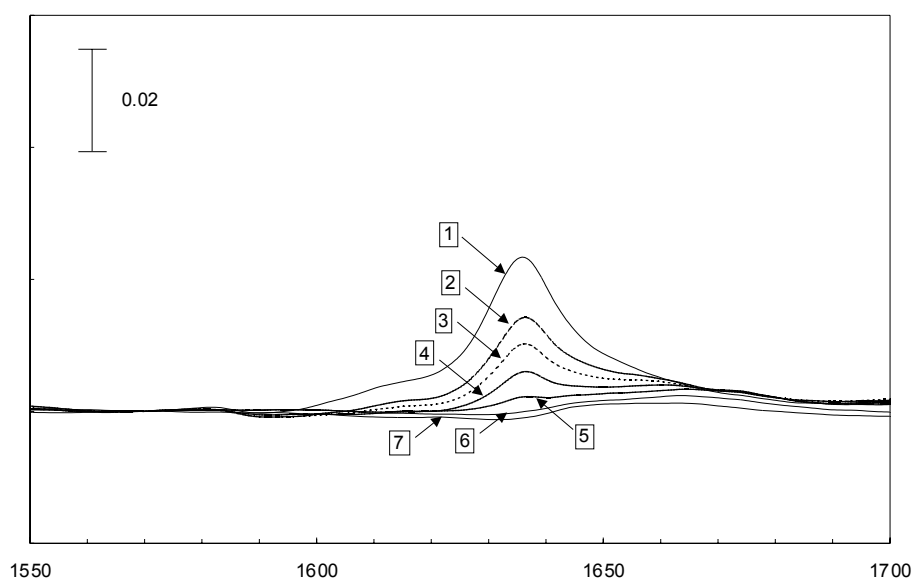Figure 10 shows the effect of aluminum introduction in Fe-[MFI] on the phenol productivity. Calcined and steamed [Fe]-MFI only produce minute amounts of phenol (0.1-

0.2 mmol·g^{-1}·h^{-1}). The incorporation of Me$_3$Al significantly increases the productivity of the hydroxylated compound. Moreover, a subsequent steaming treatment further increases the overall performance. Steaming of the starting material ([Fe]-MFI(HTS) instead of [Fe]-MFI) before Al introduction also improves the catalytic properties. As presented in chapter 4, steaming activation of Fe-[MFI] leads to additional removal of framework Fe species. This provides an explanation for the higher activity when starting from the steamed precursor. The most active sample is obtained by a steam treatment of [Fe]-MFI(HTS)+Me$_3$Al(HTS) and we surmise that the formation of the active Fe-Al-O species might be facilitated by hydrothermal conditions (*vide infra*).
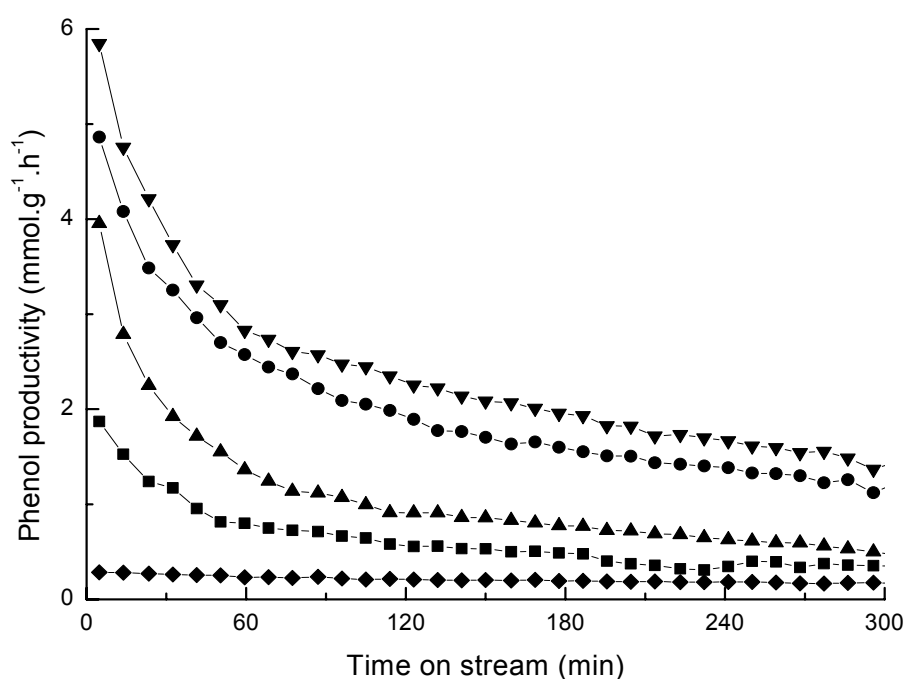
Figure 10: Phenol productivity as function of the reaction time in the oxidation of benzene with nitrous oxide (temperature: 623 K, feed composition: 1 vol.% C$_6$H$_6$, 4 vol.% N$_2$O, make-up He, GHSV = 30000 h^{-1}) for (♦) [Fe]-MFI(HTS), (■) [Fe]-MFI+Me$_3$Al, (●) [Fe]-MFI+Me$_3$Al(HTS), (▲) [Fe]-MFI(HTS)+Me$_3$Al and (▼) [Fe]-MFI(HTS)+Me$_3$Al(HTS).

Table 4 and 5 show the corresponding benzene and nitrous oxide conversions and selectivities, respectively. The incorporation of Al efficiently increases the benzene and nitrous oxide conversion and particularly their selectivities towards the formation of phenol. Further steaming treatment results in similar but more pronounced effects. Nevertheless, when the [Fe]-MFI(HTS) is used as starting material to incorporate Al, it has a different

reaction pattern. The relatively lower N_2O selectivity, compared with their Fe-[MFI]+Me$_3$Al counterparts, indicates that after a certain time part of the nitrous oxide is used for combustion of benzene and/or coke products. As outlined in chapter 2 and 3, this is probably related to the presence of some agglomerated iron oxide phases. Such species may also be present to a larger extent in the steamed [Fe]-MFI precursor than the calcined one. Subsequent introduction of Al leads to the generation of Fe-Al-O sites which are capable of producing selectively phenol from benzene but appears to leave some extra-framework Fe species in the micropores. It might very well be that the mobility of such species is hindered by the larger amount of extra-framework Al species in these materials.

Table 4: Benzene conversion and selectivity to phenol with oxidant N_2O at 623 K,Component: 4% N_2O, 1% benzene diluted in He, GHSV: 30000 h^{-1}.

	Conversion(%)			Selectivity(%)		
	5 min	1 h	5 h	5 min	1h	5 h
Fe-[MFI](HTS)	9	6	4	12	7	5
[Fe]-MFI+AlMe$_3$	10	4	1	69	75	>98
[Fe]-MFI+AlMe$_3$(HTS)	23	9	5	77	>98	>98
[Fe]-MFI(HTS)+AlMe$_3$	20	5	2	75	90	>98
[Fe]-MFI(HTS)+AlMe$_3$(HTS)	25	12	8	90	86	70

Table 5: N_2O conversion and selectivity to phenol with oxidant N_2O at 623 K, Component: 4% N_2O, 1% benzene diluted in He, GHSV: 30000 h^{-1}

	Conversion(%)			Selectivity(%)		
	5 min	1 h	5 h	5 min	1 h	5 h
Fe-[MFI](HTS)	1	1	1	35	10	2
[Fe]-MFI+AlMe$_3$	3	2	1	53	50	50
[Fe]-MFI+AlMe$_3$(HTS)	8	2	1	57	>98	>98
[Fe]-MFI(HTS)+AlMe$_3$	3	2	2	>98	50	20
[Fe]-MFI(HTS)+AlMe$_3$(HTS)	4	3	4	>98	>98	40

Figure 11 shows the IR spectra of the two steamed samples. We will limit the discussion to the development of the bands in the region of the NO$_y$ complexes but note that especially the band at 1876 cm^{-1} strongly increases upon incorporation of trimethylaluminum and oxidation. The spectrum for [Fe]-MFI+Me$_3$Al(HTS) clearly contains bands around 1615 cm^{-1} with a somewhat lower intensity than in [Fe]-MFI(HTS), bands around 1628 and 1635 cm^{-1} and

weak features around 1660 cm^{-1}. The band at 1635 cm^{-1} is related to the active Fe-Al-O species and the one at 1628 cm^{-1} was also observed for [Fe,Al]-MFI(HTS) (chapter 4). Whereas these spectra appear rather complex, the IR spectra of [Fe]-MFI(HTS)+Me$_3$Al(HTS) only exhibits one strong vibration at 1635 cm^{-1} with two very weak features at 1615 cm^{-1} and 1656 cm^{-1}. Moreover, similar to the case in figure 7 the intensity grows with increasing desorption temperature. Comparing the two materials in figure 12, [Fe]-MFI(HTS)+Me$_3$Al(HTS) contains a higher intensity of the band at 1635 cm^{-1} and this corresponds to its higher activity.
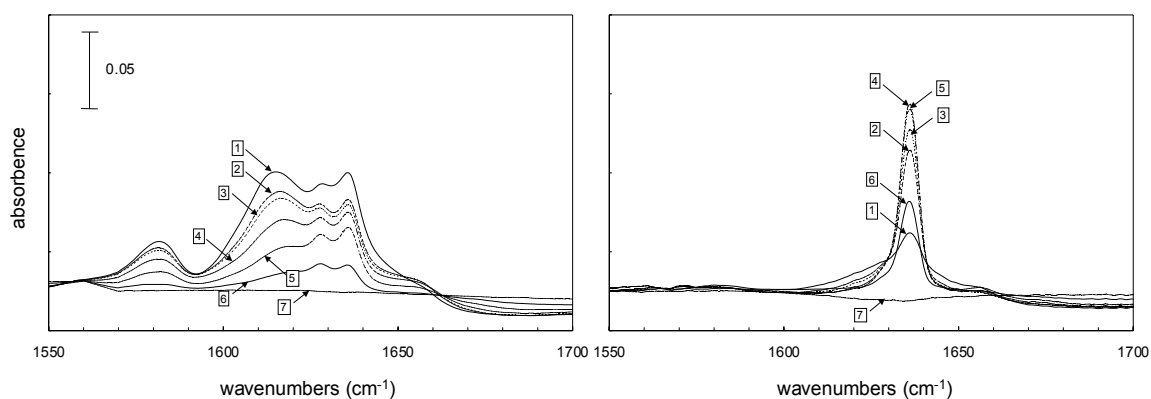

Figure 11: IR spectra after stepwise desorption of NO on [Fe]-MFI+Me$_3$Al(HTS) (left) and [Fe]-MFI(HTS)+Me$_3$Al(HTS) (right) The labels 1-7 refer to the desorption temperatures 273 K, 323 K, 373 K, 473 K, 573 K, 673 K and 773 K.

Figure 12 shows the relation between the intensity of the band at 1635 cm^{-1}, that we have speculated to derive from the active Fe-Al-O species, and the initial phenol productivity for the [Fe,Al]-MFI(x, 40, HTS) series and for [Fe,Al]-MFI(0.089, 80, HTS). It is obvious there is a linear relationship. We take this as evidence that Fe-Al-O clusters are active in the the selective oxidation of benzene to phenol. Moreover, the proportional increase of the intensity the band for [Fe,Al]-MFI(0.092, 40, HTS) compared to [Fe,Al]-MFI(0.089, 80, HTS) indicates the involvement of extra-framework Al species in the active sites. This relation is less straightforward for the Fe content and this suggests that not all the extra-framework Fe participate in the formation of active sites. This corresponds to observations that part of the Fe is aggregated, either in the micropores or external surface of the zeolites.
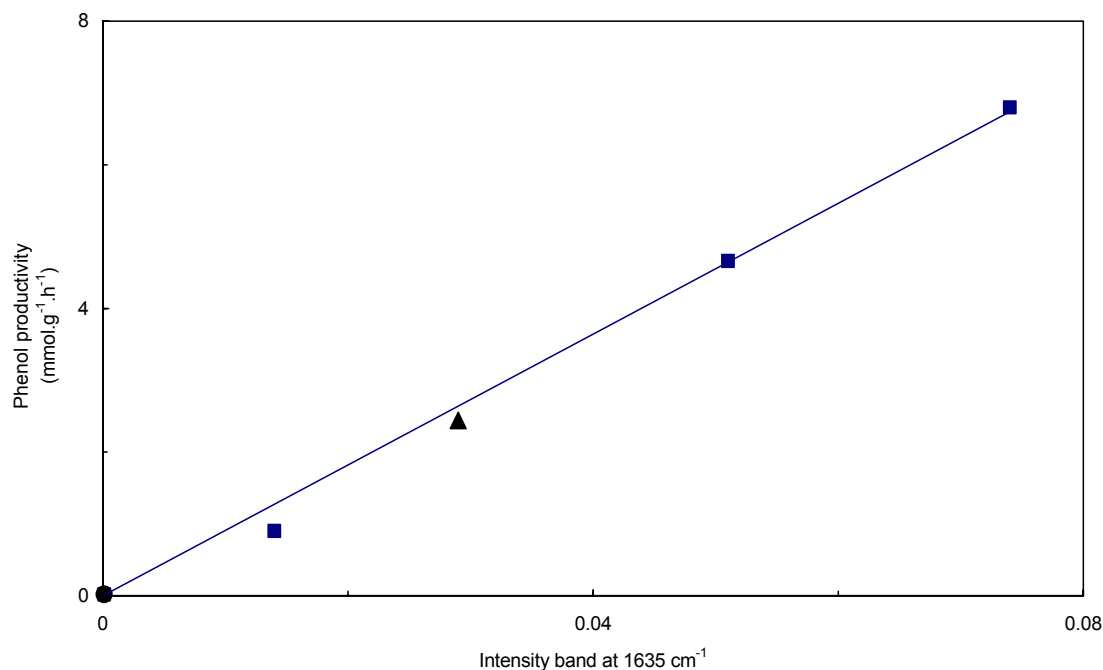
Figure 12: The relation between the active sites and the catalytic performance. Catalyst: (●) [Fe]-MFI(HTS), (■) [Fe,Al]-MFI(x, 40, HTS) , (▲) [Fe,Al]-MFI(0.089,80)(HTS), (temperature: 623 K, feed composition: 1 vol.% C_6H_6, 4 vol.% N_2O, make-up He, GHSV = 30000 h^{-1}, phenol formation after 5 min in reaction)

A third method to produce active materials is the introduction of Fe into [Al]-MFI. This can be achieved by aqueous impregnation of a suitable iron salt but this generally results in iron oxide agglomerates on the external surface. On the other hand, sublimation of $FeCl_3$ has been extensively described (*e.g.* chapter 2 and 3) and provides a method to disperse a molecular Fe species over the protonic sites of the zeolites. Figure 13 presents the phenol formation as a function of the time-on-stream over various catalysts prepared via sublimation of $FeCl_3$ on various forms of iron-free [Al]-MFI.

We did not observe the formation of phenol over steamed [Al]-MFI nor over calcined [Al]-MFI (not shown). The introduction of Fe into [Al]-MFI, *i.e.* [Al]-MFI+$FeCl_3$, results in the selective phenol formation. However, the catalyst deactivates quickly and the phenol productivity is hardly observed after *ca.* 3 h. It was shown in chapter 4 that extra-framework Al occur after removal of the template and we thus conclude these extra-framework aluminum species form active Fe-Al-O species with the introduced iron. When the material is steam-activated ([Al]-MFI+$FeCl_3$(HTS)), more aluminum is dislodged from the framework (chapter 4) to form active sites, resulting in a higher and more stable activity. Interestingly, the extra-framework introduction of Al to [Fe]-MFI or Fe to [Al]-MFI produces similar

results and this tallies with the notion of the relevance of an extra-framework species as the active site. Moreover, we surmise that the hydrothermal treatment also facilitates in the generation of the active sites, most likely due to improved mobility.
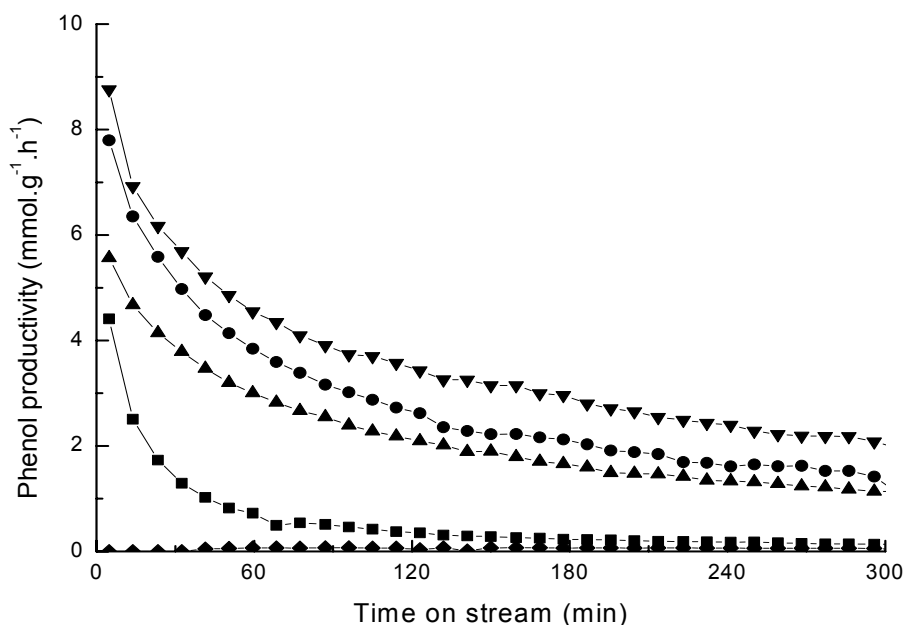
Figure 13: Phenol productivity as function of the reaction time in the oxidation of benzene with nitrous oxide (temperature: 623 K, feed composition: 1 vol.% C_6H_6, 4 vol.% N_2O, make-up He, GHSV = 30000 h^{-1}) for (♦) [Al]-MFI(HTS), (■) [Al]-MFI+FeCl$_3$, (●) [Al]-MFI+FeCl$_3$(HTS), (▲) [Al]MFI(HTS)+FeCl$_3$ and (▼) [Al]-MFI(HTS)+FeCl$_3$(HTS).

The benzene and nitrous oxide conversions and selectivities for the sublimed materials are shown in tables 6 and 7. In contrast to the results for the materials prepared by introduction of trimethylaluminum, the intrazeolite introduction of Fe causes a considerable increase in combustion rate of the catalyst. This is indicated by the relatively low selectivities. This is in line with the observation of Fe/ZSM-5 prepared by sublimation method (chapter 3) and this strengthens our surmise that combustion is due to some iron oxide particles in the micropore space of the zeolite. This could very well be cationic iron clusters that are active in the decomposition of nitrous oxide but do not generate phenol.

Table 6: Benzene conversion and selectivity to phenol with oxidant N_2O at 623 K, Component: 4% N_2O, 1% benzene diluted in He, GHSV: 30000 h^{-1}.

	Conversion(%)			Selectivity(%)		
	5 min	1 h	5 h	5 min	1h	5 h
[Al]-MFI+FeCl$_3$	31	7	5	53	27	11
[Al]-MFI+FeCl$_3$ (HTS)	42	16	6	70	90	98
[Al]-MFI(HTS)+FeCl$_3$	32	14	6	65	83	70
[Al]-MFI(HTS)+FeCl$_3$(HTS)	40	18	9	83	94	>98

Table 7: N_2O conversion and selectivity to phenol with oxidant N_2O at 623 K, Component: 4% N_2O, 1% benzene diluted in He, GHSV: 30000 h^{-1}

	Conversion(%)			Selectivity(%)		
	5 min	1 h	5 h	5 min	1 h	5 h
[Al]-MFI+FeCl$_3$	32	12	4	11	4	1
[Al]-MFI+FeCl$_3$ (HTS)	25	20	8	30	20	18
[Al]-MFI(HTS)+FeCl$_3$	22	9	7	25	32	16
[Al]-MFI(HTS)+FeCl$_3$(HTS)	19	6	7	44	65	33

It is well known that trivalent ions like Fe^{3+} or Al^{3+} become hydrated during aqueous ion exchange and even form polynuclear species. These aquated ions are generally too large to enter the micropores of zeolites. Thus, such clusters mostly end up at external surface of the zeolite. The impregnation of $Fe(NO_3)_3$ and $Al(NO_3)_3$ was used to introduce iron and aluminum to silicalite-1. The objective is to investigate the function of steaming apart from the removal of hetero-atoms from framework of the zeolites.

Figure 14 presents the reaction profile of selective oxidation of benzene to phenol by nitrous oxide for the silicalite-1-derived samples. Silicalite-1 which does not contain framework substitution sites (Si/Al > 10000) does not show any activity at all. The addition of Fe and Al via pore volume impregnation and subsequent calcination (Si-1+Imp(Fe,Al)) results in a very low productivity of phenol (~ 0.1-0.2 $mmol \cdot g^{-1} \cdot h^{-1}$). Interestingly, steaming treatment of Si-1+Imp(Fe,Al) leads to a dramatic increase of the phenol formation. The initial activity increased to 5.7 $mmol \cdot g^{-1} \cdot h^{-1}$ and a rather high stable activity was achieved(~ 2.5 $mmol \cdot g^{-1} \cdot h^{-1}$). This result indicates that steaming results in the redispersion of iron and aluminum oxides into the micropores of the zeolite. The higher mobility of metal oxide under hydrothermal conditions and especially their migration into the micropores of zeolites is a

relatively well-known process (18). Thus, it may very well be that the hydrothermal conditions are important to improve the mobility of extra-framework species and the generation of mixed oxide species in addition to the necessity to destabilize the framework and extract hetero-atoms. The present result also shows convincingly that no Brønsted acid sites are required to stabilized extra-framework Fe complexes for the formation of active sites in benzene oxidation.
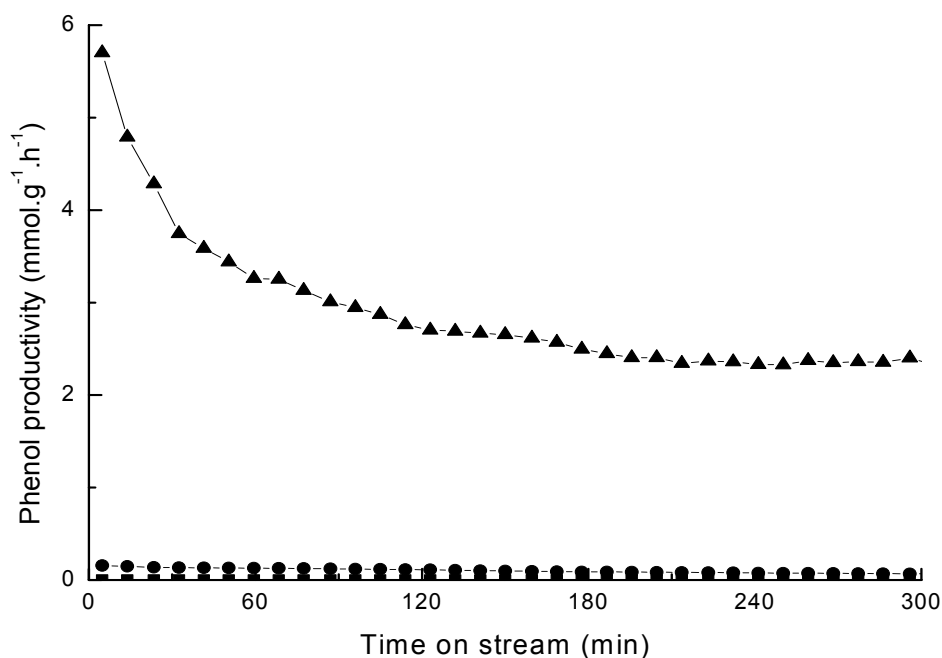

Figure 14: Phenol productivity as function of the reaction time in the oxidation of benzene with nitrous oxide (temperature: 623 K, feed composition: 1 vol.% C_6H_6, 4 vol.% N_2O, make-up He, GHSV = 30000 h^{-1}) for (■)Si-1, (●)Si-1+Imp(Fe,Al), (▲)Si-1+Imp(Fe,Al)(HTS).

As shown in table 8 and table 9, an important observation for Si-1+Imp(Fe,Al)(HTS) is that the benzene and nitrous oxide selectivities are close to 100% directly after the start of the reaction. Whereas in most other samples we observe somewhat lower selectivities and concomitantly small amounts of water and carbon oxides during the first hour of reaction time, phenol is produced almost quantitatively except for the deposition of coke in the micropores. This can be explained by the absence of framework substitutions in the supporting zeolite which implies that no cationic Fe complexes can be stabilized in the micropores. We have suggested before (chapter 3 and 4) and here that such sites may be involved in the full combustion of benzene.

Table 8: Benzene conversion and selectivity to phenol with oxidant N_2O at 623 K,Component: 4% N_2O, 1% benzene diluted in He, GHSV: 30000 h^{-1}.

	Conversion(%)			Selectivity(%)		
	5 min	1 h	5 h	5 min	1h	5 h
Si-1	0	0	0	0	0	0
Si-1+Imp(Fe,Al)	<1	<1	<1	45	>98	>98
Si-1+Imp(Fe,Al)(HTS)	23	12	9	94	>98	>98

Table 9: N_2O conversion and selectivity to phenol with oxidant N_2O at 623 K, Component: 4% N_2O, 1% benzene diluted in He, GHSV: 30000 h^{-1}

	Conversion(%)			Selectivity(%)		
	5 min	1 h	5 h	5 min	1 h	5 h
Si-1	0	0	0	0	0	0
Si-1+Imp(Fe,Al)	<1	<1	<1	20	25	25
Si-1+Imp(Fe,Al)(HTS)	5	3	2	>98	>98	>98

5.4. Discussion

The study of the influence of the iron content in isomorphously substituted MFI on the activity in the conversion of benzene to phenol indicates that an increase in the iron content results in an increase of the phenol productivity. Nevertheless, the increases in phenol productivity are not proportional to the increases in Fe content. This is a strong indication that only a limited part of the iron atoms can be incorporated in the active sites. For this class of materials, we observe that the intensity of the IR band due to NO_2 complexes interacting with extra-framework Fe-Al-O species depends on the Fe content. A linear relation between this band and the initial phenol productivity points to the relevance of extra-framework Fe-Al-O species for the selective oxidation reaction. Comparison to the intensity of this band to a sample with a lower Al content shows that the relation between productivity and intensity holds and this then confirms the presence of Al in these sites.

Initially, these zeolites produce small amounts of carbon oxides and water. However, the active sites for this full combustion apparently deactivate strongly and mostly the benzene selectivity is close to 100% after a reaction time of 1 h. We observe that the extent of full combustion increases with the iron content and this agrees with our surmise that extra-

framework Fe species and most likely cationic Fe species are active in the full combustion step. This speculation is confirmed by the catalysts prepared by post-synthesis dispersion of hetero-atoms into inactive materials. The incorporation of trimethylaluminum into the Fe-[MFI] significantly increases the selectivity of benzene to phenol (table 4) whereas the introduction of $FeCl_3$ into [Al]-MFI increases mainly the combustion of benzene (table 6). Steaming of the sublimed samples leads to an increase of phenol productivity but also to a decrease of the contribution of the full combustion. This can be explained by the extraction of Al from the framework which results in the formation a larger amount of active Fe-Al-O species and a lower amount of cationic Fe species.

It thus appears that the main function of Fe species is to dissociate nitrous oxide. The deposited oxygen atoms on the cationic sites react with another nitrous oxide molecule to produce molecular nitrogen and oxygen. These sites probably give rise to full combustion of benzene, either directly via reaction of the deposited oxygen atoms with benzene or via produced molecular oxygen. The amount of such cationic species is relatively high in calcined materials due to the higher content of framework Al sites and for sublimed materials where Fe is deposited on the cationic exchange sites.

On the other hand, extra-framework Fe-Al-O species are also able to decompose nitrous oxide. The deposited oxygen atom can be selectively inserted into a C-H bond of an adsorbed benzene molecule. We speculate that the vicinal extra-framework Al site can facilitate the selective insertion by providing a specific adsorption mode of the benzene molecule. Comparing the nitrous oxide decomposition activities of sublimed Fe catalysts (chapter 3) and isomorphously substituted samples, it may well be that the nitrous oxide decomposition rate of cationic clusters is higher than that of extra-framework Fe-Al-O species.

The results for the silicalite-1 sample into which iron- and aluminum-nitrate were impregnated provides some further clues for this model. The starting material does not contain any framework substitutions. The calcined precursor shows only a very small phenol productivity and does not produce any full combustion products. We explain this by the preferential presence of the metal oxide particles on the external zeolite surface. It might be that a very small amount of Fe-Al-O species is formed in the zeolite micropores. On the other hand, we cannot exclude that a small amount of Fe-Al-O species is located on the external surface and also catalyzes the selective oxidation reaction. Steaming results in the migration of a small fraction of the metal oxides into the micropores leading to the formation of a higher amount of Fe-Al-O species. This leads to a drastic increase of the selective conversion of benzene to phenol. As framework substitution sites are absent and are not likely to be

regenerated in the hydrothermal conditions, the sample does not contain cationic Fe species. We interpret this as the main reason for the very high selectivities for this sample already in the initial stages of the reaction. These results also stress that the extra-framework Fe-Al-O species do not require stabilization by interaction with framework substitution sites. It is however not clear whether such species are specifically formed in the zeolite micropores or that their dispersion is much higher in the micropores than on the external surface.

We interpret the finding that the active and relatively selective catalysts can be prepared by the post-synthesis dispersion of Fe to [Al]-MFI, of Al to [Fe]-MFI and even Fe and Al to silicalite-1 as strong evidence for the model where extra-framework Fe-Al-O species are the active sites in the selective oxidation of benzene to phenol.

5.5 Conclusion

A comparison of a wide range of iron- and aluminum-containing MFI materials provides further strong indications that both Fe and Al are required for the formation of extra-framework species that are active in the selective conversion of benzene to phenol. The result that an active material can be prepared via impregnation of iron and aluminum salts to silicalite-1 stresses the extra-framework nature of the species. A close inspection of the selectivities during the initial stages of the reaction points to the importance of cationic Fe species in the full combustion side reaction of benzene. Furthermore, the identification of the active species by IR spectroscopy of adsorbed NO is shown to be consistent for a series of samples with varying Fe and Al content. A further important conclusion is that the necessity of high-temperature steaming is not only to extract hetero-atoms from lattice positions for samples prepared by isomorphously substitutions, but also to increase the mobility of extra-framework species resulting in the formation of active Fe-Al-O species.

Reference

1. G. Centi, F. Cavani, F. Trifirò, Selective Oxidation by Heterogeneous Catalysis, Kluwer Academic, New York, 2001.
2. G.I. Panov, CatTech 4 (2000) 18.
3. D. Meloni, R. Monaci, V. Solinas, G. Berlier, S. Bordiga, I. Rossetti, C. Oliva and L. Forni, J. Catal. 214 (2003) 169.

4. R. Burch and C. Howitt, Appl. Catal. A 103 (1993) 135.

5. J.L. Motz, H. Heinrichen and W.F. Hölderich, J. Mol. Catal. 136 (1998) 175.

6. A. Ribera, I.W.C.E. Arends, S. de Vries, J. Pérez-Ramírez and R.A. Sheldon, J. Catal. 195 (2000) 287.

7. P. Kubánek, B. Wichterlová and Z. Sobalík J. Catal. 211 (2002) 109.

8. A.K. Uriarte, M.A. Rodkin, M.J. Gross, A.S. Kharithonov, G.I. Panov, Stud. Surf. Sci. Catal. 110 (1997) 857.

9. P. Notté, Top.Catal. 13 (2000) 387.

10. E. Selli, A. Isernia, L. Forni, PCCP 2 (2002) 3301.

11. M. García-Sánchez, P. C. M. M. Magusin, E. J. M. Hensen, P. C. Thüne, X. Rozanska and R. A. van Santen, Accepted by J. Catal

12. K. Hadjiivanov, H. Knozinger, B. Tsyntsarski and L.Dimitrov, Catal.Lett. 62 (1999) 35.

13. G. Mul, J. Pérez-Ramírez, F. Kapteijn and J.A. Moulijn, Catal. Lett. 80 (2002) 129.

14. H. –Y. Chen, T. Voskobonikov and W.M.H. Sachtler, J. Catal. 180 (1998) 171.

15. M. Lezcano, V.I. Kovalchuk and J.L. d 'Itri, Kinet Catal. 42 (2001) 10.

16. L.J. Lobree, I-Chwang, J.A. Reimer and A.T. Bell, Catal. Lett. 63 (1999) 23.

17. H.-Y Chen, El-M. El-Malki, X. Wang, R.A. van Santen and W.M.H. Sachtler, J. Mol. Catal. 162 (2000) 159.

18. E.J.M. Hensen and J.R. van Veen, Catal.Today, In press.

Summary

Iron-containing pentasil zeolites represent a complex catalytic system due to the heterogeneous nature of the iron oxide phase. Characterization of Fe/ZSM-5 and its analogues, prepared by the sublimation method (chapter 2) or via isomorphous substitution of Si by Fe during synthesis of MFI-type zeolites (chapter 4 and 5) confirms that there are a wide variety of iron-containing species in these materials regardless of the preparation method. The structure of these Fe species and their location combined with other zeolite properties including Brønsted and Lewis acidity ultimately determine the catalytic properties. A further complicating factor is that only a small portion of the iron-containing species is involved in the catalytic action. However, based on complementary information provided by different techniques (Mössbauer, ESR, IR, UV-Vis, *etc*) we can draw a rough picture of the relevance of the different types of Fe species and the nature of the active sites.

For Fe/ZSM-5 prepared by the sublimation method, the initially well-dispersed Fe species will readily migrate to various location in the zeolite matrix (cationic species and small neutral iron oxide particles inside the micropores and larger iron oxide aggregates on the external surface) in the calcination step. The combined results of various characterization techniques including Transmission Electron Microscopy (TEM), ^{57}Fe Mössbauer Absorption Spectroscopy (MAS) and UV-Vis spectroscopy indicate that a large part of the iron oxide phase is present in aggregated form on the external zeolite surface. High-temperature treatments, preferentially in the presence of water, result in various transformations of the iron oxide particles. A protolysis reation between the acidic protons and neutral iron oxide particles gives cationic Fe species. On the other hand, Fe will form a mixed oxide species together with extra-framework Al species. The presence of water during the high-temperature treatment results in a lower extent of cationic species and an increase of the amount of extra-framework Fe-Al-O particles. The increase of the fraction of Fe^{2+} species as probed by MAS might relate to such extra-framework species as also inferred from the results in chapter 4. The transformation of Fe oxide species at high temperatures leads to increased nitrous oxide decomposition rate and the different apparent activation energies indicate that various active species are involved in the catalytic action. It is noteworthy that steaming enhances the catalytic activity of Fe/ZSM-5 for the selective oxidation of benzene to phenol significantly. As several transformations occur simultaneously it is troublesome to separate their catalytic function in the nitrous oxide decomposition and the selective oxidation reaction. A tentative

model is that the selective oxidation takes place on the extra-framework Fe-Al-O species, while the competing combustion reaction proceeds over cationic species. The improvement in the selectivity after steaming may thus be attributed to the extensive removal of Al from the framework thus decreasing the number of such cationic Fe species. The most important conclusion is that there appears to be a crucial role for extra-framework Al species in the formation of active sites.

A study of the template removal in aluminum-containing MFI zeolite indicates that a small portion of the Al is removed from lattice positions. This small but noticeable amount may thus be important in the formation of extra-framework Fe-Al-O species. In contrast to the Fe/ZSM-5 prepared by sublimation method, the preparation of Fe-[MFI], [Al]-MFI and [Fe,Al]-MFI by isomorphous subsitution provides better-defined materials and allows to study the separate catalytic functions of extra-framework Fe and Al species. An extensive study of the calcination procedure to remove the template and subsequent steaming treatment show that Fe is already removed to a large extent during the first step. Its migration to extra-framework positions is more pronounced when Al is present competing for framework positions. Aluminum is much more stable in the zeolite framework and steaming activation is required to extract larger amounts from the framework. Comparison of the catalytic activities in benzene oxidation to phenol for [Fe]-MFI, [Al]-MFI (both not active) and [Fe,Al]-MFI provide strong evidence for the importance of a mixed oxide species for this reaction. Further evidence is provided by catalytic tests of designed catalysts, *i.e.* prepared by incorporation of Al into the [Fe]-MFI, incorporation of Al into the [Fe]-MFI or even impregnation of iron and aluminum nitrates into an all-silica MFI (silicalite-1). We propose the active sites to be mixed iron-aluminum oxo complexes stabilized in the micropores of MFI zeolite denoted as Fe-Al-O species. One important conclusion is that hydrothermal treatment, in addition to extract hetero-atoms from the framework, facilitates the formation of active sites. Moreover, we found that IR of adsorbed probe NO is a powerful technique to identify this species with a characteristic band at 1635 cm^{-1} different from the bands associated with 'free' iron or aluminum extra-framework species. The linear relationship between the intensity of the band at 1635 cm^{-1} and the catalytic performance clearly indicates that such Fe-Al-O is responsible for the selective oxidation of benzene to phenol by nitrous oxide.

Compared with the observation that Fe-Al-O is a prerequisite to activate N_2O to oxidize benzene selectively, it appears that nitrous oxide can be decomposed also over cationic Fe species. We can draw this conclusion based on a variety of experimental results obtained in this research. An increase in the number of such species (high temperature calcination of

sublimed Fe/ZSM-5) results in increased rate of N_2O decomposition whereas its presence leads to combustion of benzene to water and dioxide. It is not clear if the full oxidation of benzene is due to produced molecular oxygen or due to direct oxidation of benzene by oxygen deposited on the cationic species. Since Fe-[MFI], calcined or steam-activated, shows negligible activity in both nitrous oxide decomposition and hydroxylation of benzene to phenol, we take this as evidence that only a small portion of Fe oxide species participates in nitrous oxide activation. In essence, Fe stabilized by framework Al yields active sites for nitrous oxide decomposition which also result in the combustion of benzene. Stabilization of Fe in extra-framework mixed oxo complexes with aluminum yields active catalysts for the selective oxidation of benzene to phenol. This model is supported by the observation that sublimation of $FeCl_3$ into [Al]-MFI gives a very active material for nitrous oxide decomposition which however is not very selective in the oxidation of benzene. On the other hand, dispersion of Fe and Al in silicalite-1 in which no framework substitutions are present and is thus expected to give exclusively Fe-Al-O species results in a very active and selective material. The lower nitrous oxide decomposition rate of these materials suggests that optimal catalysts for nitrous oxide decomposition are those with a large amount of cationic Fe species prepared for instance by sublimation. Selective oxidation catalysts should preferentially contain no cationic species but extra-framework Fe-Al-O species. This can be achieved by starting from all-silica materials or steaming of acidic catalysts. A final interesting point is the oxidation state of the active Fe species in the selective oxidation reaction. From the MAS studies on the sublimed materials it appears that the presence of Fe^{2+} is important which coheres with recent literature. We believe there are two types of auto-reduction taking place transforming Fe^{3+} into Fe^{2+} species. One is the reduction of Fe oxide in the elevated temperature (473 K –773K) in inert gases (He). This auto-reduction is inhibited by the presence of molecular oxygen. These species with an initially high activity deactivate due to re-oxidation to Fe^{3+} (chapter 3). The Fe^{2+} oxidation state is also stabilized in extra-framework Fe-Al-O species. These species are formed in the presence of oxygen and preferentially water at relatively high temperatures. The presence of a considerable amount of Fe^{2+} in [Fe,Al]-MFI is indicated by Fe K-edge XANES. Importantly, that amount increases upon steaming confirming the involvement of an extra-framework species. These Fe^{2+} oxidation states are essentially absent in [Fe]-MFI. A preliminary interpretation of the dehydration of [Fe,Al]-MFI followed by Fe K-edge XANES (not shown) indicates that auto-reduction of Fe^{3+} to Fe^{2+} takes place during removal of adsorbed water. The exact structure of the extra-framework Fe-Al-O species is open for discussion but a tentative model is presented in figure 1.
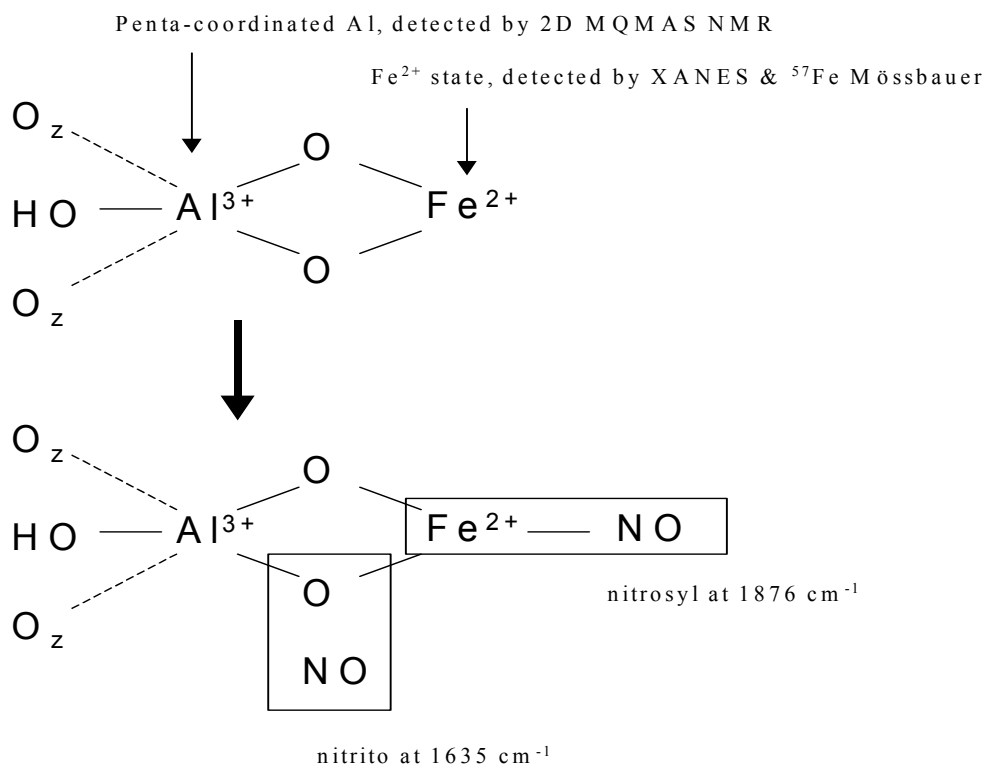
Figure 1: Tentative model for the stabilization of extra-framework Fe-Al-O complexes in the micropores of MFI zeolite. Al^{3+} is penta-coordinated to two oxygen atoms bridging to Fe^{2+}, one hydroxyl group and two framework oxygen atoms. The indicated frequencies relate to those in IR studies of the dehydrated catalyst after exposure to NO.

Samenvatting

IJzerhoudende zeolieten met de pentasil struktuur (ook wel MFI struktuur genoemd) vertonen een complex katalytisch gedrag veroorzaakt door de heterogene aard van de ijzeroxide fase. Karakterisering van Fe/ZSM-5 (ijzer in een zure MFI zeoliet) bereid via de sublimatiemethode (hoofdstuk 2 en 3) of via isomorfe substitutie van Si door Fe gedurende de synthese van het zeoliet (hoofdstuk 4 en 5) laat zien dat er verschillende deeltjes aanwezig zijn in het zeoliet met verschillende katalytische aktiviteiten. Dit hangt niet alleen sterk af van de bereidingsmethode maar ook van de gebruikte voorbehandeling. De struktuur en de lokatie van de ijzerdeeltjes bepalen samen met de andere zeoliet eigenschappen zoals de Brønsted en Lewis zuurgraad uiteindelijk de katalytische eigenschappen. Een verdere complicatie is dat voor bepaalde reakties slechts een klein deel van de ijzerhoudende deeltjes werkelijk deelneemt aan de reakties. We kunnen Gebaseerd op informatie verkregen met aanvullende technieken (Mössbauer, ESR, IR, UV-VIS, etc) een ruwe schets maken van de verschillende type ijzerdeeltjes en het belang voor verschillende katalytische reakties.

In Fe/ZSM-5 geprepareerd via de sublimatiemethode (hoofdstuk 2 en 3) zullen de aanvankelijk goed gedispergeerde Fe deeltjes makkelijk naar verschillende locaties binnen en buiten de zeolietmatrix migreren (kationen en kleine neutrale ijzeroxide deeltjes in the microporiën en grotere ijzerdeeltjes aan het buiten oppervlak) gedurende de calcinering. De gecombineerde resultaten van verschillende karateriseringstechnieken in hoofdstuk 2 (onder andere tranmissie electronen microscopie, ^{57}Fe Mössbauer Absorption Spectroscopy (MAS) en UV-VIS spectroscopie) wijzen erop dat een groot deel van de ijzeroxide fase aanwezig is als relatief grote oxidische deeltjes op het uitwendige oppervlak van het zeoliet. Hoge-temperatuurbehandelingen, preferent in de aanwezigheid van water, resulteren in verschillende tranformaties van de ijzeroxidedeeltjes. Een protolyse reactie tussen de zure protonen en de neutrale ijzeroxidedeeltjes resulteert in kationische ijzerdeeltjes. Anderzijds vormt ijzer een gemengd oxide deeltje samen met Al deeltjes die de struktuur van het zeolietrooster verlaten hebben ('extraframework' deeltjes). De aanwezigheid van water gedurende behandelingen bij hoge temperatuur resulteert in een lagere hoeveelheid van kationische deeltjes en toename van de hoeveelheid extraframework gemend Fe-Al-oxidedeeltjes. De toename van de fraktie ijzer in de 2+ oxidatietoestand gemeten met MAS kan gerelateerd worden aan dergelijke deeltjes zoals ondersteund wordt door de resultaten in hoofdstuk 4.

Hoofdstuk 3 beschrijft de katalytische aktiviteit van de katalysatoren bereid via de sublimatiemethode. De tranformatie van ijzeroxide deeltjes bij hoge temperatuur leidt tot een verhoogde snelheid in ontleding van lachgas en de verschillende schijnbare activeringsenergieën geven aan dat er verschillende deeltjes betrokken zijn bij de katalytische aktie. Het is het vermelden waard dat stomen de katalytische aktiviteit van Fe/ZSM-5 voor de selektieve oxidatie van benzeen naar phenol aanmerkelijk verbeterd. Daar er verschillende transformaties gelijktijdig plaatsvinden tijdens de voorbehandelingen bij hoge temperatuur is het moeilijk om hun funktie in de ontleding van N_2O en die in de selectieve oxidatie te onderscheiden. Een hypothetisch model is dat de selektieve oxidatie plaats vindt op een extraframework Fe-Al-oxidedeeltje terwijl de concurrerende verbrandingsreactie plaats vindt op de kationische ijzerdeeltjes. De verbetering in selektiviteit na stomen zou dus toegekend kunnen worden aan de intensieve verwijdering van Al uit het zeolietrooster. Dit geeft een vermindering van het aantal kationische ijzerdeeltjes en een toename van de hoeveelheid extraframework aluminium. De belangrijkste conclusie is dat er blijkbaar een cruciale rol is voor het extraframework Al in de vorming van aktieve plaatsen.

Een studie naar de verwijdering van templaat in aluminiumbevattende MFI zeolieten (hoofdstuk 4) toont aan dat een klein deel van het aluminium reeds verwijderd van roosterposities. Deze kleine hoeveelheid kan dus van belang zijn in de vorming van extraframework Fe-Al-oxidedeeltjes. In tegenstelling tot Fe/ZSM-5 bereid via de sublimatiemethode levert de bereiding van [Fe]-MFI, [Al]-MFI en [Fe,Al]-MFI via isomorfe substitutie van Si^{4+} door Fe^{3+} (en Al^{3+}) een beter gedefinieerd materiaal en maakt het mogelijk om de verschillende katalytische funkties van de extraframework ijzer- en aluminiumdeeltjes te bestuderen. Een diepgaande studie naar de calcineringsprocedure en een daarop volgende hydrothermale behandeling laat zien dat ijzer al gedurende de eerste stap voor een groot deel uit het zeolietrooster wordt verwijderd. De migratie van ijzer naar extraframework posities is meer uitgesproken indien Al aanwezig is en meedingt naar roosterposities. Aluminium is veel stabieler in het zeoliet rooster en aktivering via stomen is nodig om grotere hoeveelheden uit het rooster te verwijderen. Een vergelijking van de katalytisch aktiviteit in de oxidatie van benzeen naar phenol voor [Fe]-MFI, [Al]-MFI (beiden inaktief) en [Fe,Al]-MFI leveren sterke aanwijzingen voor het belang van gemengde oxide deeltjes voor deze reactie. Verder bewijs wordt geleverd door katalytische testen met speciaal ontworpen katalysatoren. Een voorbeeld is het dispergeren van Al in [Fe]-MFI of zelfs impregnatie van ijzer- en aluminiumnitraten in een silicaliet-1 zeoliet (een zeoliet met de MFI struktuur zonder roostersubstituties). Wij stellen voor dat de aktieve deeltjes bestaan uit gemengde ijzer-aluminium oxo complexen gestabiliseerd in de microporiën van het MFI

zeoliet. Een belangrijke conclusie is dat een aanvullende hydrothermale behandeling om heteroatomen (ijzer en aluminium) uit het rooster te verwijderen de vorming van aktieve plaatsen mogelijk maakt.

Daarnaast blijkt dat infrarood spectroscopie aan geadsorbeerd NO een krachtige techniek is om deze deeltjes met een karakteristieke band bij 1635 cm^{-1} te onderscheiden van de banden geassocieerd met "vrije" ijzer of aluminium extraframework deeltjes (hoofdstuk 5). Het lineaire verband tussen de intensiteit van de band bij 1635 cm^{-1} en de katalytische aktiviteit laat duidelijk zien dat zulke Fe-Al-oxidedeeltjes verantwoordelijk zijn voor de selektieve oxidatie van benzeen naar phenol door N_2O. Vergeleken met de conclusie dat de aanwezigheid Fe-Al-oxidedeeltjes een voorwaarde is voor de aktivering van lachgas om benzeen selectief te kunnen oxideren, lijkt het erop dat lachgas ook ontleed kan worden op kationische Fe deeltjes. We kunnen deze conclusie trekken gebaseerd op een verscheidenheid van experimentele resultaten verkregen tijdens het hier beschreven onderzoek. Een toename van het aantal zulke deeltjes (hoge temperatuur calcinering van gesublimeerd Fe/ZSM-5) resulteert in een toename van de ontledingssnelheid van N_2O terwijl dit tegelijkertijd leidt tot verbranding van benzeen naar water en kooldioxide. Het is niet duidelijk of deze totale oxidatie van benzeen kan worden toegewezen aan gevormd molekulair zuurstof of door directe oxidatie van benzeen door zuurstof gebonden aan de kationische deeltjes. Stabilisatie van Fe in extraframework gemengde oxo complexen met aluminium levert aktieve katalysatoren voor de selektieve oxidatie van benzeen naar phenol. Dit model wordt ondersteund door de waarneming dat sublimatie van $FeCl_3$ naar [Al]-MFI een zeer aktief materiaal levert voor de ontleding van N_2O die echter niet erg selectief is in de oxidatie van benzeen. Anderzijds resulteert de dispersie van Fe en Al in silicaliet-1 waarin geen roostersubstituties hebben plaatsgevonden en naar verwachting alleen Fe-Al-oxidedeeltjes worden gevormd in een erg aktief en selektief materiaal. De lage N_2O ontledingssnelheid van dit materiaal suggereert dat optimale katalysatoren voor N_2O ontleding diegene zijn met een groot aantal kationische Fe deeltjes bijvoorbeeld bereid via de sublimatiemethode. Selektieve oxidatie katalysatoren moeten zo weinig mogelijk kationische deeltjes bevatten en vooral extraframework Fe-Al-oxidedeeltjes. Dit kan bereikt worden door uit te gaan van een "all-silica" zeoliet of door intensief stomen van zure katalysatoren.

Een laatste interessant punt is de oxidatietoestand van de aktieve Fe deeltjes in de selektieve oxidatiereaktie. Uit MAS studies aan de gesublimeerde materialen blijkt dat de aanwezigheid van Fe^{2+} belangrijk is wat overeenkomt met literatuurresultaten. Het vermoeden bestaat dat er twee types auto-reduktie plaats vindt Fe^{3+} naar Fe^{2+} deeltjes. Eén is de reduktie van ijzeroxide bij hoge temperatuur (473-773 K) in inert gas (He). Deze auto-reduktie wordt geremd door de

aanwezigheid van molekulair zuurstof. Deze deeltjes met een initieel hoge activiteit deaktiveren door reoxidatie naar Fe^{3+} (hoofdstuk 3). De Fe^{2+} oxidatie staat wordt tevens gestabiliseerd in extraframework Fe-Al-O deeltjes. Deze deeltjes worden gevormd in de aanwezigheid van zuurstof en preferent water met relatief hoge temperaturen. De aanwezigheid van een aanzienlijke hoeveelheid Fe^{2+} in [Fe,Al]-MFI is aangetoond middels Fe K-edge XANES. Die hoeveelheid neemt toe met stomen en bevestigt aldus de betrokkenheid van een extraframework deeltje. Deze Fe^{2+} oxidatie toestand is in essentie afwezig in [Fe]-MFI. Een eerste interpretatie van de dehydratatie van [Fe,Al]-MFI gevolgd door K-edge XANES geeft aan dat auto-reduktie van Fe^{3+} naar Fe^{2+} plaats vindt gedurende de verwijdering van geadsorbeerd water. De struktuur van het extraframework Fe-Al-O deeltje is open voor discussie maar een hypothetisch model is gepresenteerd in figuur 1.

Acknowledgements

I am very grateful for my supervisor, Prof. R.A.van Santen for offering me the opportunity to pursuing the Ph.D. degree in SKA. His insight in the science and support for the research are the foundation of this thesis. I am also very thankful for many good advices of Prof. F.Kapteijn, my second promotor.

I am very grateful for Emiel Hensen for his co-operation in my research. Emiel, to work with you is very enjoyable and fruitful. He contributes so much to this project both experimentally and scientifically that it is impossible for me to separate the contributions. **This thesis is the fruit of our teamwork.** Without his whole-hearted support and strong enthusiasm in science, this research would never be finished successfully.

I would like to thank my former supervisor, Professor Xu Longya, in Dalian Institute of Chemical Physics, Chinese Academy of Sciences, for his understanding and trust in the last several years. In the time I grew up, I am grateful to many teachers for their support and help, especially Mr.Zhou Yaoming and Mr. Shao Enyu and Prof. Zhou Zhihua in Nanjing Normal University and Mr. Chen Minglu and Mr. Sun Jiqian in the middle school.

I would like to thank Barbara for her help in the initial stage of this research. The difficulty in the beginning of my scientific career taught me many basic principles to study science.

I would like to thank Joop and Robert for their technical support in the laboratory. I can not image what my experiments would be without their help.

I am indebted to many people for their experimental help and discussions in this research, especially Jos van Wolput for IR, Pieter Magusin for NMR, Patricia Kooyman (TUD) for TEM, Arian Overweg (TUD) for Mössbauer, Prof. Janssen for ESR, Misha Sychev (Kiev) for UV-Vis, Marco Hendrix and Li for XRD, Ruud for the reaction in ECN, Darek for PEP and Bruce for Raman.

I thank all of my colleagues for their consistent daily help concerning every aspect of life. Tessa, Rob, Ine, Jos, Ingrid, Pieter, Frank, Gijsbert, Christophe, Mayela, Alina, Darek Martine, Steven, Haruki, Rafaël, Nicolae, Ruben, Jarl, thank you very much. I would like to specifically mention my long-time officemate, Christophe. He made me realize that everyone has a mask. Although he seems to be rude occasionally, he is basically a gentleman.

I am very thankful to many of my Chinese friends. We had a lot of funs and happy times together and it will be in my memory forever. They are Lu Gang, Ming Weihua, Tian

Publications

Q. Zhu, E.J.M. Hensen, B.L. Mojet, J.H.M.C. van Wolput and R.A. van Santen *Chemical Communications* (2002) 1232.

Q. Zhu, B.L. Mojet, R.A.J.Janssen, E.J.M. Hensen, J. van Grondelle, P.C.M.M. Magusin and R. A. van Santen *Catalysis Letters* 81 (2002) 205

E.J.M. Hensen, Q. Zhu, P.C.M.M. Magusin and R.A. van Santen, *Chemistry for Sustainable Development* 11(2003) 31.

E.J.M. Hensen, Q. Zhu and R.A. van Santen, Extraframework Fe-Al-O species occluded in MFI zeolite as the active species in the oxidation of benzene to phenol with nitrous oxide, *Journal of Catalysis,* in press.

E.J.M. Hensen, Q. Zhu, M.M.R.M. Hendrix, A.R. Overweg, P.J. Kooyman, M.V. Sychev and R.A. van Santen, Effect of high-temperature treatment on Fe/ZSM-5 prepared by chemical vapor deposition of $FeCl_3$, I. Physicochemical characterizatin *Journal of Catalysis,* in press.

Q. Zhu, R.M. van Teeffelen, R.A. van Santen and E.J.M. Hensen, Effect of high-temperature treatment on Fe/ZSM-5 prepared by chemical vapor deposition of $FeCl_3$, II. Activity *Journal of Catalysis,* in press.

E.J.M. Hensen, Q. Zhu and R.A. van Santen, In situ Fe K-edge XANES study of iron-containing MFI zeolites: the role of aluminum in the formation of ferrous species, in preparation.

E.J.M. Hensen, Q. Zhu and R.A. van Santen, Design of catalysts active in selective oxidation of benzene to phenol with N_2O, in preparation.

Q. Zhu, E.J.M. Hensen and R.A. van Santen, The nature of Fe and Al species in the selective oxidation of benzene to phenol with N_2O over MFI type zeolite, in preparation.

Curriculum Vitae

Qingjun Zhu was born on June 4, 1974 in Hulin, a county in the northern part of China. After he finished his high school education in Xuzhou, he went to Nanjing to study chemistry (starting September 1992) and got his bachelor's degree in Nanjing Normal University. He was attracted by the complex and promising nature of heterogeneous catalysis, so he went to the catalysis center of China, Dalian Institute of Chemical Physics (DICP), to begin his graduate study. His supervisor was prof. Xu Longya and he focused on the conversion of petrochemicals. In March 1999 he transferred to the Schuit Institute of Catalysis of the Eindhoven University of Technology as a Ph.D. student in the group of prof. R.A. van Santen. The most important results in his research are presented in this thesis.